THE DEVELOPMENT OF A METAL PLATE TEST REACTOR FOR STUDYING REACTION KINETICS ON CATALYTICALLY COATED HEAT TRANSFER COMPONENTS

by

Aida Khosravi

A thesis submitted to the Department of Chemical Engineering

In conformity with the requirements for

the degree of Master of Applied Science

Queen's University

Kingston, Ontario, Canada

(September, 2012)

Copyright ©Aida Khosravi, 2012

Abstract

A novel catalytic metal plate test reactor was designed, built and commissioned. The overall dimensions of the whole assembly were 215 mm long $\times$75 mm wide $\times$60 mm deep. A strip of stainless steel with dimensions of 150 mm long$\times$15 mm wide$\times$ 1.59 mm thick was partly coated with catalyst and sealed between the two reactor parts. The design provided a single channel flow pattern that could be easily modeled to extract kinetic parameters. A key feature of the reactor design was effective heat transfer to promote isothermal operation. A series of thermocouples was incorporated into the reactor to measure the temperature profile along the reactor.

Performance of the reactor was verified using a well characterized commercially available $Cu/Zn/Al_2O_3$ catalyst from BASF. The goal of this experimentation was to determine the conversion, rate constant and activation energy for methanol steam reforming and compare these with previously published measurements.

Methanol conversion was measured at slightly higher than atmospheric pressure at temperatures of 220, 240 and 260 °C. Steam to water ratio of feed was maintained at one during the experimental program. The feed rate of methanol was varied to obtain a catalyst to feed ratio $\left(W / F_{CH_3OH}\right)$ between 6 and 20 kgs mol^{-1}. The composition of reformate and methanol conversion were studied with temperature and flow rate of the feed. An increase from 27.68 to 41.61% in methanol conversion was observed increasing the reaction temperature from 220 to 240°C.

An irreversible first order rate constant was calculated using the experimentally measured conversion and space time. The apparent activation energy (E_a) based on a first order plug flow design operation was 96±4 $k.J.mol^{-1}$ and agreed well with the values of 77-105.1 $kJmol^{-1}$ reported in the literature.

Acknowledgements

I wish to express my deepest gratitude to my supervisor, Dr. Brant A. Peppley, without whom this work could not have been accomplished. His exceptional support, leadership, and patience through these years were not only an encouragement in research fields but also taught me to be a better individual and professional.

I also wish to thank my friends and colleagues at the Queen's-RMC Fuel Cell Research Centre who have always been there for me when I needed their emotional and professional support. In particular, I would like to thank Rajesh Parmar who always cheerfully answered my endless questions. Furthermore if it was not for the direction and helping hand of Jason Wood throughout the experimental testing this project would have taken an infinitely longer time to complete. I must also thank Gordon McAlary for his contributions to this research.

Big thanks go to SOFC Canada NSERC Strategic Research Network for creating this opportunity and for providing the continuous support through the people within the network.

And finally, I would like to thank the most important people in my life, my family. My mother, Akhtar, whose unconditional love has always brightened my path when I felt the loneliest; and my father, Khosro, who taught me that there is no such word as impossible for human beings. I also deeply appreciate the support from my brother and sister, Omid and Elham, who always assured me that everything would be alright, even when I stopped believing.

Studying at the Queen's-RMC Fuel Cell Research Centre was an amazing experience that had a huge influence on my perception of life. These years have provided me with a direction and will forever influence my future decisions.

Table of Contents

List of Figures

List of Tables

Nomenclature

$C_{A,0}$	Concentration of A at the reactor entrance [mol m^{-3}]
D_{20}^{20}	Specific gravity of feed solution at 20°C
E_a	Apparent Activation Energy [kJ mol^{-1}]
$F_{A,0}$	Molar flow rate of component A at the entrance to the reactor [mol s^{-1}]
F_i	Molar flow rate of component i [mol s^{-1}]
ΔH	Enthalpy change of a reaction [kJ mol^{-1}]
ΔH_{298}°	Standard enthalpy change [kJ mol^{-1}]
k	Rate constant [m^3 kg^{-1} s^{-1}]
K_W	Thermodynamic equilibrium constant of water-gas shift reaction
m	Mass of component i [g]
M_i	Molecular weight of component i [g mol^{-1}]
n	Number of observations
n_i	Number of moles for component i
N_i	Percent of component i in dry gas product (i=CO, CO_2, H_2)
P	Pressure [units vary depending on the equation]
P°	Standard pressure [1 atm]
P_i	Partial pressure of component i [atm]
Q_F	Total volumetric flow rate of the feed mixture [ml s^{-1}]
r_{CH3OH}	Rate of methanol steam reforming reaction [mol kg^{-1} s^{-1}]
R	Ideal gas constant [= 8.134 J mol^{-1} K^{-1}, 82.05 cm^3 atm mol^{-1} K^{-1}]
R^2	Correlation coefficient for linear regression
s	Estimate of standard deviation
S_{xx}	Sum of squares of deviations of data points from their sample mean
t	Time [s]
$t_{df,\alpha/2}$	Student's t-statistics for df degrees of freedom and α significance level
T	Temperature [K or °C]
T°	Standard temperature [273.15 K]
V	Volume of the reactor [ml]
V_F	Total volumetric flow rate of dry product gas [ml s^{-1}]
V_i	Liquid volume of component i [ml]
W	Weight of the Catalyst [kg]
W_{CH3OH}	weight percent of methanol in feed mixture
$\bar{x}$	Sample mean
X_{CH3OH}	Fractional conversion of methanol
y_i	Normalized fraction of the component i in the dry product gas
$\bar{y}_{\circ}$	Predicted response value

Symbols and abbreviations

AC	Alternating Current
AFC	Alkaline Fuel Cell
ATR	Autothermal Reforming

CI	Confidence Interval
C.O.V	Coefficient of Variance
CPOX	Catalytic Partial Oxidation
DC	Direct Current
DI	De-Ionized
GC	Gas Chromatograph
GUI	Graphical User Interface
HPLC	High Pressure Liquid Chromatography
IC	Internal Combustion
IEO	International Energy Outlook
LabVIEW	Laboratory Virtual Instrumentation Engineering Workbench
LHV	Lower heating Value
MFC	Mass Flow Controller
MFM	Mass Flow Meter
NG	Natural Gas
OECD	Organization for Economy Cooperation and Development
PAFC	Phosphoric Acid Fuel Cell
PEMFC	Polymer Electrolyte Membrane Fuel Cell
POX	Partial Oxidation
PV	Process Value
PVA	Polyvinyl Alcohol
S/C	Molar water to catbon ratio
SCXI™	Signal Conditioning Extension for Instrumentation
SMR	Steam Reforming of Methanol
SR	Steam Reforming
SOFC	Solid Oxide Fuel Cell
SV	Set Value
TC	Thermocouple
TCD	Thermal Conductivity Detector
WGS	Water Gas Shift

Dimensionless group

Re	Reynolds Number
Bi	Biot Number

Greek Symbol

α	Significance level

ε_{CH3OH}	Fractional volume change on complete conversion of methanol, see Appendix E
$\mu_{y\|x0}$	Mean response of the population at x_0
ρ_F	Density of feed solution [g cm^{-3}]
ρ_i	Density of component i [g cm^{-3}]
σ	Standard deviation
τ_v	Space time with respect to reactor volume [s]
τ_w	Space time with respect to catalyst weight [kg s m^{-3}]
Φ_w	Relative equilibrium parameter for water-gas shift reaction defined by Eq. 5.10

Chapter 1

Introduction

1.1 Energy Related Challenges

Energy demand is increasing worldwide and will continue to rise due to rapidly rising human population and modernization trends across the world [1]. According to Song [2], between the years 1900 and 1997 the world population more than tripled as did the energy demand per person resulting in greater than twelve times higher global carbon dioxide emission. The U.S. Energy Information Administration [3] has stated that world energy consumption will increase by 53%, from 532 exajoules in 2008 to 812 exajoules in 2035 (Table 1.1). As nations recover from the global recession, world energy demand is expected to increase strongly as a result of robust economic growth and expanding populations in the world's developing countries. According to International Energy Outlook 2011 [3] "Energy demand in Organization for Economic Co-operation and Development (OECD) countries grows slowly over the projection period, at an average annual rate of 0.6%, whereas energy consumption in the non-OECD emerging economies expands by an average of 2.3% per year".

Future energy consumption will be driven by non-OECD demand. Whereas energy use in non-OECD nations was 7% greater than that in OECD nations in 2008, non-OECD economies will consume 38% more energy than OECD economies in 2020 in the IEO2011 Reference case and 67% more in 2035 [3].

Table 1.1 World energy consumption by country grouping, 2008-2035 (exajoules) [3]

Region	*2008*	*2015*	*2020*	*2025*	*2030*	*2035*	*Average annual percentage change 2008-2035*
OECD	257.6	264	274.8	284.5	293.8	303.8	0.6
Americas	129.6	132.9	138.1	143.3	149.3	155.7	0.7
Europe	86.7	88.1	91.6	94.6	96.8	98.9	0.5
Asia	41.3	42.9	45.0	46.6	47.9	49.2	0.6
Non-OECD	274.7	340.7	378.4	423.5	466.9	507.8	2.3
Europe and Eurasia	53.2	54.2	55.1	56.9	59.0	61.6	0.5
Asia	145.4	198.3	226.7	259.8	289.2	315.0	2.9
Middle East	27.0	32.7	35.7	39.3	43.5	47.8	2.1
Africa	19.8	22.7	24.9	27.3	30.0	33.1	1.9
Central and South America	29.2	32.7	36.1	40.1	44.9	50.4	2.0
World	532.1	604.7	653.2	708.0	760.7	811.6	1.6

Fossil fuels have been the main source of energy supply and have served human energy needs for hundreds of years. According to International Energy Agency's statistics [4], over 80% of the world primary energy supply is fossil fuel. It is clear then, the present energy consumption situation, led by fossil fuels, has major concerns such as depletion of fossil fuel reserves, rising energy costs and global warming. It is now completely established that global warming is taking place due to effluent gas emission, mainly CO_2. During the past century, global surface temperatures have increased at a rate near 0.6°C/century, but this trend has dramatically increased to a rate approaching 2.0 °C/century during the past 25 years [5]. Considering the above facts, fundamental

changes in society's energy systems are required to reduce the energy consumption rate as well as environmental impacts.

Lower rates of energy consumption, reductions in pollutants and CO_2 emissions could be achieved by the use of fuel cells in electric power plants and transportation systems. The use of fuel cells for electric power generation is attracting increasing attention, owing to a potentially superior efficiency and operational benefits compared to conventional technologies like combustion engines [6, 7].

1.2 Background

1.2.1 Fuel Cells

Fuel cells are electrochemical devices that directly convert the chemical energy of a reaction into electrical energy. The basic physical structure of a fuel cell consists of an electrolyte layer in contact with a porous anode and cathode on either side. In a typical fuel cell, gaseous fuels are fed continuously to the anode (negative electrode) compartment and an oxidant (*i.e.*, oxygen from air) is fed continuously to the cathode (positive electrode) compartment, and the electrochemical reactions take place at the electrodes to produce an electric current [8]. The electrons go through an external circuit generating an electric current while the ions move through the electrolyte toward the oppositely charged electrode. At the electrode, ions combine to create by-products, primarily water. The fuel cell operates as long as both fuel and oxidant are supplied to the electrodes, and the impact on the environment is significantly less compared to combustion engine technologies.

Fuel cells are intrinsically much more energy-efficient, and could achieve as high as 70-80% system efficiency (including heat utilization) in electric power generators using Solid Oxide Fuel Cells, and 60% (tank to wheels) efficiency [9] for transportation using Polymer Electrolyte Membrane Fuel Cells or SOFCs (versus a common efficiency of 20-35% with internal combustion (IC) engines) [2].

The fuel cell of primary interest in this work is the SOFC, which along with the molten carbonate fuel cell are commonly referred to as high temperature fuel cells.

1.2.2 Solid Oxide Fuel Cells

SOFCs utilize an oxide ion-conducting ceramic material as the electrolyte. It is therefore, simpler in concept than all the other fuel cell types as only two phases (gas and solid) are required. Furthermore, the ceramic electrolyte does not present problems with electrolyte management like liquid electrolytes that can be corrosive or difficult to handle.

SOFCs operate at the highest temperature (600-1000 °C) of the various types of fuel cells, and are the most compatible for hydrocarbon fuels compared to other types of fuel cells. Despite operating at temperatures up to 1000 °C, the SOFC electrolyte always stays in solid state. The SOFC's high operating temperature (>600 °C) allows internal reforming, promotes rapid kinetics, and produces high quality byproduct heat [8].

SOFCs can achieve the highest efficiency (defined as electrical energy produced divided by the heating value of the fuel) compared to other types of fuel cells; thus, their use can lower fuel consumption rates and, consequently, reduce fuel costs. Haldor Topsøe/Risø studies predict that 20 kW Natural Gas (NG) fuelled SOFC system reaches the electrical efficiencies from 50% to 56% (AC out/LHV in) depending on the fuel used of the system [10]. In addition to high electrical efficiencies, valuable heat can be recovered from the SOFC system; as a result, SOFCs are suitable for Combined Heat and Power systems of 2 kW to multi-MW [7].

1.2.3 Fueling the Fuel Cell

Fuel cells require hydrogen for their operation; so, there are numerous studies worldwide concerning generation and storage of hydrogen. The lack of hydrogen infrastructure, in the short term, along with the highly attractive energy density of liquid fossil fuel has created wide spread

research efforts in the field of distributed small-scale and on-board hydrogen generation from various hydrocarbon [6].

Fuel reforming is a technical term used to describe the complex chemical process of converting hydrocarbon fuels, usually by the aid of suitable catalyst, into a hydrogen-rich gas stream. This hydrogen-rich product gas, commonly called reformate, can then be used to feed various types of fuel cells.

SOFCs are known for their fuel flexibility compared to other type of fuel cells. Table 1.2 summarizes general fuel requirements, and the impact of gas components on five different types of fuel cells. There is generally no need to add a further unit for gas clean-up to remove CO, CO_2, and CH_4 since they have no significant detrimental effects on the performance of a SOFC anode.

Table 1.2 The fuel requirements for the principal types of fuel cells [7]

Gas Species	*PEMFC*	*AFC*	*PAFC*	*MCFC*	*SOFC*
H_2	Fuel	Fuel	Fuel	Fuel	Fuel
CO	Poison (>10 ppm)	Poison	Poison (>0.5%)	Fuel	Fuel
CH_4	Diluent	Poison	Diluent	Diluent	Diluent
CO_2 and H_2O	Diluent	Poison	Diluent	Diluent	Diluent
S (as H_2S and COS)	Few studies	Unknown	Poison (>50 ppm)	Poison (>0.5 ppm)	Poison (>1.0 ppm)

Essentially the lower the operating temperature of the fuel cell, the more stringent the requirements for contaminant removal and the greater demand placed on fuel processor.

1.2.4 Structured and Micro-structured Reactors

The first major success of monolith supported catalyst was in automobile exhaust treatment. Subsequently other applications were developed, environmental applications being by far of the greatest interest [11]. Structured reactors have been used in automotive emission control since the

1970s to reduce nitrous oxides and oxidize carbon monoxide and hydrocarbons from internal combustion engine exhaust [12]. The catalyst support substrate is in fact an integral part to the reactor system that brings the catalyst into maximum exposure to the reactants. The active catalyst is deposited as a washcoat onto the surface of the structured support. These supports should withstand a variety of severe operating conditions as well as providing reasonable durability of the washcoat.

These uniform catalyst support structures can vary from plates and channels to foams, and they commonly utilize ceramic or metal materials as supports, see Figure 1.1. Ceramic and metallic substrates offer good mechanical strength. The substrate material dictates the thermal behavior of the reactor. Where ceramic acts as insulator and behaves as nearly adiabatic, metal substrates transfer heat much more effectively in axial and radial direction promoting isothermal behavior. Consequently, metallic substrates are particularly attractive for more heat demanding reactions.

The other appealing application of structured reactors in recent years has been in fuel reforming technology. These types of reactors are of great interest due to their capability to transfer heat effectively, where fixed bed reactors are generally considered inefficient for highly endothermic reaction such as steam reforming. Lower pressure drop and full utilization of the catalyst potential can be achieved in structured reactors while rapid temperature changes can weaken particulates causing attrition and blockage resulting in decreased catalyst activity and increased pressure drop in fixed bed reactors. Ceramic and metallic structures also offer a uniform reactant access to the catalytic surface and good mechanical strength while catalyst pellets can face attrition issues under the pressure of the weight of a packed bed.

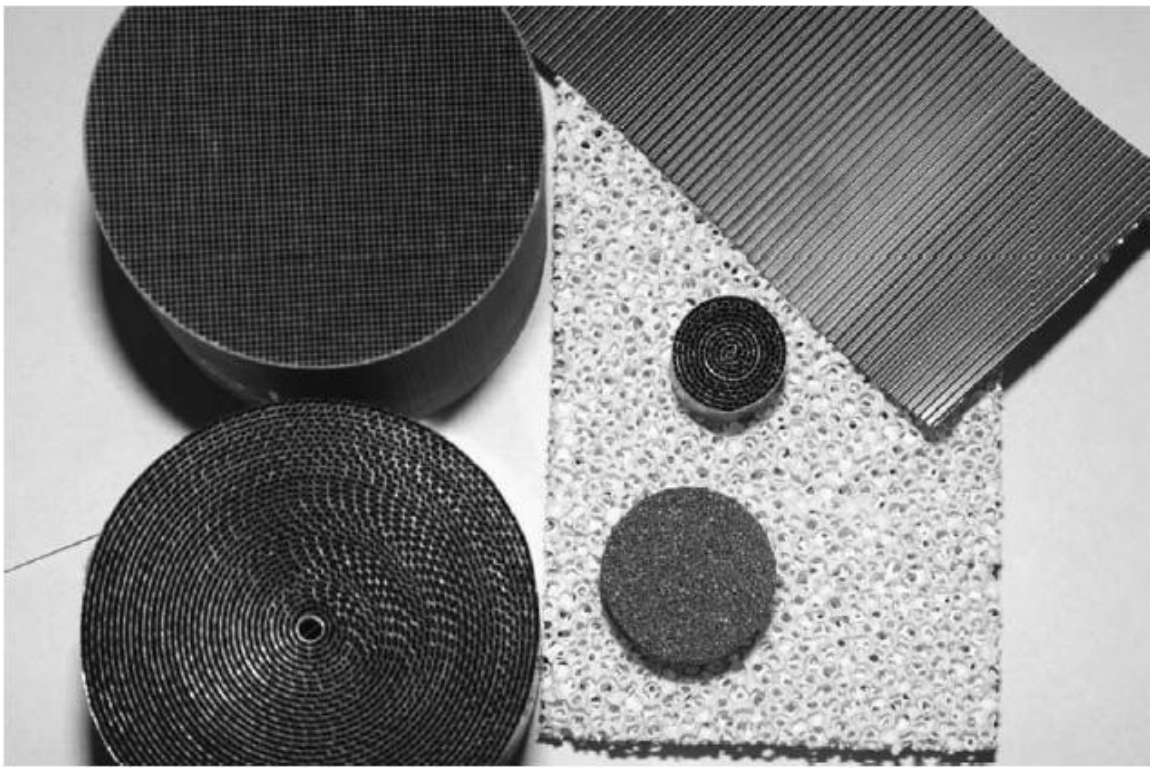

Figure 1.1 Examples of catalyst substrates (clockwise from upper left): ceramic monolith, corrugated metal foil sheet, small metal monolith, fine metal foam, coarse ceramic foam, large metal monolith [13]

1.3 Research Opportunities for Improved Fuel Reformer Design

There are numerous studies to find an optimum combination of fuel, catalyst, reactor type, and process that allows for compact, lightweight and efficient reformers introducing a quick response to transition modes with an acceptable hydrogen production rate to meet the strict cost targets and performance reliability. Considering the advantages of structured and micro-structured reactors, researchers have been trying to develop a compact and effective structured fuel reformer since the choice of reformer has significant impact on overall efficiency and operating characteristics of fuel cell systems.

Effective heat transfer is critical when it comes to highly endothermic reactions such as steam reforming; besides, an appropriate reactor design is crucial for accurate kinetic measurements.

Difficulties occur with fixed bed when highly heat demanding reactions are investigated where axial and radial temperature gradients happen due to poor heat transfer across the bed [14].

Metallic substrates, as mentioned before, are a promising alternative for highly endothermic or exothermic reactors. However, there are two major fields that require detailed investigation:

- The adhesion problem that occurs because of non-porous nature of metals, and different thermal expansion coefficients between metal substrate and catalyst layer.
- Effective design depending on purpose and operation characterization of the reformer.

Regardless of the structural support material the issue is always the same: developing a highly catalytically active but stable coating while strongly bonded to a sometimes incompatible and low surface area support material [15]. When using ceramic as a substrate, the porosity of ceramic material promotes good bonding with the washcoat. Metal substrates on the other hand, need to go through some pre-treatment to develop a porous surface and extra care must be taken that they are compatible with the supported catalyst to ensure a reasonable wash-coat/substrate adhesion and durability [13].

1.4 Objectives of this Thesis

The first objective of this work was to design, build, and commission a laboratory fuel reforming test reactor for measuring the activity of catalyst coatings applied to metal substrates. The design must provide a simple laminar flow pattern that can be easily modeled so that kinetics parameters can be determined.

The second objective was to calibrate the gas analysis system and develop a method to generate precise and reproducible experimental results using the system. A mass balance around the system must close to less than 5%.

The Third objective of this work was to collect kinetic data for the catalytic steam reforming of methanol over a $Cu/ZnO/Al_2O_3$ catalyst in the metal plate reactor. These results were to be compared with published literature in order to verify the performance of the test system.

1.5 Thesis Structure

The present work introduces a new design of metal plate fuel reforming reactor that allows repeatable estimation of the activity of catalyst coatings developed for micro-structured reactors. This work covers reactor design, test system development, and experimental method for catalyst layer activity measurement.

Chapter 2 of the thesis provides an overview of structured and micro-structured reactors briefly outlined in Section 1.2.4, including advantages over conventional technologies. Chapter 2 will also review and compare detailed procedures and available techniques for coating catalysts onto metallic substrates. The chapter also reviews results from literature in the field of methanol reforming in micro-reactors.

Chapter 3 discusses the design of the reactor. Operational challenges and obstacles are also discussed terms of the criteria for the specific design.

A detailed description of the test system as well as the experimental procedure is given in Chapter 4. The system is discussed in detail including description of major components and their features. The chapter also describes the experimental protocol for data acquisition. An overview of the challenges encountered and solutions that were applied is given as a great deal of effort was spent assembling and troubleshooting the analysis and metering subsystems.

The data collected for the determination of conversion and rate constant for the $Cu/ZnO/Al_2O_3$ catalyst is presented in Chapter 5. A comparison of these measurements with previously published activity measurements is given including a discussion of the differences that were observed.

Conclusion and recommendations are given in Chapter 6. A list of suggestions for the improvement of the reformer and the test system is also provided.

Chapter 2

Literature Review and Theory

The first section of this chapter introduces structured and micro-structured reactors and compares them with conventional technologies with an emphasis on relevant applications to this thesis. The focus is on the literature utilizing metallic structured supports since this work is concerned with a metal plate reactor. The second section discusses catalyst selection and the potential of methanol steam reforming. The third section is dedicated to a review of the literature on the development of catalyst coated metal substrates. The final section of this chapter reviews some of the structured micro-reactors from the literature and their testing conditions.

2.1 Structured and Micro-Structured Reactors for Catalytic Reactions

Structured reactors offer great advantages when it comes to compact design and process volume reduction. Structured catalysts are typically monolith supported catalysts where the monolith is commonly manufactured from ceramic or metal materials [12, 13, 16]. The monolith support structures are not, in most cases, catalytically active by themselves; therefore, there is a need to deposit a very thin layer of catalytically active material onto the surface of the structured support. Enormous development effort has been required to develop methods for depositing the catalyst components but the advantages associated with modern monolith based reactors have outweighed the cost and effort. A variety of methods for catalyzing the wall of the monolith are now available. Exact procedures vary with the type of structured support surface and the specific application; however, extra care has to be taken for metallic substrates to ensure the acceptable adhesion between metal and the catalyst layer [17].

Structured reactors were first introduced for large scale for car exhaust emission control, in the 1970s offering large geometric surface area along with more compact and lighter reactors. Lighter weight promotes rapid warm up of the catalyst favoring greater conversion of pollutants. By around

1980, all automobile manufacturers designed their catalytic converters using catalyst coated ceramic monoliths [17].

The success of structured catalyst in automobile and environmental applications persuaded other industries to develop the technology for their own specific means. In recent years micro-reactors have been attractive to researchers for diverse applications such as, hydrogenations, dehydrogenations, dehydrations [18], and fuel reforming [18-37].

In most documents structured reactors are regarded as micro-structured when carrying channel(s) or similar fluid paths are with a size below few millimeters, these two terms might be used interchangeably in this text. This thesis does not concentrate on the complicated manufacturing processes of different types of monolith; however, there is literature focusing on production techniques [11] that the reader can refer to.

2.1.1 Advantages of Structured Reactors

Ceramic or metal monoliths offer a wide variety of advantages over packed beds for almost all unit operations; mainly related to reduced pressure drop, mechanical integrity, improved heat transfer and reduction in size [17, 23, 24]. The open structure also allows their use in high dust environment without concern from plugging. These factors and advantages are discussed in details below [17].

Pressure Drop

Regardless of the construction material the open frontal area and open concept of structured reactors result in very little resistance to flow; consequently, the pressure drop across these reactors is much smaller compared to inherently large pressure drop in fixed beds. The bed porosity is 40% for spherical particles while monoliths have open frontal area approaching 85% [17]. Lower pressure drop leads to lower resistance to flow or back pressure on the system and therefore lower energy loss.

The substrate material of construction (ceramic or metallic) can further affect the pressure drop. Metallic supports can be manufactured with very thin walls compared to ceramics. This additional open surface area for a given cell density (number of channels, their diameters and wall thickness determine the cell density, expressed in cell per square inch [17]) means that pressure drop across metallic monoliths can be lower than across ceramic monoliths [13].

Heat and Mass Transfer

Improved heat and mass transfer is a crucial drive for applying micro-structured reactors instead of conventional apparatuses. Small channel diameters considerably enhance heat and mass transfer rates in structured systems regardless of the support material. Hass-Santo *et al.* [38] have reported overall heat transfer coefficients up to 1700 W/m^2K for gas-gas and up to 54000 W/m^2K for water-water heat transfer. As a result these reactors are attractive for processes that require fast heating and cooling of the reaction mixture, quick response to transitions, and fast start ups.

Metallic substrates also have superior heat transfer properties to ceramics due to their higher thermal conductivities that allows utilizing the full potential of the catalyst for highly endothermic or exothermic reactions, avoids hot spot formation, and promotes isothermal behavior. It was shown that with a catalytic partial oxidation of alcohol to aldehyde, the yield could be increased from 85% in conventional systems up to 96% in micro-channel reactors, simply because the reaction could be run under nearly isothermal conditions [38].

Geometric Surface Area to Volume Ratio

Structured reactors are the most efficient for reactions that require high geometric surface area. The specific surface in conventional laboratory and production vessels is usually 100 m^2/m^3 and seldom exceeds 1000 m^2/m^3; while in micro-structured reactors this ratio can be in the range of 10000-50000 m^2/m^3 [39].

Mechanical Strength

Particulate catalysts can weaken under the pressure of the weight of a packed bed, or in motion in fluidized bed, or in the presence of an aggressive chemical environment such as high temperature and partial pressure of hydrogen and steam, or rapid temperature changes during transient operation. This would cause attrition and blocking; therefore, decreasing catalytic activity and increasing pressure drop [13].

Ceramic and metallic monoliths offer good mechanical strength due to their uniform body structures. They allow more freedom for orientation in the system and are more resistant to mechanical and thermal shocks while particulate catalyst supports can face issues in severe reaction conditions.

Process Safety

Structured and micro-structured reactors are recognized for their inherent safety during operation due to the small inventories of reactants and products [39], and flame arresting capabilities [38]. For such process safety capabilities, Haas-Santo *et al.* [38] have demonstrated the heterogeneously catalyzed reaction of explosive mixture of hydrogen and oxygen in a micro-channel reactor.

It is also worthwhile to mention that the open structure allows the use of these reactors in high dust environment, such as coal-fired power plants and diesel exhaust without concern from plugging. For extreme operating conditions where there is a heavy accumulation of dust, the monolith allows easy cleaning by air lancing or chemical washing [17].

With all the advantages mentioned for monolithic reactors, there are still challenges such as durability and activity of the catalyst. Greater catalyst loading and increase in porosity inside the coating (particularly on metallic substrates) are required to increase the durability of catalyst [32].

2.1.2 Substrate Material of Construction

Monolithic structures are commonly manufactured from ceramic or metal, but can be also be made of plastic [17]. Metallic monoliths can be manufactured more easily compared to ceramics, and due to their mechanical strength, they can be found in different forms such as walls [14, 15], foams [40-44], micro-channels [21, 22, 25-28, 35, 37, 45-51], and wire meshes [52].

The substrate material determines the behavior of the reactor and affects coating and adhesion of the catalyst layer. It is important to consider factors such as cost, weight, maximum temperature capability, heat management, *etc.*, and find the best matching substrate candidate for any specific application. A list of chemical and physical properties for ceramic materials is presented by Heck *et al.* [17].

Ceramics act as an insulator and operate approximately adiabatically, so they can be used for reactions such as autothermal reforming. Catalyzed ceramic monoliths are great alternatives for autothermal reaction since they eliminate the limitation of heat transfer; therefore, the heat generated from partial oxidation reaction can be directly utilized by the steam reforming reaction [17].

As mentioned previously, metals are another widely used material for structures and can transfer heat more effectively in the axial and radial direction promoting an isothermal behavior along the reactor. They are attractive for processes that require quick response, fast start up and transitions [22]. For instance, metal micro-reactors are great candidates for a highly endothermic steam reforming reactions, where it is necessary to supply large amount of heat to maintain the reaction rate [25, 30].

<u>Ceramic vs. Metallic Substrates</u>

Multi-cell ceramic monoliths made from cordierite ($2MgO\ 2Al_2O_3\ 5SiO_2$) were first used in large scale in the mid-1970s for a catalytic converters on new vehicles in the US [13, 17]. The porosity of

the cordierite material ensures good bonding with the washcoat material. Washcoated cordierite monoliths are widely used in three way gasoline converters, which simultaneously convert CO, HC and NO_x to CO_2, H_2O and N_2 when operated in the stoicheometric air ratio to fuel in the exhaust of the internal combustion engine [17].

The parallel channel ceramic monolith is essentially an adiabatic reactor limiting temperature control. These types of reactors are not suitable for many petrochemical reactions where selectivity is governed by temperature. Metallic substrates were employed, solving these operational problems with their high temperature resistance and thermal conductivity. Being resistant to mechanical shocks, metal monoliths can be machined to have thinner walls and allow micro-reactor configurations. With open frontal areas approaching 90% [17] and smaller channel size, they also offer even lower pressure drop and greater geometric areas compared to ceramics. However, it should be kept in mind that micro-structured reactors made of metals are not suitable for chemical reactions where corrosive reactants are involved. Ceramic materials are the perfect choice for these kinds of applications.

The general method for metal monoliths and structured supports is to deposit a layer that has a specific surface area and hosts the noble metal catalyst [53]. In rare occasions, the entire metal monolith can be fabricated using the catalytically active material (*e.g.*, silver heat exchange for oxidative dehydrogenation) [25]. The problem arises for coated metal monoliths when the thermal expansion coefficient of the ceramic oxide coating and the metallic substrate are significantly different, so the adhesion between them becomes an issue resulting in catalyst lifetime and durability deficiencies. As a result, metallic substrates generally must go through some pre-treatment to compensate for the problems of thermal mismatch seen in these types of reactors. This is the topic of section 2.3.

2.2 Reforming of Hydrocarbons

Fuel reforming is generally classified into three modes; steam reforming (SR), partial oxidation (POX), and autothermal reforming (ATR). Each of these processes has advantages and disadvantages with respect to process requirements for heat transfer, mass transfer, choice of materials and safety issues. The choice of type of reformer has a significant impact on the overall efficiency and operating characteristics of a given fuel cell system. A number of excellent publications are available on common methods of fuel reforming and fuel processor designs [2, 6, 7].

SR is the most commonly used industrial reforming method and offers higher hydrogen product concentrations compared to POX and ATR. Literature reports 70-80% hydrogen concentration in steam reforming products and 30-50% for POX and ATR [54, 55]. Steam reforming of natural gas is a well known and widely used commercial process to produce large quantities of hydrogen in petroleum refining processes [56]. Equation 2.1 shows the SR reaction that converts hydrocarbons into a mixture of carbon monoxide and hydrogen.

$$C_nH_m + nH_2O \rightarrow nCO + \left(\frac{m}{2} + n\right)H_2 \qquad \Delta H > 0 \qquad \textbf{2.1}$$

This reaction is highly endothermic and requires heat to be supplied to maintain the reactor temperature; as a result, the reactor design is limited due to heat transfer issues. Additional equipment required for heat is one of the main drawbacks to steam reforming and the amount of heat required causes slow dynamic response to any transition; however, SR is a very effective method for fuel reforming if the reformer design allows high heat transfer along the reactor. Reformate from steam reforming usually also contains unconverted steam and, to a lesser extent, some unconverted fuel, and carbon dioxide [6]. The water gas shift (WGS) reaction increases the hydrogen and carbon dioxide concentration of the product reformate as well.

$$CO + H_2O \leftrightarrow CO_2 + H_2 \qquad \Delta H^{\circ}_{298} = -40.1 k\ J\ mol^{-1} \qquad \textbf{2.2}$$

In another reforming method, hydrocarbons can be converted to hydrogen via partial oxidation (POX). In POX, hydrocarbon fuel reacts with sub-stoichiometric amount of oxygen or air to produce hydrogen and carbon monoxide. Partial oxidation can be carried out at high temperatures (typically 1200-1500 °C) without a catalyst. Such high temperature partial oxidation has been employed on a large scale by several companies but does not scale down well, and control of the reaction is problematic [7]. The process becomes known as catalytic partial oxidation (CPOX) if a catalyst is employed and the temperature is reduced.

Providing pure oxygen either on a large or small scale is usually not a viable option; therefore, the reaction is usually done using air to provide the oxygen, which results in an overall decrease in reactor efficiency and dilutes the hydrogen product gas since nitrogen is a non-reactive molecule in the reaction [57].

$$C_nH_m + \frac{n}{2}\left(O_2 + 3.75N_2\right) \rightarrow nCO + \frac{m}{2}H_2 + 3.75\left(\frac{n}{2}\right)N_2 \qquad \Delta H < 0 \qquad \textbf{2.3}$$

Exothermic partial oxidation using air is a much simpler system that does not require additional heat supply, but has lower hydrogen yield compared to SR and ATR. Partial oxidation of higher alkanes, however, presents several problems such as flame occurrence during vaporization and mixing, soot formation associated with combustion of fuel-rich gases, and coke formation on reactor walls and on catalysts [58].

Autothermal reforming is another commonly used fuel reforming method. ATR is in fact oxidative steam reforming that usually describes a process in which both steam and oxidant (oxygen, or more normally air) are fed with the fuel to a catalytic reactor. It can, therefore, be considered as a combination of partial oxidation and steam reforming [7], processes that have already been described above.

$$C_nH_m + x(O_2 + 3.75\,N_2) + (n-2x)H_2O \rightarrow n\,CO + \left(n - 2x + \frac{m}{2}\right)H_2 + 3.75x\,N_2 \qquad \textbf{2.4}$$

$$\Delta H \approx 0$$

As seen in Equation 2.4, the advantage of autothermal reforming is that both the endothermic steam reforming (Equation 2.1) and the exothermic partial oxidation reactions (Equation **2.3**) occur together; so, no heat needs to be supplied or removed from the system. However, this is not the case in practical systems because heat losses need to be compensated. Usually an optimum oxygen/carbon ratio exists for each fuel under thermally neutral conditions to achieve optimum efficiency [6].

2.2.1 Steam Reforming of Methanol (SRM)

Methanol has been identified as a highly suitable liquid fuel for hydrogen production because of its low reforming temperature, easier handling than methane or other gaseous fuels, good miscibility with water, and low content of sulfur compounds [21, 23, 24, 34]. Methanol can be catalytically converted to a hydrogen rich stream via following three main reactions.

Steam reforming of methanol:

$$CH_3OH + H_2O \rightleftarrows CO_2 + 3H_2 \qquad \Delta H^{\circ}_{298} = 48.96\ \text{kJ mol}^{-1} \qquad \textbf{2.5}$$

Methanol decomposition:

$$CH_3OH \rightleftarrows 2H_2 + CO \qquad \Delta H^{\circ}_{298} = 90.13\ \text{kJ mol}^{-1} \qquad \textbf{2.6}$$

Water-gas shift reaction:

$$CO + H_2O \rightleftarrows CO_2 + H_2 \qquad \Delta H^{\circ}_{298} = -41.17\ \text{kJ mol}^{-1} \qquad \textbf{2.7}$$

Steam reforming of methanol enables the production of hydrogen at relatively low temperatures in the range of 230-300 °C; therefore, only a relatively small amount of CO (< 2%) is formed [35].

Steam reforming of methanol is an endothermic reaction and it is considered to be one of the important methods for hydrogen generation from the viewpoint of feasibility for various kinds of on-site energy systems. As is the case for any endothermic reaction, it is necessary to provide the reactor with sufficient heat to maintain the reaction rate. Reuse *et al.* [35] designed a micro-structured reactor to bring heat directly to the core of the reactor by coupling an exothermic combustion zone. This was one of the first publications dealing with coupled methanol steam reforming reactor. The design of Reuse *et al.* will be described in section 2.4.

2.2.2 Choice of Catalyst Formulation

A commonly used catalyst for methanol steam reforming is oxide supported copper. The presence of zinc oxide was found to be beneficial for the catalyst stability under reaction conditions [35]. From the literature, water to methanol molar ratios higher than one are beneficial for catalyst activity and enhance the carbon dioxide selectivity which resulting in greater H_2 yield by reaction 2.5 (see above).

The group of catalysts showing the highest activity for methanol steam reforming has composition of $Cu/ZnO/Al_2O_3$, which is also the catalyst for methanol synthesis. Methanol and steam in the presence of a $Cu/ZnO/Al_2O_3$ catalyst at temperatures greater than 160°C react to form a hydrogen-rich gas [59]. $Cu/ZnO/Al_2O_3$ catalyst has been shown in numerous studies to have high hydrogen and carbon dioxide selectivity while producing minor quantities of carbon monoxide.

Generally, there are four types of catalysts for steam reforming of methanol in the literature under the category of micro-structured reactors, $Cu/ZnO/Al_2O_3$, $Cu/Cr_2O_3/Al_2O_3$, $Cu/CeO_2/Al_2O_3$, and Pd/ZnO. Bravo *et al.* [25], Park *et al.* [34], Cominos *et al.* [29], Lim *et al.* [23], Karim *et al.* [24], Won *et al.* [37], Yu *et al.* [21], and Hwang *et al.* [30] used $Cu/ZnO/Al_2O_3$ in micro-channels. The other types such as $Cu/Cr_2O_3/Al_2O_3$, $Cu/CeO_2/Al_2O_3$, and Pd/ZnO were tested in studies by Zapf *et al.* [28], Men *et al.* [27, 47], and Pfeifer *et al.* [60] respectively. As is noticed, $Cu/ZnO/Al_2O_3$ is the most commonly used catalyst for the methanol steam reforming purpose and was used in this thesis.

In general, the catalyzed substrate is first prepared, and then integrated into the reactor. The problem in structured reactors, however, is the poor durability of the catalyst. Section 2.3 discusses catalyst preparation and coating to prepare the catalyzed metal substrates.

2.3 Development of Catalyst Coated metal Substrate

The design of structured reactors creates some extra engineering demands when coating different substrate materials. It is generally accepted that it is more difficult to achieve and adhere catalyst coating on a metal than a ceramic. The coating of active catalysts onto metallic walls, regardless of their shape (plate, foam, tube, *etc*.) and size (micro or larger) is generally problematic due to an intrinsically low geometric surface of metal while highly developed surface areas are needed to get active catalytic surface. Different types of metals are utilized for different purposes, metals like aluminum (for alumina deposit) or special steels (aluminum containing or stainless steel) might be more suitable. However, the preferred material for most industrial reactors is stainless steel owing to its good thermal conductivity, easy processing chemical inertness, and relatively low cost [15].

Many methods are described in the literature for depositing a catalyst layer on a surface depending on the properties of the surface and the catalyst that has to be deposited. Every system, regardless of all the details and special case requirements, usually consists of a catalytic active phase, catalyst support, and substrate or wall. Despite all the variation in details to develop the catalyzed metal substrate, the general procedure stays relatively the same: substrate pre-treatment, catalyst preparation/ deposition, drying and calcination.

2.3.1 Pre-Treatment of the Substrate

The pre-treatment of the substrate is gaining more and more importance because it allows increasing adherence of the catalytic layer; and thus, the life time of the structured catalyst [16]. Early work in the area attempted the direct deposition of the active phase (usually noble metals) onto the metal substrate [16]. It was, however, soon confirmed that an intermediate layer of a catalyst support would help to obtain a higher and more stable dispersion of the active phase [11].

A wide range of pre-treatments are described in the literature such as: heat treatments, mechanical roughening, chemical etching, anodic oxidation (if the substrate contains aluminum), and boehmite primer deposition. Thermal treatment is probably the most widely used procedure in the literature to improve the roughness of the metallic surface and increase the specific surface area. Phase separation occurs at high temperature (840 °C); aluminum oxides are probably formed on the surface of aluminum containing alloys [16]. Passive oxides like $(Fe,Cr)_2O_3$ are present on the surface of *e.g.* 316L alloy; however, a pre-treatment is necessary to increase the oxide layer density [15].

Zhao *et al.* [53] studied the influencing factors on the adhesion between the γ-Al_2O_3 layer and the FeCrAl metallic support including support oxidation. The FeCrAl alloy foils were first ultrasonically cleaned in alkaline and then acidic solution, and then thoroughly rinsed in de-ionized water to remove oil, primary oxidation and other impurities. In order to investigate the effect of different oxidation temperatures and times, FeCrAl alloy foils were then calcined for different oxidation times; 5, 10 and 20 h at 950 °C.

Figure 2.1 shows the morphology of the metallic surfaces oxidized for different durations. As shown, all oxidized surfaces formed whiskers, which greatly increased the specific surface area of the oxidized layer. On the other hand, with increasing temperature, the dimension of crystal grains formed on a surface oxidation layer increased; *i.e.*, there is a reduction in the specific surface area. Zhao found that pre-oxidation at 950 °C for 10 h were the optimal conditions. He also indicated, by oxidizing the foil at 1050 °C for only 30 min, it could reach almost the same coating adhesion level as 900 °C for 10 h.

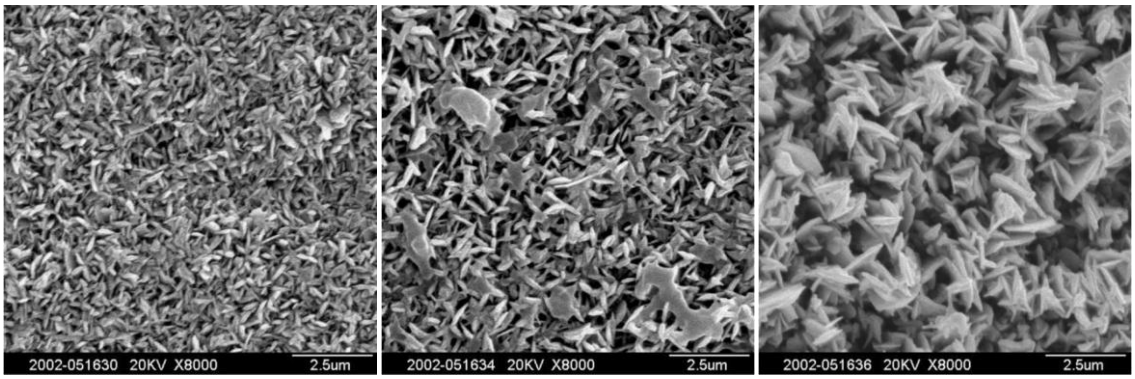

(a) (b) (c)

Figure 2.1 Morphology of the metallic surface pre-oxidized at 950 °C for different times: (a) 5, (b) 10, and (c) 20 h [53]

Another method for substrate enhancement is to apply primer to the metal substrate before the actual catalyst coating. The coating by primer (*e.g.*, boehmite) improves the adhesion between the catalyst slurry layer and metallic substrate, also may act as barrier to hinder the diffusion of unwanted elements of the metal during reaction. There are several requirements porous oxide coating have to fulfill for catalytic applications in micro-reactors. A coating should provide a large surface area to enhance the substrate from the low geometric area of the metal to the required high surface area of the active coating when wet impregnated with catalytically active species. This means that the material needs to have a high porosity so that many active centers are created. Furthermore, mechanical stability and adhesion to the metallic substrate are crucial [53]. The major problem arises when thermal expansion coefficient of the metallic support is different from the ceramic oxide washcoat affecting the durability and mechanical strength of the coating.

Other pre-treatment methods are applied on smaller scale. A thorough review on these different methods is presented by Meille [16].

2.3.2 Catalyst Preparation/Coating, Drying/Calcination

This section deals with methods used to prepare and disperse the finished material (catalyst support or active phase/support) on pre-treated support samples. Generally the standard ingredients of

catalyst slurry are: powder (catalyst support or catalyst itself), binder, acid, and water (or another solvent). The concentration of all ingredients varies largely from one researcher to another, and also depends on the nature of the surface to coat and the desired thickness of the layer [16]. The size of the suspended particles also influences the adhesion to the substrate and is a key factor to obtain a uniform coating. Drying and calcinations/activation steps may be necessary to strengthen the holding of layers after catalyst deposition.

There are mainly two types of preparation and coating procedure in the literature for methanol reforming catalysts. One method involves preparation of catalyst support and deposit a comparatively thick layer of support material on the substrate, followed by wet impregnation of the metal solution as nitrate or other soluble forms [21, 28, 29, 45]. The other method lies on the interesting aspect of slurry preparation that allows depositing ready-to-use (*e.g.*, commercially available) catalyst as well. Many research groups have used commercially available $Cu/ZnO/Al_2O_3$ catalyst [24, 25, 30, 32, 33, 37]; however, to achieve reasonable bonding the substrate has to be undercoated with a primer before the catalyst coating is applied. It is reported that adhesive coating layer has been acquired from both techniques; examples for both methods are provided in the following.

Zapf *et al.* [28], Cominos *et al.* [29], and Yu *et al.* [21, 45] developed a catalyst coated metal substrate with a very good adhesion, high porosity and reasonable catalyst distribution by applying a washcoating/co-impregnation technique. Zapf *et al.* [28] for instance, obtained an adherent γ-Al_2O_3 layer on stainless steel micro-channels, suspending 20 g γ-Al_2O_3 (3 μm particles), 75 g de-ionized water, 5 g polyvinyl alcohol (PVA) and 1 g acetic acid. Cominos also used PVA as a drying control agent to reduce crack formation of the alumina layer. The adhesion of the alumina layer is improved due to the addition of PVA by decreasing the evaporation rate of water and thus preventing a sudden shrinking of alumina layer at the initial stage of drying [30]. The washcoated plates were then calcined in an oven for 1 h at a temperature of 600 °C. Before impregnation,

washcoated substrates were evacuated in an exiccator to remove air form the pores. For the impregnation, 10 wt% aqueous solutions of targeted compound nitrates ($Cu(NO_3)_2$,$Cr(NO_3)_3$) were used. After impregnation and drying, samples were calcined again. Generally the calcination temperature of the impregnated wash-coats is kept 20-50°C above the respective operation temperature of the reaction. Cominos *et al.* [29] used the same preparation method as Zapf *et al.* [28] applying a γ-Al_2O_3 washcoat to prepare Cu/ZnO/Al_2O_3 catalyst coating on stainless steel substrates. Channels in the plates were then filled with γ-Al_2O_3 suspension and any excess on the top was wiped off. After calcinations the washcoated plates were placed in vacuum to remove air from pores. Carbon dioxide was subsequently passed to fill the pores as it readily dissolves in the nitrate solution used for impregnating the alumina with Cu and Zn. Cominos prepared 3 different samples with different catalyst loadings (8 wt% and 16 wt%) and copper-to-zinc ratios (1:1 and 3:1); the samples calcined at a temperature of 300°C. Among them catalyst with a higher loading (16%) and copper-to-zinc ratio (3:1) exhibited higher activity and a more stable performance for methanol steam reforming reaction. Results of his work will be discussed in next section. Yu *et al.* [21, 45] also used the same method to produce stainless steel containing aluminum that supported Cu/ZnO/Al_2O_3 catalyst coating for methanol steam reforming. Yu optimized several preparation parameters that control the structural characteristics of the catalyst coating. Yu reported, as also confirmed by Cominos *et al.*, the catalyst activity was directly related to copper metal surface area. Their reactor was initially coated with γ-Al_2O_3 to increase the surface area and enable dispersion of the catalytic material. After catalyst support deposition, samples were dried in air and calcined at 500°C. Copper and zinc oxides were then deposited by wet impregnation on the γ-Al_2O_3 coating with an aqueous solution of $Cu(NO_3)_2.3H_2O$,$Zn(NO_3)_2.6H_2O$,$Ce(NO_3)_3.6H_2O$. Samples were impregnated and dried at 120 °C in air for 2 h. subsequently calcined at 450 for 4 h. Methanol steam reforming activities for the corresponding Ce-doped catalyst coatings were compared in Yu's work and will be discussed in section 2.4.

In a different method, many research groups have used commercial catalyst for preparing $Cu/ZnO/Al_2O_3$ catalyst slurry. Park *et al.* [34] for instance, used ICI Synetix 33-5 catalyst to prepare slurry made of ICI Synetix 33-5, 20 wt% alumina sol, distilled water and 2-propanol. Small amount of 2-propanol was added to reduce the surface tension as the surface tension of solvent is very important in micro-channel catalyst coating. Alumina sol was undercoated on the surface in order to enhance the adhesion between catalyst and substrate. The catalyst slurry was well stirred for 2 h before the suspension of powdered catalyst and alumina sol was coated on the preformed alumina layer. After drying in air catalyst coated metal structure was calcined at 300-400°C before being tested for methanol steam reforming reaction. Won *et al.* [37] developed a catalyst coated stainless steel substrate by mixing 0.2 g $Cu/ZnO/Al_2O_3$ (ICI 33-5, CuO 50%, ZnO 33%, Al_2O_3 8%) catalyst with 1 ml zirconia sol solution and 1 ml isopropanol. They primed the substrate with zirconia sol before the application of catalyst slurry. Coated substrates were calcined at 350-400°C to strengthen the catalyst layer. In order to enhance the adhesion, zirconia sol was undercoated on micro-channels. The sol was prepared by adding nitric acid to a zirconium isopropoxide isopropanol complex. Zirconia powder was mixed to create a sol gel solution and isopropanol was added to adjust viscosity. Kundu *et al.* [32] also performed steam reforming of methanol in stainless steel micro-channels coated with commercial catalyst ($Cu/ZnO/Al_2O_3$-MDC-3: *Süd-Chemie*). Different sols, alumina, Zirconia, and mixed sol of alumina/zircon (molar ratio 1:1) as a binder for catalyst were studied in his work to compare the stability and performance. Mixed alumina and zirconia produced better performance as he reported.

2.4 Micro-Reactor Performance for Methanol Steam Reforming

It is determined from the literature that the reactor product for methanol steam reforming only consists of hydrogen, carbon dioxide, carbon monoxide, and unreacted methanol and water. Methanol steam reforming is typically carried out in the presence of metal oxide supported catalyst

at temperatures ranging from 200 to 300°C. An appropriate feed ratio of water to methanol and proper control of temperature is required to minimize the amount of CO formed in the process.

As emphasized in previous sections, structured and micro-structured technology results in compact designs that save both cost and weight. This has a secondary benefit of having a smaller reactor to heat; so, that there can be rapid thermal responses to transient behavior. Whether the application is a load-following stationary fuel cell or an on-site hydrogen generator stepping up from standby mode to full operation, the reactors need to be able to respond quickly to changes in temperature and flow rates [13].

Bravo *et al*. [25] compared the activity of a wall coated catalyst with a packed bed in their studies. They determined that their 4.1 mm packed bed reactor was subjected to heat transfer limitation during steam reforming of methanol. They reported that the measured activity of the catalyst was lower than the catalyst intrinsic activity due to the large temperature gradient in their packed bed reactor. As illustrated in Figure 2.2, they found that the apparent catalyst activity of the wall coated catalyst showed improvement over the same catalyst in packed bed form.

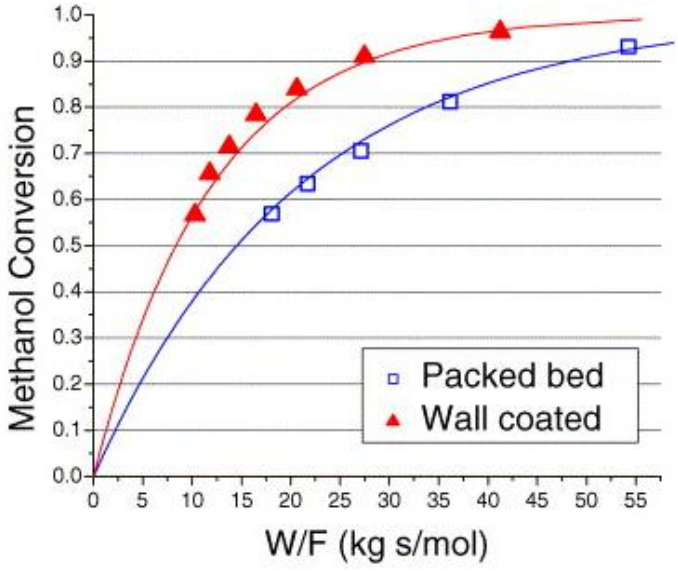

Figure 2.2 Activity for methanol steam reforming reaction for a packed bed and wall coated reactors (From Bravo *et al.* [25])

A perfect example of compact design is a coupled methanol steam reforming/total oxidation special two-passage micro-structured reactor by Reuse *et al.* [35]. The reactor consists of stacked plates (Figure 2.3) and could be used in the co-current or counter-current heat exchanger mode in which the reforming and oxidation reactions can be performed separately. The plates were 78 mm long, 23mm wide and 200 μm thick. Channels are "S" shaped: 17 rounded channels are split up to give 34 straight channels with a total length of 30 mm. They were 320 μm wide and 100 μm deep. Only the straight part was used for the reactions. The plates for the second reaction were the mirror image of the first one. All plates are stacked together in the housing (Figure 2.3). In the middle of the stack a special plate, designed for temperature measurements, is inserted.

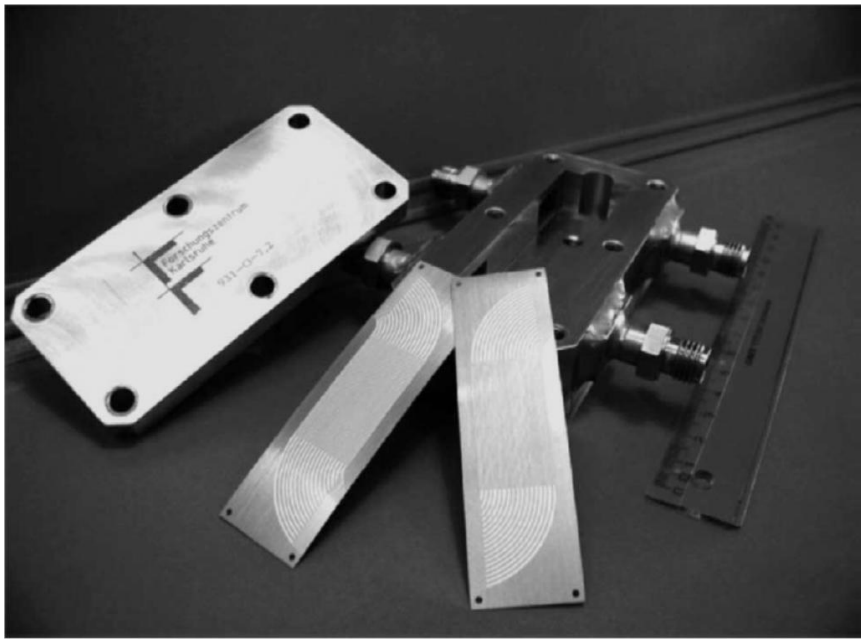

Figure 2.3 Micro-structured plates, and housing of the two-passage micro-structured reactor [35]

2.4.1 Effect of Steam to Carbon Ratio

For methanol-steam reforming, the product CO concentration decreases with an increase in steam to carbon ratio. Yu *et al.* [45] reported a CO concentration in dry reformate of about 2.05% when the water/methanol molar ratio is 0.8. This amount decreased to 1.02 % with increasing steam to

carbon ratio up to 1.3. It is shown in Figure 2.4 that increasing the water/methanol molar ratio reduces the outlet CO concentration..

According to Equation 2.5 the stoichiometric value for H_2O/CH_3OH is one in the steam reforming reaction. However, it is known from Equations 2.6 and 2.7 (methanol decomposition and WGS) that excess H_2O promotes methanol conversion and reduces the CO concentration by shifting the WGS equilibrium towards the right [45]. However, the increase of steam to carbon ratio increased the burden of heating, it also means a decrease of methanol feed rate at a constant feed rate of liquid fuel causing a decrease in H_2 production at higher steam to carbon ratios, so the ratio between 1.2 and 1.5 is reported reasonable in literature. The optimum ratio varies due to many factors such as feed flow rate, type and amount of catalyst coating.

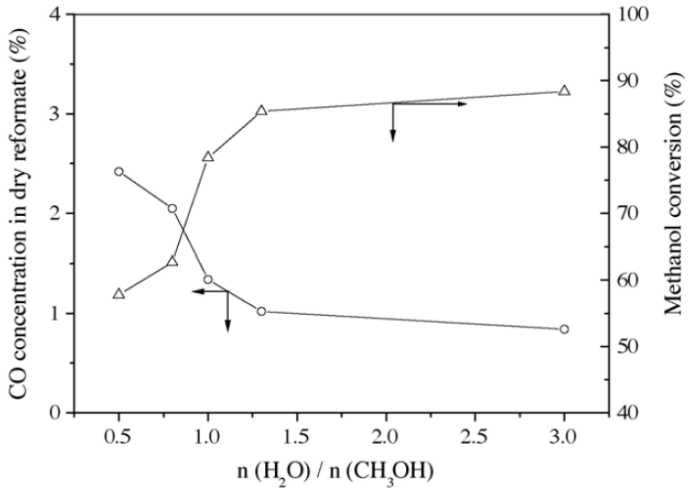

Figure 2.4 Effect of H_2O/CH_3OH molar ratio on conversion and CO concentration (T= 272°C, feed flow rate= 6 cm^3h^{-1} [45]

2.5 Summary

Advantages of micro-structured reactors were discussed and compared to conventional packed beds.

Different reforming reactions of hydrocarbons were discussed and the literature was reviewed on steam reforming of methanol as well as common catalyst and coating procedures for methanol steam reforming.

The literature provided various examples of micro-structured reactors and established some insight into potential design concepts for the test reactor.

Chapter 3

Design and Development of a Catalyst Coated Metal Plate Steam Reformer

3.1 Overview

As stated one of the main goals of the work was to design and verify the performance of a catalytic plate reactor.

The catalyst coated plate test reactor was designed and built at Queen's University. The final design was the result of numerous trials and revisions. Section 3.2 describes the design process and the most important design features of the reactor. Issues concerning preparation of the coated plates, the assembling, and sealing of the reactor are outlined in the subsequent section. It is important to note that the reactor was designed to eventually have the capability for higher hydrocarbon reforming such as diesel although the work described in this thesis will only examine its performance for methanol steam reforming. This reaction was chosen because of its simplicity, which allowed for the timely completion of the process of commissioning the reactor and the development of operational procedures for the new test system using a simple and well understood reforming reaction.

3.2 Reactor Design

Key criteria were identified for the design of the plate type reformer. The design was to satisfy following criteria:

- Resistance to corrosion and thermal cycling for temperatures up to 950°C
- Simple geometry that would be relatively easy to mathematically model
- Minimal pressure drop along the reactor

- Good heat transfer to promote isothermal behavior for the reaction
- Accurate measurement of the temperature profile along the reactor
- Allowance for easy change out of catalyst plate
- Produce accurate data suitable for the estimation of kinetic parameters

3.2.1 Overall Geometry and Flow Channel Configuration

A single channel reactor design was chosen. The reactor consisted of two main structural pieces: a top part and a bottom part with overall dimensions of 215 mm long $\times$75 mm wide $\times$60 mm deep. A strip of stainless steel plate, 150 mm long$\times$15 mm wide$\times$ 1.59 mm thick that was partly coated with catalyst, was sealed between the top and bottom parts of the reactor. Figure 3.1 shows these key parts of the reactor.

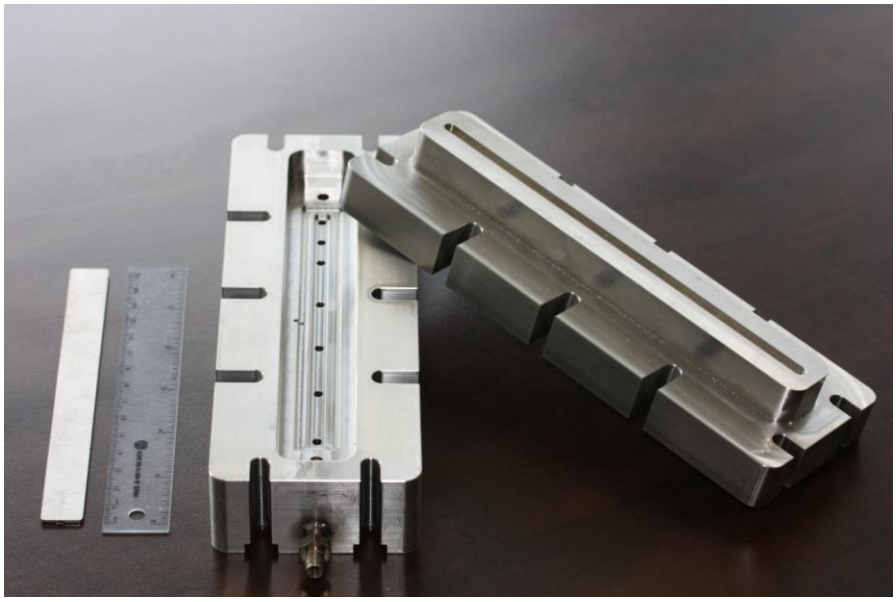

Figure 3.1 Initial reactor design before modification to improve sealing

Figure 3.2 shows a profile view of the geometry to be modeled. The gas path is a rectangular, 5 mm wide $\times$ 2 mm deep, channel where one wall is the catalyst coated strip with a 5mm wide thin layer of catalyst.

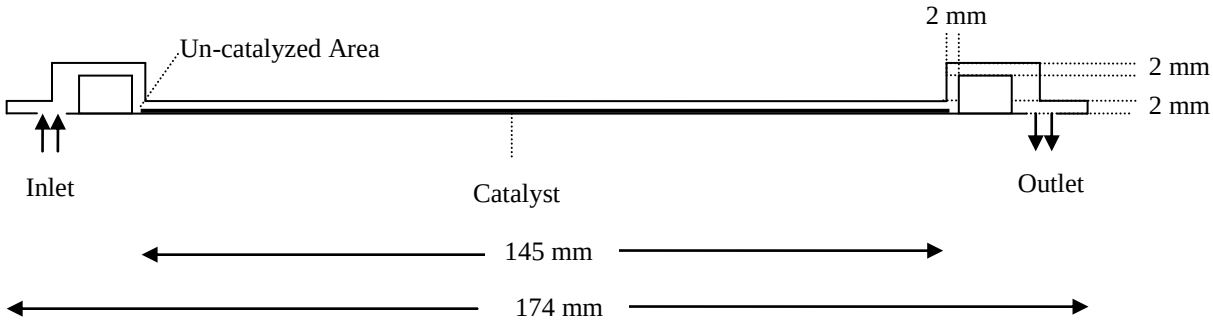

Figure 3.2 View of the reaction channel

As the Reynolds number is less than 2000, a no slip condition at the wall is assured with a parabolic flow profile along the channel. This single narrow rectangular channel with a thin layer of catalyst on one side has been shown to be easy to model [61].

A Biot number (Bi) analysis was used to confirm the isothermal behavior on the metal underneath the catalyst coated metal strip. The numerical value of Biot number was determined to be much smaller than one indicating uniform temperature condition for the reactor. The isothermal operation of the reformer was also confirmed with experimental measurements that will be presented in Chapter 5.

3.2.2 Thermocouples Placement

The holes shown on the bottom part of the reactor (see Figure 3.1) accommodated seven K-type thermocouples that touched the catalyst plate from underneath. A multiple-bore ceramic tube from McMaster-Carr was cut into 1.5 cm pieces to accommodate wire thermocouples inside the slots on the bottom part of the reactor. The leads from the thermocouples to outside of the reactor furnace

were protected by 3 mm diameter, high temperature braded ceramic thermocouple wire insulation, see Figure 3.3.

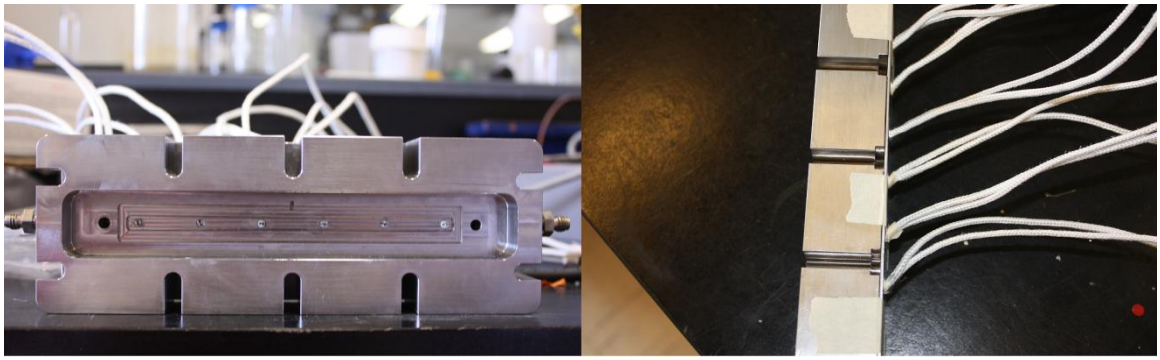

Figure 3.3 Wire thermocouples in bottom part of the reactor

Six equally spaced thermocouples closely tracked the temperature profile along the catalyst plate. The thermocouples were made with 0.5 mm diameter wire and responded quickly to changes in reaction conditions. The calibration of the individual thermocouples was monitored by ensuring that the reading of all six thermocouples in the reactor agreed when no reaction was occurring. These reading were found to be within 3 °C. A seventh thermocouple was later accommodated between the last two thermocouple slots near the exit. This thermocouple was used with the high temperature safety shut off system.

3.2.3 Catalyst Loading

In order to facilitate the quick changing of the catalyst coated plate, the reactor was designed in a flange configuration where ten bolts could be easily removed and the reactor opened to replace the catalyst coated strip.

Accurate and repeatable activity measurements required that the conversion be in the kinetically limited region and that the product gas flow rate be sufficient to achieve steady state product composition within a reasonable period of time (60-80 min). The volume of the reactor and the loading of the catalyst were designed such that these criteria were met.

3.2.4 Reactor Sealing

Achieving appropriate sealing was one of the most challenging and time consuming issues during the reactor development process. During the process of selecting the correct gasket and achieving good sealing the reactor was leak tested then disassembled to examine the pressure marks on the gasket to determine the probable spots for leakage. It was determined that the main leakage occurred at a small gap between the inlet and outlet ports and the catalyst region. Two tabs were added on the top part of the reactor to apply sealing pressure on these areas. A channel was machined over these tabs to provide a path for gas (See Figure 3.4).

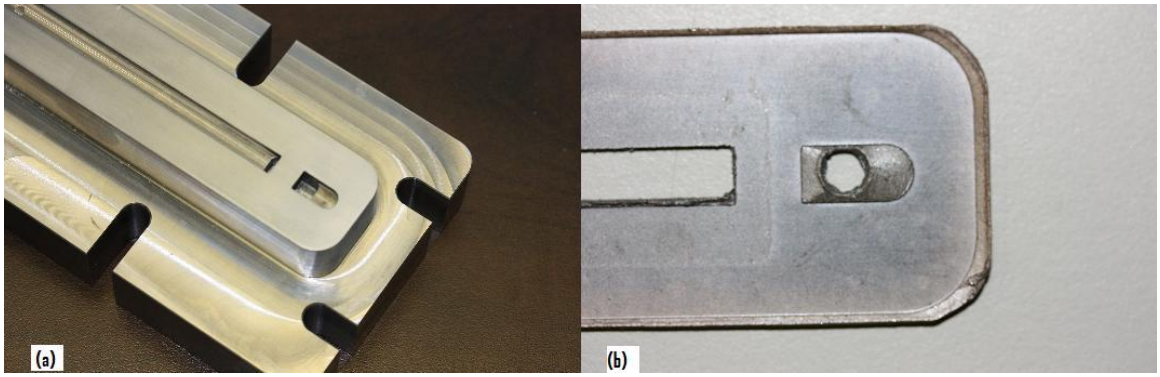

Figure 3.4 (a) Reactor top part modification, (b) Gasket pressure marks

A suitable gasket material had to tolerate temperatures up to 950°C required for higher hydrocarbons reforming while being capable of sealing the large sealing surface area between the top and bottom parts of the reactor. Various gasket samples were tested. Thermiculite 866 provided by Flexitallic was found to provide acceptable sealing at the operating condition for hydrocarbon reforming. The specific form of Thermaculite 866 that is smooth on both sides with an uncompressed thickness of 1.5 mm was used for under the catalyst strip and 0.7 mm for between the top and bottom flange.

Two gaskets were used in sealing the reactor. The first was cut from a 1.5 mm thick sheet with dimensions of 145 mm×6 mm. Seven holes were also made in this strip to accommodate the thermocouples. The purpose of this piece was simply to hold the thermocouples in place and keep

them from moving. The other gasket was cut for an exact shape of gasket from a 0.7 mm thick sheet with holes for inlet and outlet streams and a designated slot for the catalyst. Picture of these gaskets can be seen in Figure 3.5. This gasket was the most important factor to determine proper sealing of the reactor. Extra attention was paid cutting this gasket to make sure it was dimensionally exact and all parts were perfectly aligned.

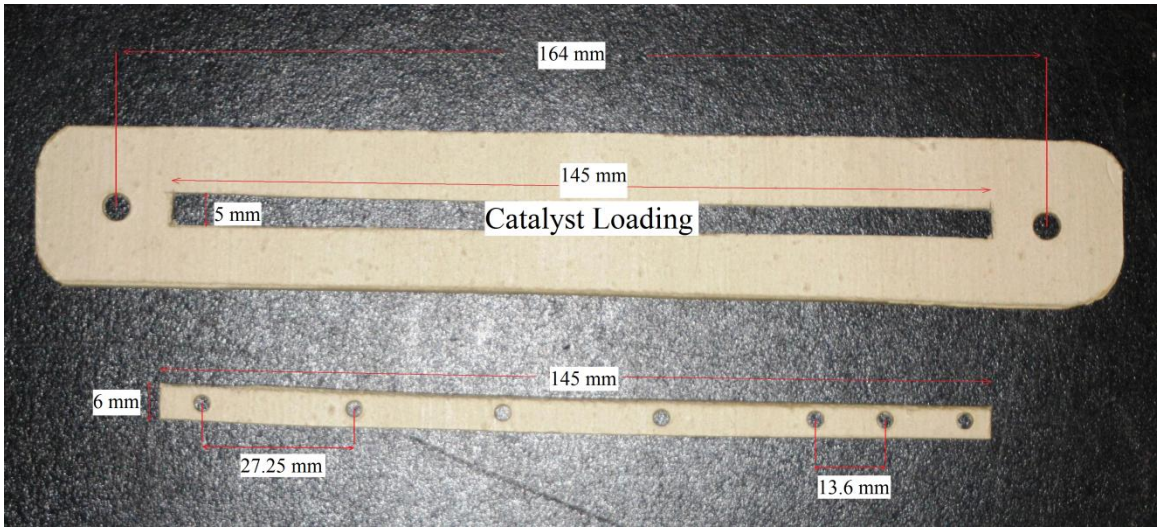

Figure 3.5 Picture of cut out gaskets for underneath (a) and top (b) of the metal plate

3.3 Assembling the Reactor and Leak Test

Certain steps were taken every time to assemble the reactor. This made sure of the same proper sealing every time that the catalyst had to be changed. These steps are listed below:

1. The 1.5 mm thick gasket with the holes for thermocouples was placed in the appropriate slot in the lower plate of the bottom part of the reactor so that the thermocouples holes in the reactor aligned with those in the gasket.
2. The metal strip onto which the catalyst was to be deposited was placed into the slot above the gasket.

3. The second gasket which had been cut to allow the catalyst to be exposed to the flowing reactants was placed over the top of the metal plate. This gasket also had holes at each end for the inlet and outlet streams.

4. The desired amount of catalyst that had been weighed before was poured onto the designed slot of the top gasket on the metal strip.

5. Pieces of glass wool were placed on the inlet and outlet path on the top part of the reactor. This ensured that the catalyst particles stayed in place while handling the reactor.

6. The upper flange was placed on top of the gasket to form the seal between the catalyst metal plate and the bottom of the upper flange.

7. The bolts were finger tightened into the holes around the perimeter of the reactor. It was important to apply a light coat of copper anti-seize lubricant on the bolt threads before being tightened. This greatly reduced the chances of encountering seized nuts during the next removal.

8. The whole reactor was placed on the lower platen of the hydraulic press.

9. A set of square metal bars was placed across the top of the reactor and one single metal bar covered them from one end to the end. This was done to provide an even pressure distribution between the bolts and across the entire upper surface once the hydraulic pressure is applied.

10. The hydraulic press was pumped up to almost 14 MPa (2000 psi), then the individual bolts surrounding the reactor were tightened up to 17.2 Nm with a torque wrench. This torque value was determined, after extensive trials, to be sufficient to seal the reactor if the gasket that had been properly cut. It was extremely important to tighten the bolts a very small amount at a time up to 17.2 Nm in a cross pattern manner. This further ensured the even distribution of pressure across the entire surface.

A picture of the closed reactor is shown in Figure 3.6.

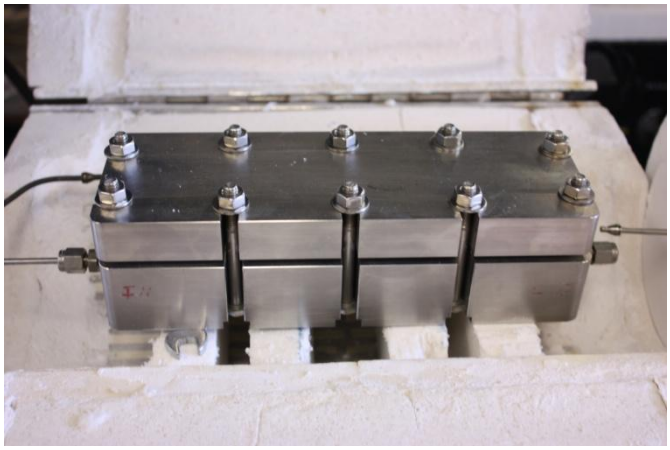

Figure 3.6 View of the closed reactor

Leak Testing the Assembled Reactor

After the reactor was assembled it was pressurized to 280 kPa (~40psi) with a combustible gas mixture. Using a combustible gas detector, the outside of the reactor housing was scanned to determine if there was any leak from the upper portion or lower portion of the reactor.

The entire reactor assembly was then placed into the reactor test system oven connected to the inlet feed supply. With the exit capped the system was then pressurized with nitrogen to 105 kPa gauge (~15 psig) and the decrease of the nitrogen flow was monitored. If the reactor was leak free the nitrogen flow would decrease to zero almost instantaneously. If a leak was detected, it was necessary to disassemble the reactor and replace gaskets (note: using leak detector was not an option because the soap damaged the gasket and reactor could not be sealed).

3.4 Summary

The design and development process of the metal plate reactor was discussed. The methodology of designing the reactor met the requirements of testing the catalytic coated plate for micro-structure catalytic kinetic testing.

The assembly method provided an adequate sealing of the reactor. Once the reactor was assembled and verified to be leak free it was taken into the reactor test system to evaluate its performance.

Chapter 4

Reformer Test Station Set Up and Experimental Methodology

This chapter describes the experimental system used to test the plate type wall reactor described in Chapter 3 and the method developed to collect rate data for the catalytic steam reforming of methanol over a $CuO/Zn/Al_2O_3$ catalyst. A detailed overview of the configuration of the experimental equipment is provided, followed by a description of how the system functions. Calibration methods for various system components and how their accuracy is verified will also be discussed. Finally an overview of the testing procedure will be provided.

4.1 Apparatus and Instrumentation

This section discusses the fluid and electrical interconnections for the experimental apparatus. Each subsystem will also be described in detail.

A schematic diagram of the experimental system is shown in Figure 4.1. The tubing throughout the apparatus is nominally 1/16, 1/8, and 1/4 inch OD stainless steel used with stainless steel Swagelok connections.

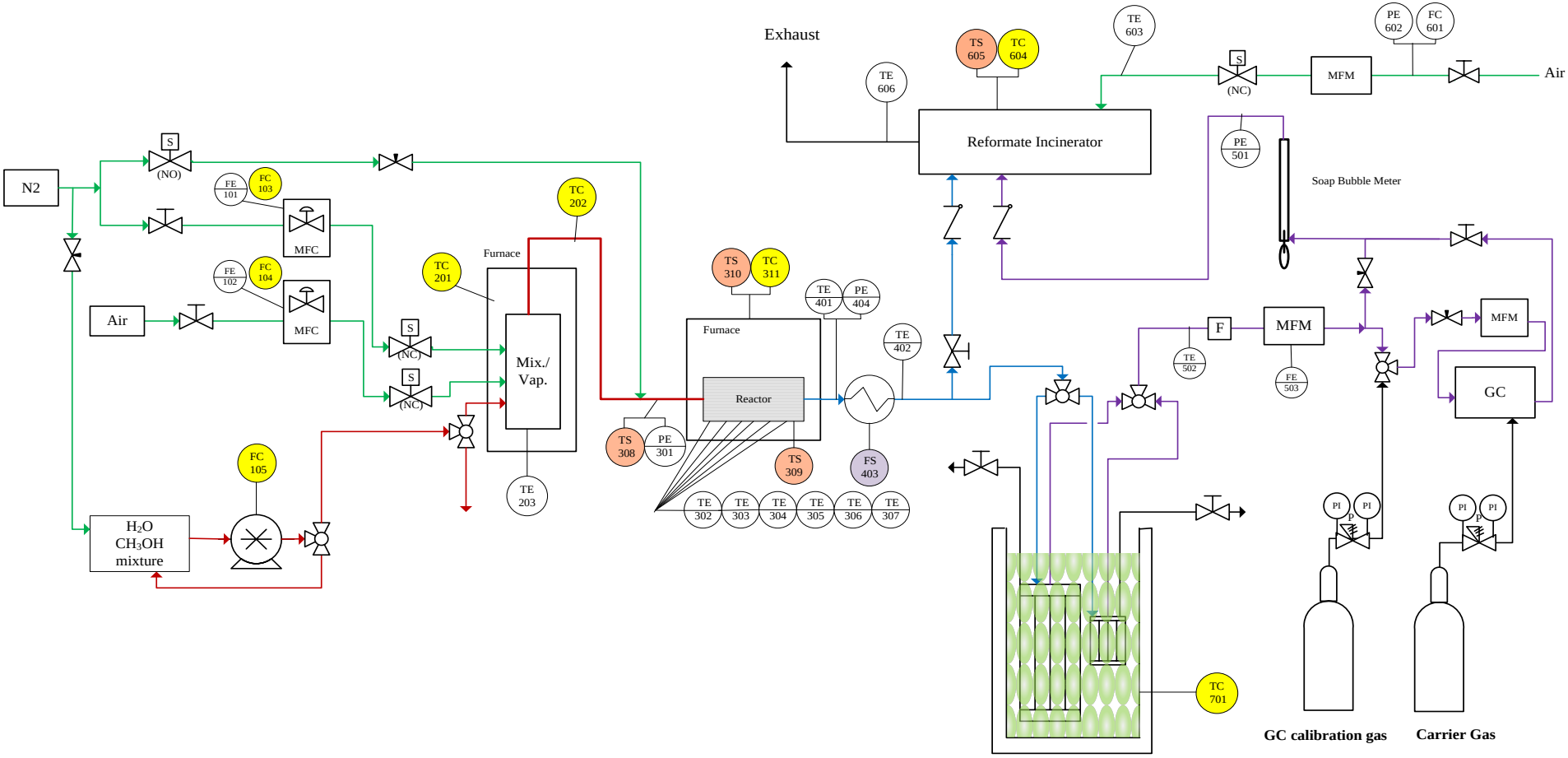

Figure 4.1 Schematic diagram of the metal plate reformer test station

Legend for Figure 4.1

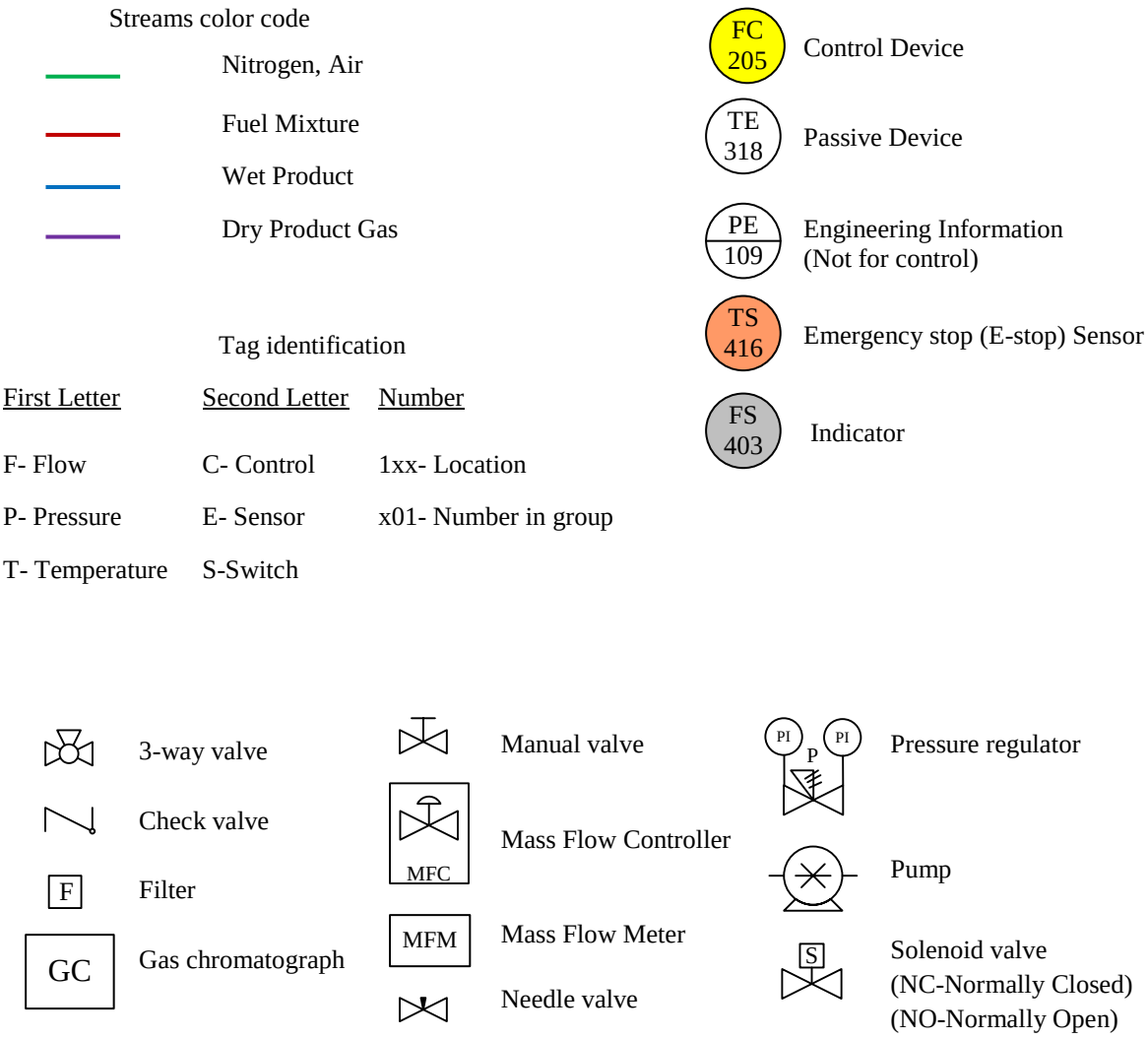

A wide range of components was required to test the performance of the reformer. The major components of the system are listed in Table 4.1. A great deal of effort and time was required to assemble, troubleshoot, and calibrate the analysis equipment as well as the reformer itself.

Table 4.1 Set up main components

Component	Manufacturer	Model	Specs
N_2 MFC	Aalborg	FMA5508	0-100 mL/min
Air MFC	Aalborg	GFCM17	0-200 mL/min
HPLC pump	Gilson	305	0.125-25 ml/min
Mixer vaporizer	Autoclave Engineers	301B-2430	
Mixer vaporizer furnace	Vulcan	3-550	1225˚C Max, 3-step multi stage programmable
Heated transfer line	Autoclave Engineers	405A-8273	6'x 0.062" 120VAC, K-type TC
Heated transfer line temperature controller	Digi-Sence		120VAC, 10A
Reactor furnace	Unknown	Unknown	With custom controller
Reformer inlet pressure transducer	Transicoil	152CP110	0-10 psig
Reformer outlet pressure transducer	Transicoil	152CP110	0-10psig
Heat exchanger	In house	N/A	Tube in tube
Condenser circulator	Cole-Parmer	Polystat	
Condenser immersion chiller	PolyScience	KR-80A	120VAC
Dry gas-product MFM	Aalborg	GFM171	0-500 mL/min
Pre-GC MFM	Toptrak	821-2	0-200 sccm
Gas Chromatograph	HP-5890		
Soap film meter outlet pressure	Transicoil	150C-P030D	0-8" H_2O
Soap film-meter	Wilmad Lab Glass		100 mL
Analog to digital conversion	National Instruments	SCXI	
Software	National Instruments	LabVIEW™ ver.6	

4.1.1 Liquid Feed and Mixer Vaporizer System

A High Pressure Liquid Chromatography (HPLC) piston pump, Gilson model 305, was used to supply methanol and water mixture to the mixer vaporizer at a precise flow rate. The flow rate

range was between 0.125-25 cm^3/min for the 25SC head. The manufacturer's specifications for this pump head indicate that the minimum value is not the absolute limit and the flow rate can be adjusted down to 0.01% of the maximum flow rate.

HPLC grade methanol as supplied by Caledon Chemicals and de-ionized (DI) water were mixed at the desired ratio in a one liter Erlenmeyer flask. This solution was continuously purged with nitrogen to exclude dissolved oxygen and avoid bubble formation in the pump head. A needle valve installed on the nitrogen manifold upstream of the nitrogen MFC (see Figure 4.1 controlled the nitrogen flow through a 1/8 inch tube to the feed container. The feed solution was drawn from the Erlenmeyer reservoir via a 1/8 inch Teflon tube connected to the HPLC pump head. A metal frit filter was attached to the end of this inlet tube to prevent particulates from being drawn to the pump and damaging the check valve on the pump head. Right after the pump a three-way valve either directed the fluid back into the reservoir for priming purposes, or to the mixer vaporizer. The pump head needed to be primed to avoid damage that can occur if the pump head is operated dry. Control of the liquid feed flow rate was set manually on the pump control panel.

Liquid feed was delivered to an Autoclave Engineers mixer vaporizer by a 1/16 inch OD tube. The mixer vaporizer was machined from a 164×38 mm stainless steel bar and was capable of mixing up to five streams. Temperature control of the mixer vaporizer was achieved using a 3-step multi stage programmable Volcan® 3-550 furnace. A thermocouple mounted on the wall of the mixer vaporizer measured the temperature.

4.1.2 Gas Feed and Flow Measurement System

Nitrogen and Air Feed

Two Aalborg mass-flow controllers (MFCs) provided feed gases to the mixer vaporizer. One MFC, rated for 0-100 ml/min, metered nitrogen, and a second one, rated for 0-200 ml/min, metered air. Nitrogen generally is used as a diluent. Although in this work only pure steam reforming was studied, an air supply was included in the design to provide for autothermal

reforming for future work. The flow rates were monitored continuously to ensure that they remained constant at the specified flow.

Dry product-Gas Flow Rate

The flow rate of the dry product-gas stream exiting the condenser was a critical measure needed to analyze kinetic data. A 0-500 mL/min MFM monitored the dry product-gas flow rate. However, the MFM was calibrated for air, therefore, did not provide an accurate reading for the variable product gas flow composition. An accurate measurement of the dry product-gas flow rate was obtained using a 100 cm^3 Wilmad-LabGlass soap-film meter and a stop watch. At least six readings were taken for each flow rate determination to ensure that the flow was steady and to obtain an estimate of the variance of the flow. The MFM located upstream of the soap film-meter was primarily used to ensure that steady-state was achieved.

4.1.3 System Heating and Temperature Control

Mixer Vaporizer Furnace

Temperature control of the mixer vaporizer was achieved using the programmable controller built into the Volcan 3-550 furnace. The temperature was set at 200°C. The furnace temperature reading was provided to the controller by a K-type thermocouple located in the wall of the furnace compartment. As mentioned above, the actual mixer vaporizer temperature was monitored by a separate K-type thermocouple mounted directly on the vaporizer housing.

Heated Transfer Line

A six foot heated transfer line, which was maintained at a constant temperature of 200°C, delivered feed vapor from the mixer vaporizer to the reactor. The temperature was controlled by a Digi-Sence temperature controller. The temperature of the heated transfer line was also kept at 200°C to ensure that the feed remained in the vapor state between the mixer vaporizer and reactor furnace.

Reactor Clam Shell Furnace

The reactor was heated in a custom clam shell furnace. The furnace temperature was controlled by a Watlow 96 temperature controller.

The controller was equipped with a dedicated over-temperature Watlow Limit LV switch, and an external E-stop loop connector. However, this safety feature was redundant as there was another reactor furnace temperature safety switch in the system safety box which will be described in Section 4.1.6.

4.1.4 Condenser System

The exit gas from the reactor consisted of a mixture of un-reacted methanol and steam combined with the product gases H_2, CO, CO_2, and possibly diluting nitrogen. The un-reacted methanol and steam were condensed and collected in either a 500 cm^3 or a 65 cm^3 condenser vessel. The condensers were connected in parallel so that the large condenser could be used for the high liquid feed rates while the 65 cm^3 condenser was available to minimize the residence time of the reactor outlet for faster measurements. The inlet of the condenser system was a 3-way valve that directs the gas stream to either the small or large condenser vessel, or stops flow to both. The outlet of the condenser system was similar to the inlet as the small and large condenser vessels connect as the 3-way valve with the common port of the valve continuing the gas flow to the rest of the test system. When selecting either the large or small condenser it had to be ensured that both the inlet and outlet 3-way valves both connect the same condenser size.

Both condensers were submerged in a chilled glycol solution. The glycol solution was cooled using a PolyScience chiller that could only be turned on or off with an immersion probe. The temperature of the condensers was kept at -10 °C with a Cole-Parmer digital circulator.

The glycol level in the condenser chiller was kept around 2 to 3 inches from the top of the insulated container. The glycol level increased as water from the air condensed on the cold finger cooling the glycol. The glycol level had to be monitored regularly as this added water would

eventually overflow the container. Although this was not the case for the short term use of the condenser for this work, the glycol in the condenser chiller will get diluted over time due to the water added from the condensation around the cold finger. If the glycol is too diluted, the solution may actually freeze in the chiller and prevent proper circulation around the condensers. The glycol concentration can be monitored using a hydrometer.

Methanol-water solution was drained from condensers using a syringe through a pre-installed plumbing to the bottom of each vessel while the vessel was pressurized by blocking the outlet flow path.

4.1.5 Dry Product-Gas Composition Analysis

Regular analysis of the product gas composition was performed using a temperature programmed Gas Chromatograph (GC) equipped with a Thermal Conductivity Detector (TCD). A HP-5890 programmable GC was used for the analysis of the dry gas mixtures. The gas stream from the condenser passed through a six-port sample injection valve equipped with a 250 μL sample loop. The components in the product gas were separated on a Restek 2 m $\times$ 1 mm I.D. micro packed ShinCarbon ST 100/120 mesh column. The packed column inside the GC oven required no physical support other than that provided by proper installation at inlet and detector fitting. The GC features and programs through the experiment were as follows:

- Sample size: 1 mL
- Injector temperature: 100 °C
- Oven temperature: 40 °C (hold for 3 min.) to 250 °C at 16 °/min ramp (hold for 10 min.)
- Detector temperature: 270 °C
- Carrier gas: 8.5% H_2 in helium
- Carrier gas flow rate: 10 mL/min

The signal from TCD of the GC was sent to a SRI single channel serial port model 203 and then to a computer program called PeakSimple Chromatography Data System. The 8.5% H_2 in helium carrier gas caused a completely negative H_2 peak, so the GC was programmed to switch automatically the signal polarity before and after the hydrogen peak had been eluted. Each gas chromatogram was saved to the computer for further data processing.

The retention time of the H_2 peak was 0.7 minutes while CO and CO_2 came off at 2 and 7 minutes respectively. N_2 peak also was recognized at 1.8 minutes if the condenser had not completely flushed nitrogen out by the time that the GC was taken. No other peaks were detected during operation of the system.

4.1.6 Electrical connections

Electrical connections devices, sensors, and controllers were very important features of the test system set up. Designed electrical connections ensured proper control and safety of the system as well as proper data recording for future calculations. Main components used with data logging and controls were:

- Signal box
- Safety box
- National Instruments SCXI module with two I/O cards
- PC running LabVIEW

Signal and safety boxes were certainly the two most critical components on the set up which are further explained below. SCXI module and LabVIEW program are also discussed in detail in Section 4.1.7.

Signal Box

Signal box was considered one of the most important electrical features in the set up. The signal box was used to:

- Connect MFCs, pressure sensors, and the heat exchanger flow switch to the PC via the SCXI™ (Signal Conditioning Extension for Instrumentation) module.
- Power devices via an adjustable 12 VDC power supply.
- Relay the valve off signal from safety box to the MFCs during E-stop (connection was the cable from the rear panel of the signal box to the rear of the safety box).
- Relay an E-stop status signal from the safety box to SCXI module (connection is the cable from the rear panel of the signal box to the rear of the safety box).

Figure 4.2 demonstrates the front panel of the signal box. Before running an experiment one had to ensure that the override switches on the interface box were set on the middle (normal) position.

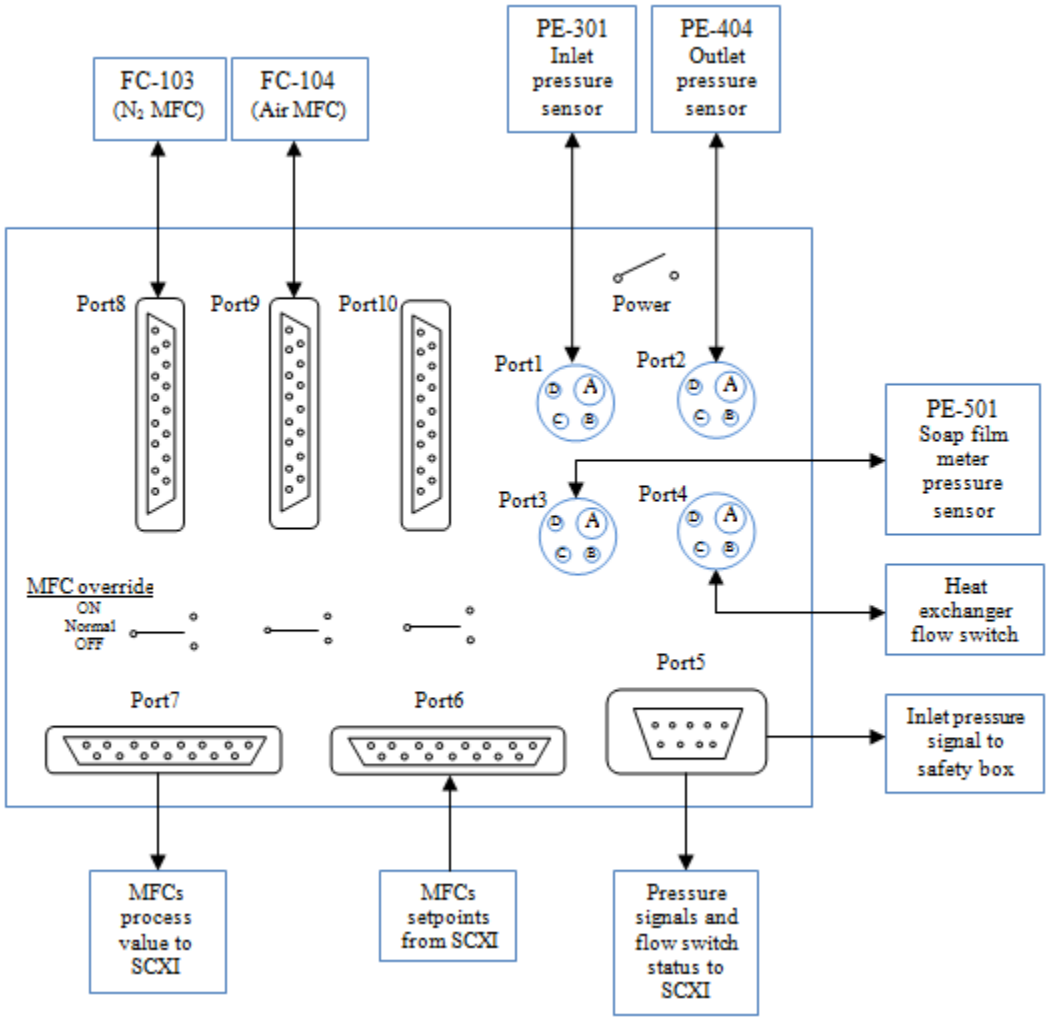

Figure 4.2 Signal box connections front panel

Safety Box

Another very important feature to be noted from electrical connections is the safety box. The safety box monitored pressure and temperatures of several locations, and puts the system in a state of E-stop if set limits were exceeded. The four signals monitored in this E-stop system and their limits were:

1. Reactor temperature < 1015 °C
2. Reactor furnace temperature < 1000 °C
3. Catalytic converter temperature < 600 °C
4. Reactor inlet pressure < 9 psig

An E-stop might also be initiated by pressing the E-stop button located beside the computer monitor. The black restart button on the safety box should be pressed in order to continue with the process after the system was put into E-stop.

In the event of an emergency stop, power was cut to the devices fed from the safety box via a power strip. In this case, all solenoid valves returned to their normal de-energized state. This ensured no flow through the air and nitrogen MFCs, and also opened the nitrogen purge that is connected to the reactor inlet. Power to the pump also was shut off in an E-stop situation to stop reactant flow to the reactor. Overall, the effect of the safety box mechanism was to force inert gas through the reformer while stopping reactants flow. Relatively large amount of combustible gases were forced out of the reformer quickly in this scenario, so it was designed to turn off the heat as well the air flow to the combustor in order to prevent potential unintentional ignition of the mixture.

A relay in the safety box connected pin 12 of both MFCs to ground. This connection was made via a cable running from the rear of the signal box to the rear of the safety box. Pulling this pin to ground forced the MFC valve off (closed). This was done because attempting to send a set point

to the MFC during E-stop with the flow path blocked may be harmful to the MFC and throw off the calibration.

4.1.7 Computer Control and Data Logging

Continuous monitoring of system conditions, *e.g.*, temperatures, pressures, and flow were important in order to ensure a steady-state was achieved during kinetic measurements. Computer control and data acquisition was achieved using a National Instruments SCXI 1000 system with a custom LabVIEW interface. The program Graphical User Interface (GUI) is shown in Figure 4.3.

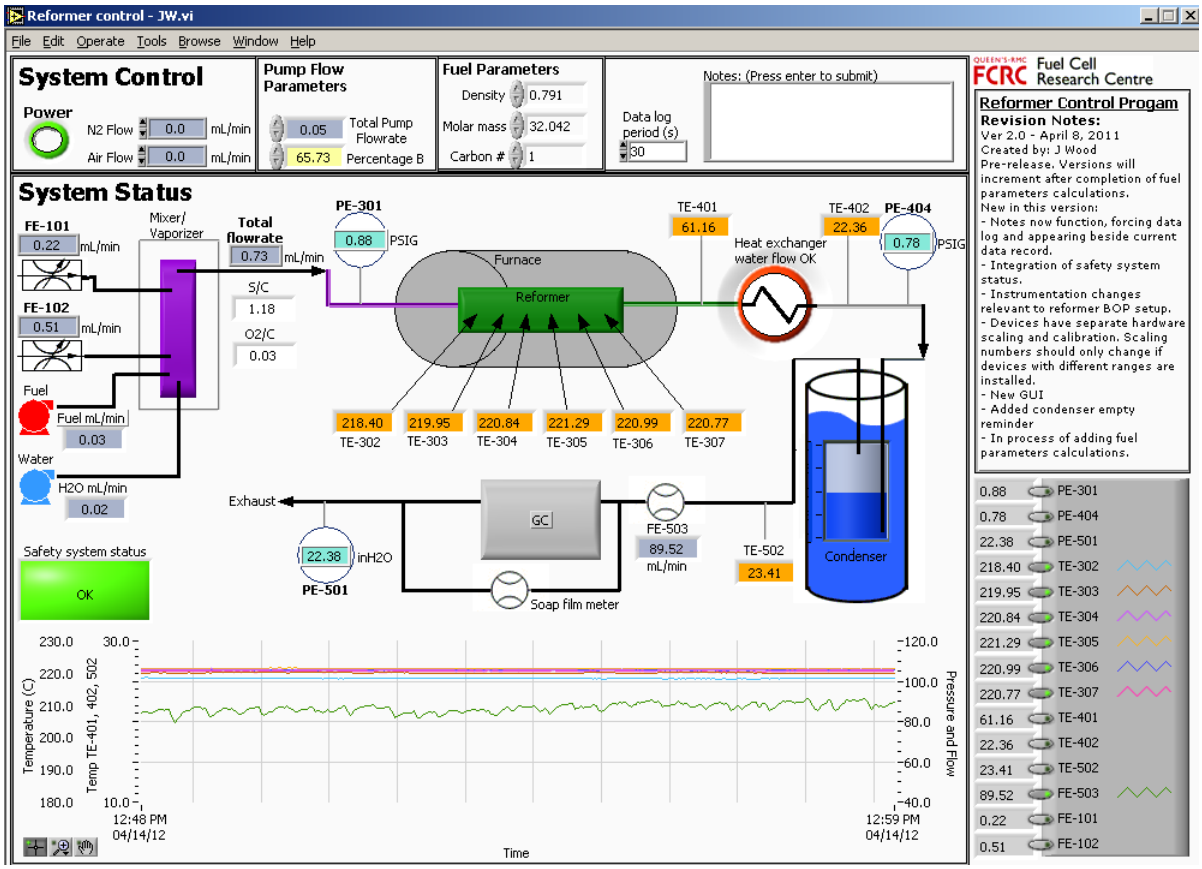

Figure 4.3 Screen shot of LabVIEW program for the system

The computer controlled air and N_2 flow thorough MFCs, and the following signals (see Table 4.2) were read and logged by the computer. Log files were saved in a comma separated values

(csv) format and could be opened in spreadsheet software such as Microsoft Excel or Open Office.

Table 4.2 Recorded signals (connecter card SCXI-1303)

Measuring	**Sensor output**	**Voltage range**	**Sensor range**	**Description**	**Tag on LabVIEW**
Flow	0-5 VDC	0-5	0-100 mL/min	N_2 MFC readback	FE-101
Flow	0-5 VDC	0-5	0-200 mL/min	Air MFC readback	FE-102
Pressure	4-20 mA	0.996-4.98	0-10 psig	Reformer inlet pressure	PE-301
Temperature	mV			Reformer TC_1	TE-302
Temperature	mV			Reformer TC_2	TE-303
Temperature	mV			Reformer TC_3	TE-304
Temperature	mV			Reformer TC_4	TE-305
Temperature	mV			Reformer TC_5	TE-306
Temperature	mV			Reformer TC_6	TE-307
Temperature	mV			Post reformer furnace	TE-401
Temperature	mV			Post heat exchanger	TE-402
Flow	0 or 4.5 V	0-5	Set at 0.1 GPM H_2O	H_2O flow switch for Heat Exchanger	FS-403
Pressure	4-20 mA	0.996-4.98	0-10 psig	Reformer outlet pressure	PE-404
Pressure	4-20 mA	0.996-4.98	0-8" H_2O	Soap film meter outlet pressure	PE-501
Temperature	mV			Post condenser	TE-502
Flow	4-20 mA	0.996-4.98	0-500 mL/min	Dry gas-product	FE-503

4.2 Equipment Calibration and Error Analysis

Making quantitative measurements is always accompanied by errors and necessitates an understanding of statistics and error analysis. Careful equipment calibration was essential to yield an acceptable accuracy during the experiment. Calibrations were carried out on the pump, mass flow controllers, pressure transducers and gas chromatograph, the result of which are explained further below. A review of statistical methods for error analysis of equipment is presented below,

followed by a specific calibration procedure for each piece. Detailed discussion of typical errors and error propagation through the experiment is given in chapter 5 as well as a complete set of sample calculations for one set of experimental results.

Set points and actual (observed) values were recorded for each piece of equipment, and the equation for a line of best fit was determined using a simple least squares regression. The equation $\hat{y} = b_0 + b_1 x$ was used to predict or estimate the mean response at $x = x_0$. Each line of the best fit was forced through the origin and a 95 % confidence interval was constructed for $\mu_{Y|x_0}$. A 100(1-α) % confidence interval on the mean response can be constructed for a random variable,

$$T = \frac{\hat{Y}_0 - \mu_{Y|x_0}}{s\sqrt{\frac{1}{n} + \frac{(x_0 - \bar{x})^2}{S_{xx}}}} \qquad \textbf{4.1}$$

which has a student t-distribution with $n-2$ degrees of freedom [62]. This leads to the following equation for a 100(1-α) % confidence interval for the mean response $\mu_{Y|x_0}$.

$$\hat{y}_0 - t_{\alpha/2} s\sqrt{\frac{1}{n} + \frac{(x_0 - \bar{x})^2}{S_{xx}}} \le \mu_{Y|x_0} \le \hat{y}_0 + t_{\alpha/2} s\sqrt{\frac{1}{n} + \frac{(x_0 - \bar{x})^2}{S_{xx}}} \qquad \textbf{4.2}$$

where $t_{\alpha/2}$ is a value of the t-distribution with $n-2$ degrees of freedom.

4.2.1 Gas Chromatograph

GC calibration was one of the most time consuming and complicated aspect of assembling the system. Particular attention had to be paid to this calibration as it was the most important piece of equipment to determine kinetic data and had a greater effect on the error compared to those associated with flow controllers and the pump. Numerous mechanical problems were encountered

and a number of parts were replaced and modified in response to various problems encountered during the calibration process.

A major problem was identified with the valve system causing significant baseline drift, variation in retention times and difference in calculated peak area were experienced from one run to another. It was suspected that the original 6-port valve did not switch all the way any time injection occurred. To determine the issue only carrier gas was run through column with the exit end on the column disconnected. Carrier gas flow was measured while purge A was set to OFF (position 1). Setting purge A to ON (position 2) flow would drop during change (flow path momentarily blocked), see Figure 4.4. Flow should return to previously measured value in a matter of a few seconds. If not, then it was probable that the valve did not fully rotate into position and the flow path is fully or partially restricted.

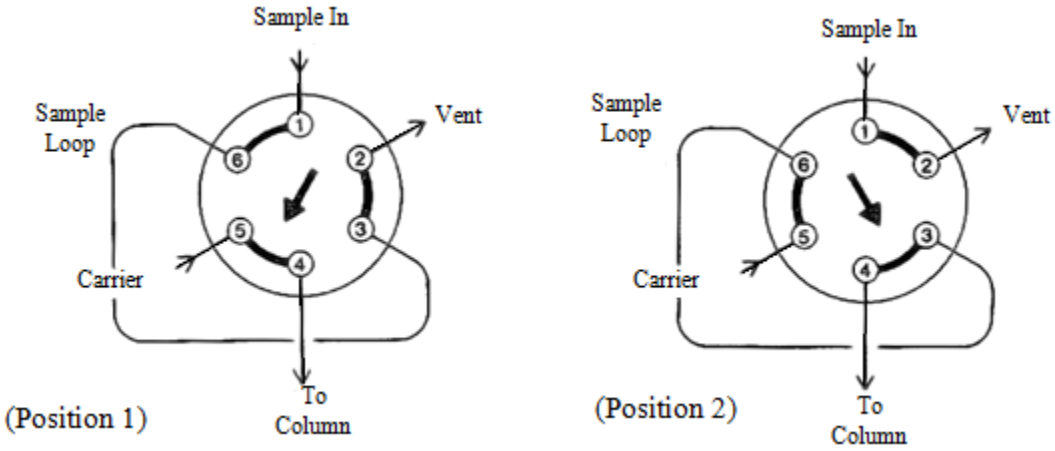

Figure 4.4 Injection valve positions

Finally, the original Valco 6-port injection valve was found to be faulty, not fully opening the pathways when switched causing baseline drift. The valve was replaced with a much newer valve taken from a Varian 3800 GC.

GC calibration was performed and checked on a regular basis using two different gas mixtures to assure that the relative calibration did not change with time. Composition for each of the calibration gas mixtures is given in Table 4.3.

Table 4.3 Calibration gas mixtures for GC

Compound	Nominal Concentration (Mixture#1)	Nominal Concentration (Mixture#2)
Hydrogen	53%	66.7%
Nitrogen	20%	0.7%
Carbon Monoxide	7%	16.1%
Carbon Dioxide	5%	16.5%
Methane	10%	0
Ethylene	2%	0
Ethane	2%	0
Propane	1%	0

Calibration with known composition and concentration provided information for later qualitative and quantitative analysis of unknown mixture during experiment program. Retention time for a given solute was used to identify the compound while the experimental conditions (column, temperature, and carrier gas flow) were kept identical to those used to analyze the specimen [63], see Section 4.1.5 . The GC was calibrated by injecting different gas mixtures, and the response of the detector was integrated to obtain peak areas for H_2, N_2, CO, and CO_2. As mentioned in Section 4.3.7, no other components were detected in the product stream. Appendix A shows the best fit of the calibration curves and the 95% confidence intervals of the predicted values. These graphs have been expanded in the range of concentrations which were measured during the experimental program. It was determined that the error associated with GC is much larger than the flow controllers and the pump error.

4.2.2 Pressure, and Flow Signal Calibration

Pressure and flow signals coming into the SCXI module go through two separate calibration calculations.

Engineering Multiplier and Offset

The raw signals from pressure sensors and flow controllers needed to be converted from signal levels on LabVIEW to appropriate pressure or flow units. This is referred to as the Engineering Multiplier and Offset (mX+b). The values for the Engineering Multiplier and Offset were calculated as follows:

Engineering Multiplier = Device process range/ (Full scale signal – Zero signal)

Engineering Offset = Engineering Multiplier $\times$ Device zero signal $\times$ (-1)

The full scale and zero signals will be in volts and may be a value such as 5 and 0. For devices that output current *i.e.*, 4-20 mA, there are 249 Ohm sense resistors in the SCXI that convert the current signal into a voltage signal, in this case 0.996 to 4.98 volts (see Table 4.2). For example, the Engineering Multiplier for a pressure sensor that reads up to 10 psig and outputs 4-20 mA is calculated as, 10/ (4.98-0.996) = 2.51. Engineering Offset for the above pressure sensor is then, $2.51 \times 0.996 \times$ (-1) = -2.499. It is important to note that Engineering Multiplier and Offset should only be modified if sensor hardware is altered.

Device calibration Multiplier and Offset

After the raw signals from devices are converted to pressure or flow units, the signals had to run through another mX+b calculation in order to calibrate the instrument read back to accurate values. If the signals coming into the software are completely accurate then the multiplier and offset would be 1 and 0 respectively. Generally devices should be put through a multi-point calibration. The calibration curve can then be used to obtain a trend line giving the appropriate slope and intercept values to be plugged into LabVIEW software. It was important to set the device Multiplier and Offset to 1 and 0 when performing a multi-point calibration.

Nitrogen flow controller (FE-101) and dry-product gas flow meter (FE-503) were calibrated using a 100 mL stop watch and a soap bubble meter. Reactor inlet and outlet pressure sensors (PE-301, PE-404) were calibrated using a Molblox RFM-M from DH instruments. The pressure sensor after soap bubble meter (PE-501) was calibrated using a monometer since the output was inches of water. Linear relationship (mX+b) was derived for each device and then input into LabVIEW software. These values the associated plots are presented in Appendix A.

4.2.3 HPLC Pumps Verification

The accuracy of the pump flowing fuel and water had significant influence on the experiments. The volumetric rate of liquid feed delivery was measured using a stop watch and measuring the actual delivered liquid over a given period of time. The maximum error in determination of the pump delivered flow rate was 0.8567%. A plot of actual delivered liquid over pumps reading is given in Appendix A.

4.3 Experimental Procedure

This section describes the general experimental procedure for different set of conditions, and provides further explanation of the applied experimental program.

4.3.1 Pre-start Checklist

Before proceeding to actual experimental procedure, the following steps had to be taken. These were referred to as pre-start checklist. These steps are mostly to ensure the safety of the process and to protect equipment.

Nitrogen and Air Source Pressure

Feed gas source pressure (*e.g.*, Nitrogen and air) needed to be high enough to create an acceptable difference across the MFCs. As stated by Aalborg MFCs, calibrations were performed at conditions of 14.7 psia and 21.1 °C. For the best accuracy, it is recommended to keep the MFC source pressure the same as the pressure used during calibration. Nitrogen and air source pressure

were set at 15 psia and were checked each time before proceeding to the experiment. One had to note that nitrogen source pressure had to be set before adjusting the nitrogen purge rate which is described below.

Nitrogen Purge Rate

Setting nitrogen purge rate was an important step due to safety considerations and had to be checked before experimental runs. To set the nitrogen purge rate it had to be sure that the nitrogen source pressure was correctly set and a piece of tubing connected to the inlet and outlet while the reactor was not in place. This precaution was taken to make sure that catalyst powder inside the reactor did not get displaced by higher nitrogen flow rates while setting to desirable purge rate. Proper needle valve was used to set the purge flow rate at 100 mL/min while the system was put into E-stop. This rate could be verified with FE-503.

Hardware E-stop Limits

Operation of the safety box was described in Section 4.1.6. As previously mentioned the safety box monitored pressure and temperatures at several locations of the process, and puts the system in a state of E-stop if set limits were exceeded. The four signals monitored in this E-stop system and their limits were:

1. Reactor temperature < 1015 °C
2. Reactor furnace temperature < 1000 °C
3. Catalytic converter temperature < 600 °C
4. Reactor inlet pressure < 9 psig

4.3.2 Catalyst Loading and Reactor Installation

BASF K3-110 is a relatively inexpensive and non-hazardous material and presents no serious disposal or storage problem. It is a low-temperature shift catalyst primarily for use in the

production of hydrogen for refinery operations and ammonia synthesis or for producing synthesis gas for methanol production [64]. Table 4.4 summarizes the basic characteristics of the catalyst.

Table 4.4 Physical characteristics of BASF K3-110 catalyst [64]

Characteristic	*Value*
wt. % CuO	40
wt. % ZnO	40
wt. % Al_2O_3	20
Nitrogen B.E.T. Area	102 ± 4 m^2 g^{-1}
Pore Volume	0.35 mL g^{-1}
Copper Area	9.83 m^2 g^{-1}

As previously mentioned in Chapter 2, the coating of catalyst onto metallic walls is generally problematic due to an intrinsically low surface area of metals. To obtain the catalyst coated metal plate a method was developed consisted of three steps.

These steps were followed to coat almost one third the metal plate in the middle where the feed vapor would travel along. The first, step was to pre-treat and prepare the metal plate in order to achieve an adhesive catalyst layer.

The pre-treatment itself consisted of three separate actions: cleaning, thermal treatment and primer deposition. The 316L stainless steel plates were first ultrasonically cleaned in 1 N nitric acid for 10 minutes and then thoroughly rinsed with DI water. This was done to remove any impurities or other primary oxides on the metal surface. Thermal treatment improved the roughness by oxides formation on the metallic surface. Metal stripes were heated to 800°C and kept at that temperature for 2 hours, and let to cool down slowly. The difference in color and roughness of a fresh and treated metal strips were completely noticeable at this point. See Figure 4.5.

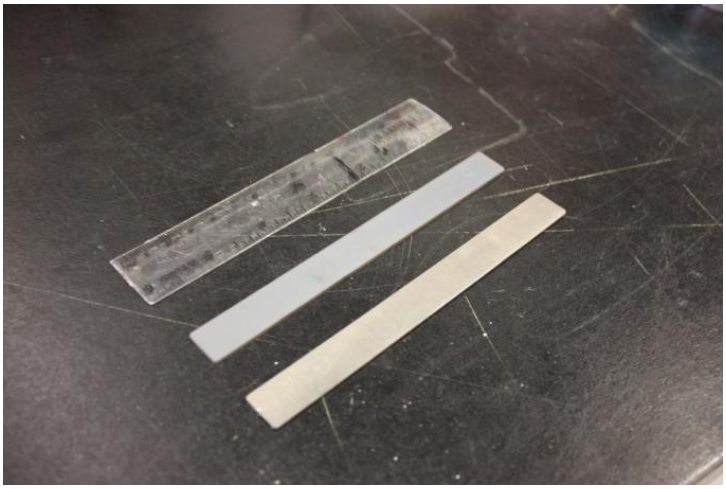

Figure 4.5 Thermally treated and fresh metal substrate (the object at the back is a 15 cm ruler)

As the final step of the pre-treatment procedure, γ-Al_2O_3 slurry primer was prepared and coated on the metal stripe. The substrate had to be primed before the catalyst coating was applied to achieve reasonable boding between layers. This step might be referred to as a part of the coating procedure rather than pre-treatment. In order to prepare the primer slurry, the same method as Zapf *et al.* [28] was used. First 5 g of binder [polyvinyl alcohol Alfa Aesar] was dissolved in 75 mL DI water in a beaker. This mixture was stirred smoothly by a magnetic stirrer at 60°C for 2 hours, and left over night without stirring. 20 g of 3 micron 99.97% metal basis γ-Al_2O_3 powder and 1 g of 1 N acetic acid were added to the mixture successively without stirring [51]. This mixture was stirred at 60°C for 2 hours and then left for 3 days without heating. At least a day was given to the mixture before application in order to give enough time to release the air bubbles trapped during stirring.

The slurry was coated on the metal strips applying two different techniques. The most common method to coat the metal strips was dip coating. In this method the metal strips were immersed into the primer slurry at a constant speed while the unwanted area on the substrate was covered with masking tape. The substrate was kept inside the slurry for few minutes and withdrawn very slowly at a constant speed. A thin layer was deposited on the substrate.

Screen printing was another technique was used to deposit the γ-Al_2O_3 primer. The substrates were placed underneath a silk screen where the unwanted areas were masked on the screen itself and slurry was poured on the screen surface. Slurry was forced through the mesh openings by a squeegee. This technique provided a thinner layer of γ-Al_2O_3 on the substrates; however, multiple layers could be applied to achieve a desirable thickness for the deposit.

Freshly coated substrates were dried at room temperature and then calcined in an oven for 1 hour at a temperature of 600°C. Both dip coating and screen printing techniques generated adhesive layer of primer on metal substrates and they were ready to be coated with catalyst.

The second step on the coating process was to coat the pre-treated metal strips with slurry of BASF K3-110 catalyst. The 5 mm diameter $\times$ 3 mm long catalyst pellets were crushed with a mortar and pestle. Obtained catalyst particles were then placed between 80 and 100 mesh screens and dusted with compressed air to ensure that no fines remained attached to the catalyst particles. A significant amount of fine powder was usually removed by this method. The exact same procedure as γ-Al_2O_3 primer was used to prepare BASF catalyst slurry. This catalyst was deposited on the pre-treated substrates by dip coating. Samples were dried at room temperature and then calcined at 600°C. However, after the calcination process the catalyst flaked of easily and the adhesion between the catalyst and the primer layer was deemed unacceptable.

Despite all the effort, the coating process was found to require extremely more time and effort than initially anticipated. In order to be able to carry on to the main objective of this work, *i.e.* the design of an experimental system to test the plate type reactor, it was proposed to use a thin layer of the BASF K3-110 catalyst particles on the metal plate without being coated. As an alternative an exact desirable amount of catalyst particles was weighed and was filled in the gasket slot using a funnel. The reactor was then assembled as is described in Section 3.3.

Four semicircular shapes were cut off an Al-Si ceramic fiber to set the already assembled reactor inside the cylinder shape clam shell furnace at the same level of inlet and outlet tubing. The two ends of the furnace were then capped with ceramic insulation with holes to accommodate inlet and outlet of the reformer.

4.3.3 System Temperature Control

Temperature control was an important matter that had to be carefully set and monitored at the beginning and through the process. The temperature controllers for mixer vaporizer furnace, heated transfer line and combustor were described in Section 4.1.3. First step in the beginning of an experiment run was to set the temperature for these pieces of equipment to 200 °C. Then, the temperature of the reactor clam shell furnace was set to the desired value. For different sets of experimental runs this temperature was set at 220, 240, and 260 °C. A sufficient amount of time had to be given until the reactor itself reached a desirable temperature which was verified by the thermocouples accommodated inside the reactor.

4.3.4 System Operation

Three main operation variables for the experimental testing were reaction temperature, steam to carbon ratio (S/C), and flow rate of methanol to calculate $W/F_{CH3OH,0}$ ($kg.s.mol^{-1}$). The experimental range for these main variables was based on limitations associated with pump head, reactor design, previous results reported in literature, and properties of the BASF K-110 catalyst. The S/C ratio was set according to the stoichiometric amount of water required in the system from Equation 2.5. This ratio was nominally set at 1 through the whole experimental program; however, it was kept at slightly higher values in order to avoid carbon formation in the system. Feed flow rate was also of great importance as it is used to compare experimental data with literature. The reactor was tested at three different temperatures, 220, 240, and 260 °C. For each temperature the methanol flow rate was varied over four different settings. Catalyst deactivation was also studied for each of above temperatures as a function of time.

4.3.5 Feed Ratio and Composition Measurements

De-ionized (DI) water and HPLC grade methanol as supplied by Caledon Chemicals were pre-mixed at the desired ratio in a 1000 cm^3 Erlenmeyer flask using Equation 4.3.

$$\frac{S}{C}=\frac{n_{H_2O}}{n_{CH_3OH}}=\frac{V_{H_2O}\times\rho_{H_2O}\times {}^{1}\!/\!_{M_{H_2O}}}{V_{CH_3OH}\times\rho_{CH_3OH}\times {}^{1}\!/\!_{M_{CH_3OH}}}=\frac{\left({}^{\rho}\!/\!_{M}\right)_{H_2O}\times V_{H_2O}}{\left({}^{\rho}\!/\!_{M}\right)_{CH_3OH}\times V_{CH_3OH}}=2.24\frac{V_{H_2O}}{V_{CH_3OH}} \qquad \textbf{4.3}$$

691.65 mL methanol and 308.44 mL DI water were mixed to obtain desirable feed composition of S/C ratio of 1.

Control of the liquid feed flow rate was set manually on the pump control panel. Exact feed composition and flow rate were determined by measuring the specific gravity of the feed mixture at 20 °C. The specific gravity was calculated using a 10 mL density bottle calibrated with DI water at 20 °C. Feed solution was de-gassed by bubbling nitrogen before filling the density bottle. The accuracy for specific gravity measurement was approximately $\pm 0.0191\%$. The actual composition of the feed mixture was then determined using interpolation of the specific gravity versus composition data from CRC Handbook of Chemistry and Physics [65].

4.3.6 Catalyst Activation and Conditioning

Available BASF K3-110 catalyst was in the calcined oxide state, and the copper oxide in the catalyst had to be conditioned in a reducing atmosphere to be activated [64]. Once the reactor had been installed into the furnace, the reactor was heated to 220 °C and a feed of 1:1 S/C was introduced at a flow rate of 0.065 mL/min. This flow was maintained for several hours until temperature, conversion and product composition had stabilized. It was observed, however, that the conversion was much lower after 24 hours of operation compared to the first few hours due to significant deactivation of the new catalyst. Therefore, the data in this work are gathered after 24 hours of operation of the catalyst.

4.3.7 Product Gas Sampling and Analysis and Required Measurements

To start an experiment the green LabVIEW power button was pressed (see Figure 4.3). The program started by requesting a file name and destination to be used for data logging. One had to make sure the system is out of E-stop to make a run. If not, the black push button on the safety box is the reset for the safety system.

To collect rate data regular, analysis of the product gas composition was performed using a temperature programmed GC. After passing the desired flow rate of feed through the reactor, unreacted steam and methanol vapor was trapped in a condenser in a bath maintained at -10 °C. To perform a mass balance for the system, methanol-water solution was drained from the condenser using a syringe through a pre-installed plumbing to the bottom of each vessel while the vessel was pressurized by blocking the outlet flow path. The exact flow rate of dry product gas was determined using the soap film meter before taking each GC samples. At least 6 readings for the stop watch were taken, and their average used to determine a flow rate.

By actuating a six-port sampling valve on the GC, 1 mL samples of the dry gas product gas were injected into the GC column for separation and analysis. A detailed description of the GC program and calibration procedure is given in Section 4.1.5 and 4.2.1. Sufficient time was allowed before any attempt to take a GC sample, so the reactor stabilized at a new flow rate. It was important to ensure the sample gas flow was approximately the same as calibration conditions through the sample loop. This could be achieved by adjusting the needle valves before the soap film meter and the GC. GC would start automatically after starting the PeakSimple software. The same conditions had to be manually input to PeakSimple and the GC. Chromatographs were then saved, along with the run number and date for further analysis. The above procedure was repeated for different valued of $W/F_{CH3OH,0}$. The values of $W/F_{CH3OH,0}$ were chosen experimentally to enable adequate measurements of product composition. No efforts were made in order to optimize this value with respect to catalyst performance.

The following experimental measurements were required for each set of experiments:

1. The specific gravity of methanol-water mixture at 20 ºC.
2. The flow rate of the methanol-water liquid feed.
3. The barometric pressure and room temperature.
4. The integrated peak area of the thermal conductivity detector response for each component in the chromatograms of the dry gas outlet.
5. The flow rate of dry gas from the condenser.
6. Temperature of the reactor.
7. Mass of catalyst.

The mass of the condensate collected in the condenser was also measured for mass balance calculations. This is discussed in Section 5.5.1.

4.3.8 Catalyst Standby

Over the course of the experimental studies it was found that the conditions under which the reactor was held on standby, between kinetic experiments, had a significant effect on the activity of the catalyst. A feed rate of water-methanol (0.065 mL/min) was fed to the reactor as it was used to activate the catalyst for the first time. The temperature was lowered to 240 °C if the experimental temperature was at 260 °C; otherwise, it was kept the same.

4.4 Summary

Important features of the test set up and calibration of the key components of the system were described in this chapter. The experimental procedure was established to evaluate the performance of the metal plate reactor.

Chapter 5

Result and Discussion

5.1 Overview

This chapter presents results from a series of experimental studies of methanol steam reforming on a commercially available $Cu/ZnO/Al_2O_3$ catalyst, BASF K3-110, using the plate type wall reactor described in Chapter 3. A brief description of the data collection procedure is given followed by presentation and analysis of the results.

A number of experiments were done to test the reactor system and to obtain estimates of the performance of a well characterized catalyst for a range of conditions in order to compare with published results. The main input variables to characterize the performance of the reactor were reaction temperature and flow rate of the feed. The reformate composition was determined for each set of experimental conditions while the effect of main input variables on methanol conversion was analyzed. The important issues for catalyst conditioning and catalyst deactivation are also discussed.

A 0.7 g sample of catalyst was used in testing the reactor. The catalyst operated for 336 hours. All the experiments were carried out near atmospheric pressure at temperatures of 220, 240, and 260°C. Four different values for feed flow rate were tested for each temperature. The steam to methanol ratio was held at slightly above one. Methanol conversion and product composition versus W/F_{CH3OH} data and methanol conversion versus time-on-line data were collected. The catalyst was conditioned for 24 hours at 220°C at W/F_{CH3OH} of 37.5 kg s mol^{-1}.

5.2 Data Collection

All the data presented in this work is for the steady-state operation of the reformer. As mentioned in Chapter 4, an important feature of the apparatus was the continuous monitoring of the

conditions in the reactor. This made it possible to ensure that steady-state was achieved before taking a gas chromatograph.

Data points for temperature, pressure, and flow rates were collected every 30 seconds. It was verified that the reformer was running at steady-state by observing that the temperature profile in the reactor, as well as other temperatures and pressure through the system remained constant with time. The assumption of steady-state was further confirmed by comparing the reformate composition from consecutive gas chromatograms. Following a change in feed rate 90 minutes was allowed for the system to come to steady-state and all lines to be flushed thoroughly with the new product composition.

For each experimental condition, two or three reformate samples were analyzed until the gas composition of consecutive GCs change by less than 4%. The data presented are based on the average of the final two samples. Overall 22 test runs were done at 13 different sets of experimental conditions. The experiments were carried out from the lowest temperature, 220°C, to the highest, 260°C. The feed rates were changed from lowest value to the highest.

Experimental conditions for the runs and overall methanol conversion are shown in Table 5.1. An extended table of experimental results is presented in Appendix B.

Table 5.1 Experimental conditions and selected results in chronological order

Run	Reaction nominal temperature (°C)	Cumulative Time on-line (hr)	Feed total flow rate (ml/min)	Methanol molar flow rate (μmol/s)	Dry product gas total volumetric flow rate (ml /s)	Fractional fuel Conversion
1	220	25	0.124	35.66	1.32	0.42
2	220	28	0.1688	48.50	1.53	0.36
3	220	32	0.2284	65.62	1.58	0.28
4	220	35	0.3973	114.13	1.77	0.18
5	240	51	0.124	35.87	1.97	0.63
6	240	54	0.1688	48.79	2.24	0.52
7	240	59	0.2284	66.01	2.39	0.41
8	240	62	0.3973	114.81	2.84	0.28
9	260	75	0.124	35.79	2.56	0.82
10	260	78	0.1688	48.68	2.91	0.72
11	260	81	0.2284	65.86	3.34	0.58
12	260	83	0.3973	114.55	4.49	0.43
13	240	100	0.124	35.70	1.65	0.52
14	240	103	0.1688	48.55	1.82	0.43
15	240	106	0.2284	65.69	1.88	0.32
16	240	110	0.3973	114.25	1.96	0.19
17	260	156	0.124	35.596	1.95	0.62
18	260	160	0.1688	48.41	2.17	0.51
19	260	163	0.2284	65.496	2.40	0.42
20	260	166	0.3973	113.91	2.82	0.28
21	240	276	0.4440	128.14	1.40	0.13
22	220	302	0.3973	114.90	0.62	0.06

5.3 Sample Calculations and Propagation of Error

Evaluation of replicate runs was carried out to test the experimental error. As shown in Chapter 4, the students t-distribution was used to determine the errors associated with the gas chromatograph

and the input flow rates of the reactants. Calculated values such as the fuel conversion, product generation were dependent on those measurements, so the associated errors for each measurement propagated throughout those calculations.

An estimate of the error in the calculated value of the methanol conversion was obtained by combining the error from various measurements and calculations. A complete set of sample calculations for one set of experimental results is given in Appendix C. These calculations are similar to those equations used by Peppley [64]. The average error in the measurement of the conversion of methanol, using 95% confidence intervals for the calibration curves, was estimated to be approximately 2%. For example, for the sample calculation $X_{CH_3OH} = 0.63 \pm 0.02$ $(\text{or } 63 \pm 2 \text{ mol}\%)$.

5.4 Reformer Temperature Profile

Table 5.2 shows the average temperature for each thermocouple along the length of the catalyst zone for $W/F_{CH3OH,0}$ =10.6 kg s mol^{-1} and temperatures of 220, 240 and 260°C. The temperature profile for no flow at 220°C is also included for comparison. The position of thermocouples along the reaction channel was described in Chapter 3. The first thermocouple was positioned at 8.25 mm from the inlet and 5 other thermocouples were along the channel in 27 mm intervals. The error associated with the K-type thermocouples is 2.2°C.

The lowest temperature always occurred at the first thermocouple that was the closest to the entrance of the reactor. And the highest temperature was associated with the middle thermocouple. A maximum variation of 2°C was observed along the reactor. The fact that there is the same trend for the temperature variation with and without the reactants flow rates indicated that variability in the temperature was not associated with heat transfer limitations at the reaction conditions.

Table 5.2 Temperature profile along the reactor

$W/F_{CH3OH,0}$ (kg.s/mol)	Nominal Set point (°C)	TC1 (°C)	TC2 (°C)	TC3 (°C)	TC4 (°C)	TC5 (°C)	TC6 (°C)
10.6	260	258	260	260	261	260	260
10.6	240	237	239	240	241	241	241
10.6	220	218	220	221	222	221	221
0	220	219	220	221	221	221	220

5.5 Performance of the Reformer

5.5.1 Mass Balances

The most important aspect of performance of the system was to ensure that the mass balance closes. Three runs were selected to verify the mass balance. These runs required that the mass of the liquid collected in the condenser be accurately measured. The density of the condensate solution was also determined so that the composition of the condensate could also be specified.

For all of these tests the mass balance always closed to less than 5% error. Detail for these runs is given in Appendix D.

5.5.2 Conversion

Fuel conversion and product composition were used to evaluate the reactor performance for kinetic measurements. As previously mentioned, all of the composition data presented in this thesis are on a dry molar basis, *i.e.* the water vapor was removed from the reformate gas prior to the measurement by the gas chromatograph.

The simplest expression of conversion of methanol is:

$$X_{CH_3OH} = \frac{[\text{moles of methanol consumed}]}{[\text{moles of methanol fed}]} = \frac{F_{CH_3OH,0} - F_{CH_3OH}}{F_{CH_3OH,0}} \quad \textbf{5.1}$$

where $F_{CH_3OH,0}$ is the molar flow rate of methanol at the inlet of the reactor and F_{CH_3OH} is the molar flow rate of methanol in the outlet stream. However, there was no direct method for measuring the exit flow rate of methanol. Mole balances for each of the atomic species in the system were used to express conversion of methanol in terms of the flow rates of hydrogen and carbon monoxide. This will give the advantage of conversion measurement based on the molar flow rates of two dry product gases, hydrogen and carbon monoxide, that are directly analyzed by GC. Furthermore, because CO_2 can potentially be dissolved in the condensate, using the H_2 and CO flow rate is less prone to error.

For the reactions methanol steam reforming reaction the material balances for carbon, hydrogen and oxygen atoms are as follows:

$$F_{CH_3OH,0} = F_{CH_3OH} + F_{CO_2} + F_{CO} \quad \text{(C-balance)} \quad \textbf{5.2}$$

$$4F_{CH_3OH,0} + 2F_{H_2O,0} = 4F_{CH_3OH} + 2F_{H_2O} + 2F_{H_2} \quad \text{(H-balance)} \quad \textbf{5.3}$$

$$F_{CH_3OH,0} + F_{H_2O,0} = F_{CH_3OH} + F_{H_2O} + 2F_{CO_2} + F_{CO} \quad \text{(O-balance)} \quad \textbf{5.4}$$

To obtain an expression for the methanol moles consumed two times Equation 5.4 was subtracted from Equation 5.3.

$$2F_{CH_3OH,0} - 2F_{CH_3OH} = 2F_{H_2} - 4F_{CO_2} - 2F_{CO} \quad \textbf{5.5}$$

Equation **5.5** is divided by 2 and next F_{CO_2} is substitute from Equation **5.2**.

$$F_{CH_3OH,0} - F_{CH_3OH} = F_{H_2} - 2\left(F_{CH_3OH,0} - F_{CH_3OH} - F_{CO}\right) - F_{CO} \quad \textbf{5.6}$$

After rearranging Equation **5.6** gives an expression for the moles of methanol consumed as:

$$F_{CH_3OH,0} - F_{CH_3OH} = \frac{F_{H_2} + F_{CO}}{3} \qquad \textbf{5.7}$$

Substituting this into Equation **5.1**, the conversion of methanol is obtained in terms of the production of hydrogen and carbon monoxide.

$$X_{CH_3OH} = \frac{F_{H_2} + F_{CO}}{3F_{CH_3OH,0}} \qquad \textbf{5.8}$$

Using Equation 5.8, methanol conversion for various flow rates was determined. Figure 5.1 shows methanol conversion versus W/ $F_{CH3OH,0}$ at 220, 240 and 260°C. For all these curves the feed was methanol and water of nominal S/C ratio of 1. These results were collected during the period of 25 to 83 hours of time on line. As mentioned above, an initial conditioning period of 24 hours preceded data collection and this was believed to be sufficient for the catalyst activity to stabilize such that deactivation would have a minimal effect of subsequent measurements.

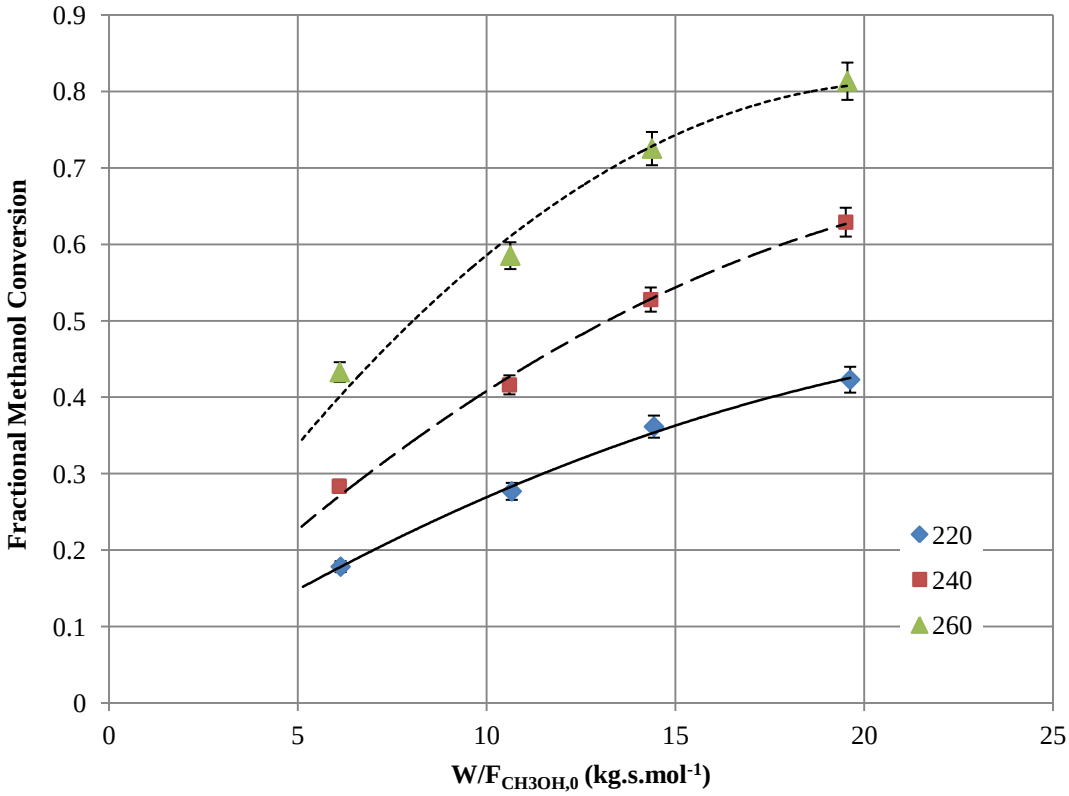

Figure 5.1 First set of results for conversion of methanol versus $W/F_{CH3OH,0}$ for BASF K3-110 at 220, 240 and 260°C, S/C ratio =1, 80-100 mesh catalyst particles

5.5.3 Catalyst Deactivation

Figure 5.2 shows that there was a significant decrease in methanol conversion due to the deactivation of the catalyst between the periods from 25 to 156 hours on line. Table 5.3 also shows the deactivation behavior of the catalyst at 260°C for $W/F_{CH3OH,0}$=10.6.

Table 5.3 Deactivation of BASF K3-110 during methanol steam reforming: Temperature 260°C, $W/F_{CH3OH,0}$=10.6, S/C=1

Time on line	*Rate of H_2 Production (µmol/s)*	*Rate of CO_2 Production (µmol/s)*	*Rate of CO Production (µmol/s)*	*Conversion*
75	116±3	34±1	0.59±0.04	0.58±0.03
156	79±2	24±1	0.47±0.09	0.42±0.01

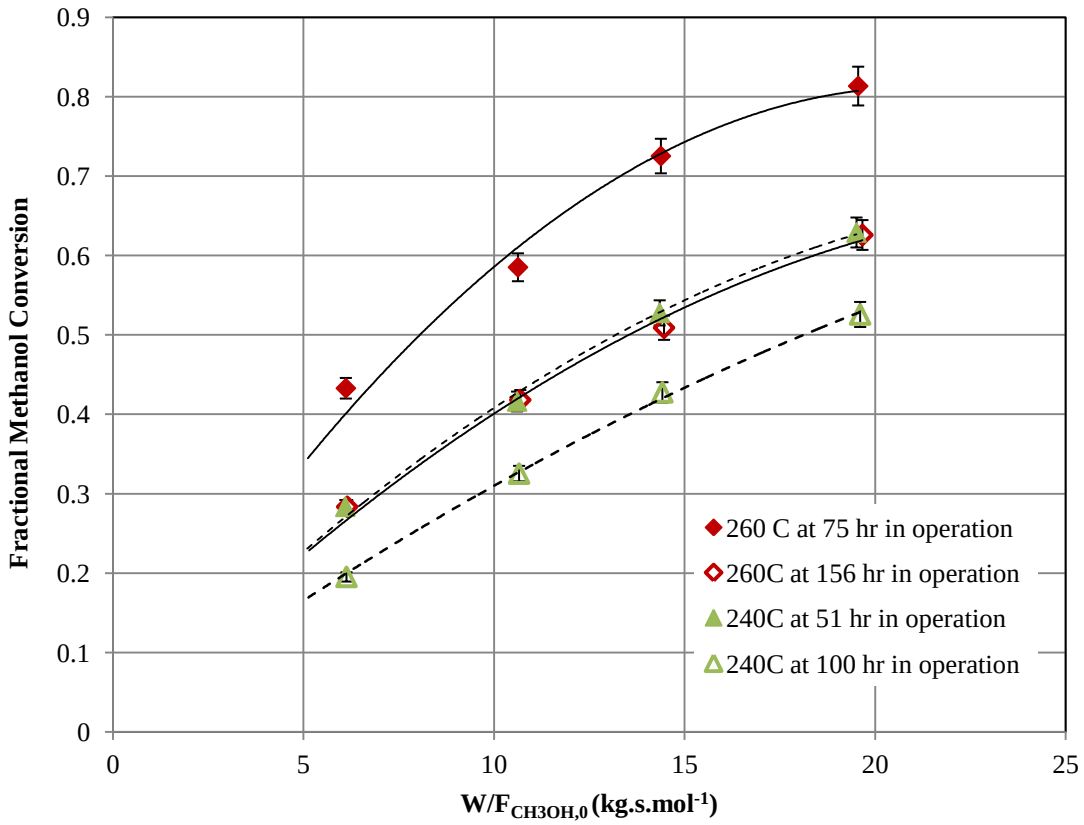

Figure 5.2 Decrease in methanol conversion due to deactivation of the catalyst at 240 and 260°C, S/C=1, between 51 and 156 hours on line

Table 5.3 shows that the rate of deactivation of the processes that produce CO_2 was different than the rate of deactivation for those producing CO. Overall, the rate of CO_2 production decreased to almost 70% of its initial value in 81 hours, whereas the rate of CO was 80% of its initial value

after the same period of time. The fact that the deactivation of the catalyst activity for the CO producing processes can be measured independently to those producing CO_2 can be important when studying the processes occurring on the surface of the catalyst.

5.5.4 Measurement of Composition vs. Water-Gas Shift Reaction Equilibrium

As can be seen in Figure 5.3 there is a correlation between the increase in carbon monoxide content and decrease in carbon dioxide content in the product gas when moving from lower to higher reaction temperature which would be expected according to the WGS equilibrium.

This pattern is indicative of the water-gas shift reaction shown in Equation 5.9.

$$CO + H_2O \rightleftarrows CO_2 + H_2 \qquad \Delta H^{\circ}_{298} = -41.17\ \text{kJ mol}^{-1} \qquad \textbf{5.9}$$

In the presence of the steam reforming reaction, the water gas shift reaction will almost always occur [7]. The equilibrium WGS reaction plays an important role in determining the final composition for methanol steam reforming.

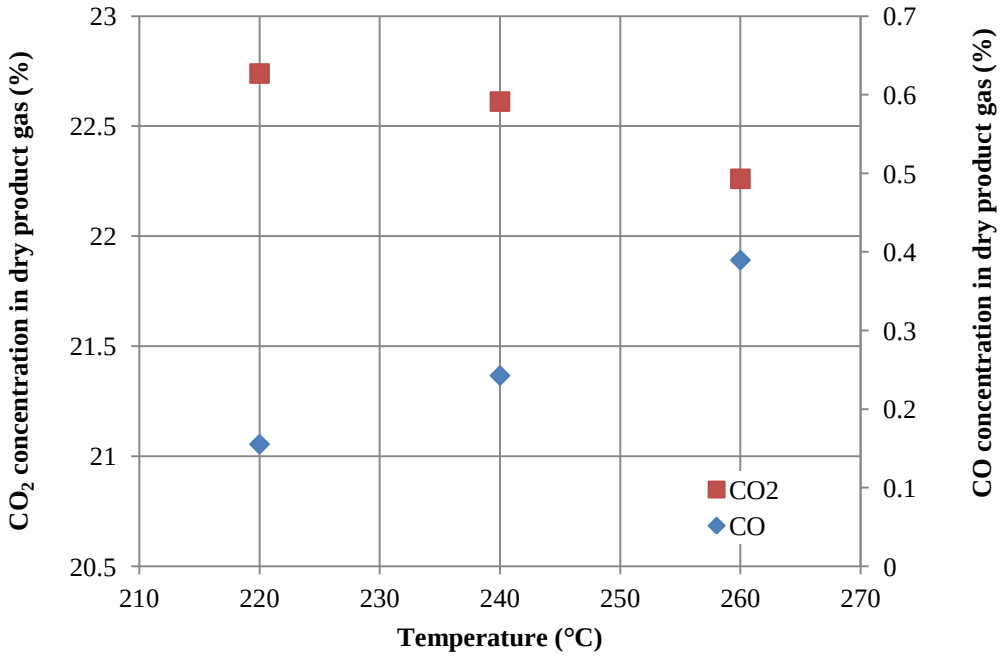

Figure 5.3 Carbon dioxide and carbon monoxide content in product gas versus temperature, $W/F_{CH3OH,0}$= 10.6 (kg.s.mol^{-1}), S/C= 1

As the temperature increased, the WGS reaction was driven to the left due to its exothermic nature reducing the amount of hydrogen and carbon dioxide in the product gas. This relationship is easily seen in Figure 5.3. As the temperature increased, the CO content in the product gas increased from 0.15% at 220 to 0.38% at 260 °C while CO2 content decreased from 22.73% to 22.41%.

In Figure 5.4, the ratio Φ_W given by Equation 5.10 is plotted against conversion. The Φ_W parameter represents the product composition relative to the WGS equilibrium.

$$\Phi_W = \left(\frac{P_{CO_2} P_{H_2}}{P_{CO} P_{H_2O}} \right) \frac{1}{K_W} \qquad \textbf{5.10}$$

The value of Φ_W will be equal to 1.0 when the gas composition is at WGS equilibrium, <1.0 when the partial pressure of the products are less than equilibrium and >1.0 when the partial pressures of the products are greater than equilibrium.

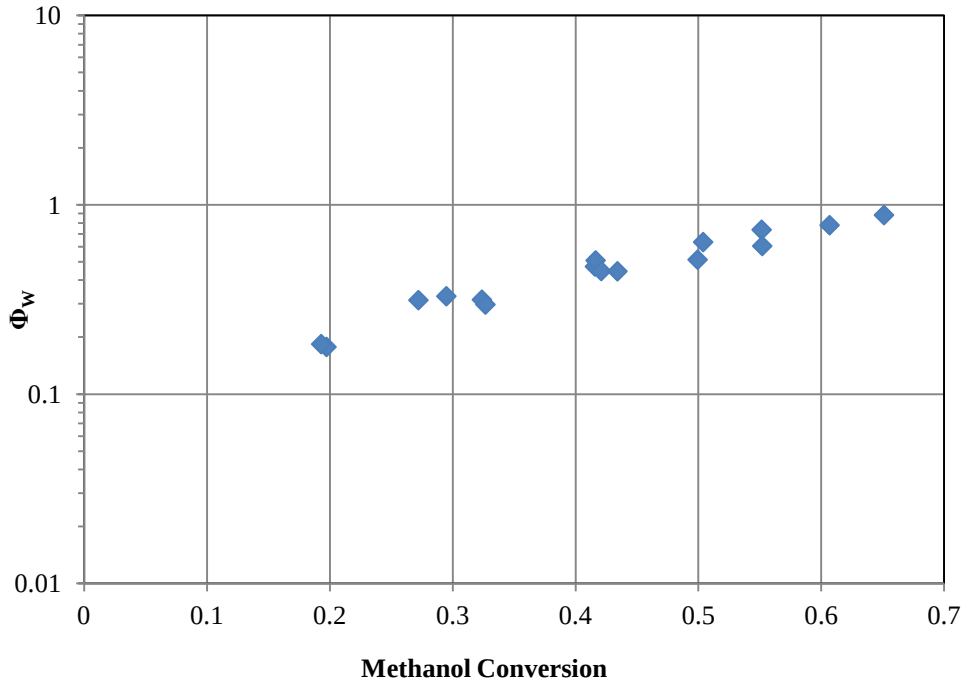

Figure 5.4 Φ_W versus fractional conversion, Temperature= 240, various flow rates, S/C= 1

Figure 5.5 compares the results from Peppley *et al.* [59, 66] with the measured Φ_W in this work. The measured Φ_W in this work is slightly lower than the prediction from Peppley's model. This means more CO had been produced initially. This, however, is not surprising considering the differences between the reactor in his work and the metal plate reactor for this thesis. The fact that slightly more CO is being produced in the metal plate reactor might be due to the catalyst being directly in contact with the metal plate and at a slightly higher average temperature. The key point is that the same overall trend reported by Peppley is clearly seen for the data of this work.

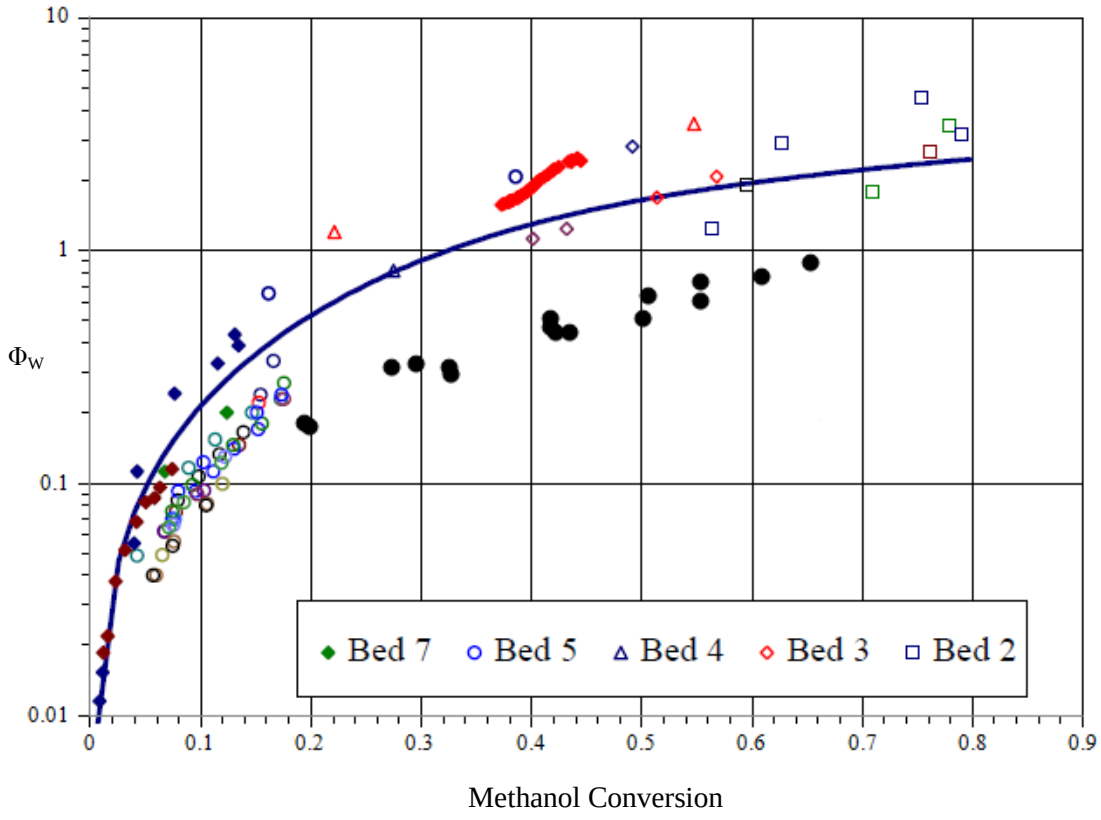

Figure 5.5 Comparison of Φ_W versus methanol conversion for BASF K3-110 at 240°C in metal plate reactor with prediction of model from Peppley *et al.* [59, 66] for the same catalyst in packed bed reactor (●) data from this work, the rest from Peppley *et al.*

5.5.5 First Order Rate Constant and Activation Energy

A preliminary kinetic analysis was made by considering the runs performed at different feed flow rates. The method for calculating the first order rate constant is described in Appendix E.

Table 5.4 shows the average values for the first order rate constant for methanol steam reforming over the BASF K3-110. The rate constant is only a function of temperature; however, the catalyst had changed between the runs at the same temperature due to deactivation. So, the rate constant was different as the time on line increased. It can be seen for runs 13-16, the 240°C rate constant is lower compared to run 5-8 due to the deactivation of the catalyst.

Table 5.4 First order rate constants for the experimental runs

Temperature	Runs	$k_{avg.}$ ($m^3\ kg^{-1}\ s^{-1}$)	σ
220	1-4	2.03×10^{-6}	6×10^{-8}
240	5-8	3.75×10^{-6}	4×10^{-8}
260	9-12	6.88×10^{-6}	6×10^{-8}
240	13-16	2.58×10^{-6}	2×10^{-8}
260	17-20	3.68×10^{-6}	3×10^{-8}
240	21	1.51×10^{-6}	2×10^{-8}
220	22	6.23×10^{-7}	2×10^{-8}

Apparent Activation Energies Comparison

The first order rate constant was calculated using the experimentally measured conversion of methanol and space time. According to the obtained results it was clear that there was rapid deactivation occurring between runs 1-16, so it was decided to only use the last runs in order to obtain an estimate for the rate constant. To determine the $k(T)$ and the activation energy an Arrhenius function describing the rate constant variation with temperature was determined. As demonstrated in Figure 5.6, the rate constant behaves according to Arrhenius-type expression at experimental temperatures. An Arrhenius exponential function was fitted to the experimentally obtained values of $k(T)$. The equation is given below:

$$k(T) = 9.89 \times 10^{3} \exp\left(\frac{-(96 \pm 4)\left[\text{kJ mol}^{-1}\right]}{RT}\right) \qquad \textbf{5.11}$$

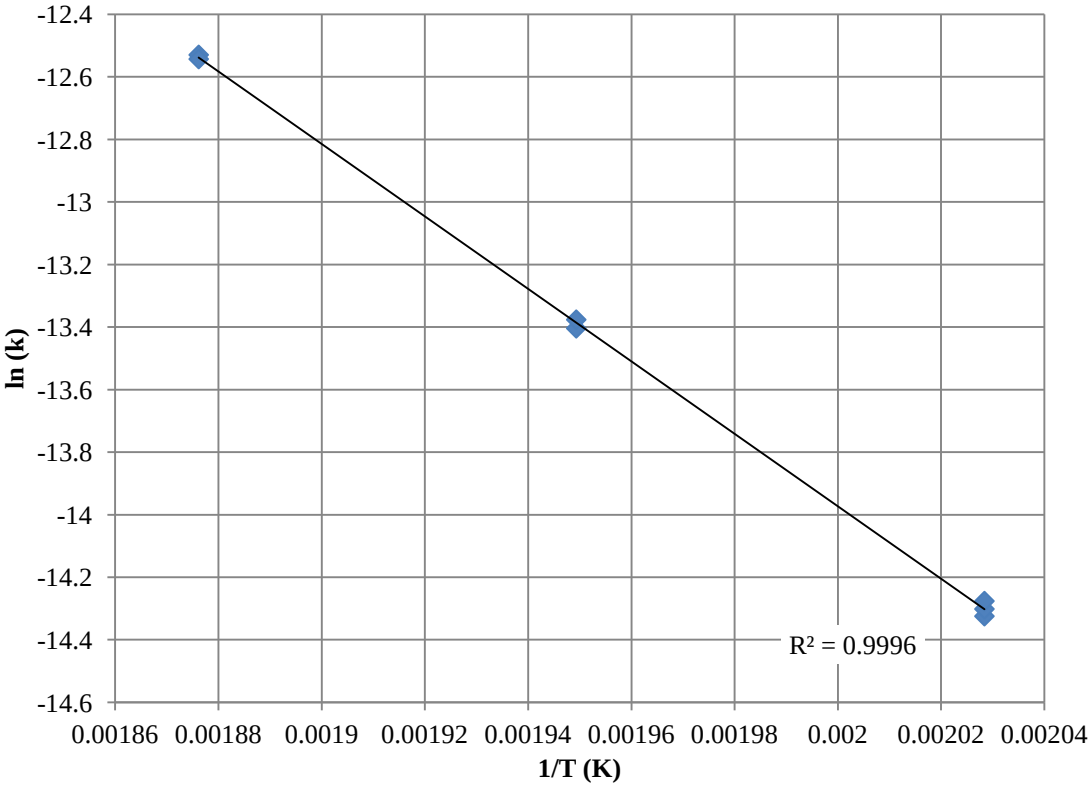

Figure 5.6 First order reaction rate constant as a function of temperature

The Arrhenius plot shows a satisfactory linear regression and the calculated apparent activation energy (E_a) of 96 kJmol^{-1} agrees well with values of 77-105 kJ mol^{-1} reported in the literature for similar Cu based catalysts (see Table 5.5).

Table 5.5 Apparent activation energies values from literature for methanol steam reforming reaction over $Cu/Zn/Al_2O_3$ catalysts as estimated by kinetic experiments

E_a (k J mol^{-1})	*Experimental Temperature Range (°C)*	*Reference*
102.8	180-280	Peppley *et al.* [66]
77-91	150-270	Amphlett *et al.* [67]
105.1	170-260	Jiang *et al.* [68]
100.9	175-220	Agrell *et al.* [69]
77.7	160-200	Santacesaria *et al.* [70]

Peppley *et al.* [66], Santacesaria *et al.* [70], and Jiang *et al.* [68] have reported the activation energy for a commercial $CuO/ZnO/Al_2O_3$ provided by BASF. Jiang *et al.* studied various copper-based catalyst prepared in lab and two commercial catalysts (BASF S3-85 and Harshaw Cu-0203-T). Their attention was focused on BASF catalyst since it was reported to have the highest activity. They estimated the value of 105.1 $kJmol^{-1}$ for the activation energy. Activation energy of 77.7 kJ mol^{-1} was reported by Santacesaria *et al.* [70].

Peppley *et al.* [59, 66] employed the exact same BASF K3-110, and they reported an activation energy of 102.8 kJ mol^{-1} based on a Langmuir–Hinshelwood rate expressions.

In general, the value for activation energy of 96±4 (kJ mol^{-1}) obtained in this work compares well to the research concerning determining the activation energy for quite similar catalysts. The fact that the obtained value is well among the range reported in the literature validates the catalyst coated metal plate reactor designed in this work.

Chapter 6

Conclusions and Recommendations

6.1 Overview

The main objective of this thesis, as stated in Section 1.5 of the introduction, was to design and commission a metal plate fuel reformer to study reaction kinetics of coated heat transfer surfaces. The metal plate reactor was successfully developed and its performance was tested for methanol steam reforming over a well characterized commercially available $CuO/ZnO/Al_2O_3$ catalyst, BASF K3-110. However, all the design features of the reactor and test station have capabilities for higher hydrocarbon reforming such as diesel. The reactor key design features included accurate measurement of the temperature profile along the reactor.

This reactor was tested for a variety of methanol steam reforming operating conditions. The performance of the reactor was investigated for various feed flow rates and reaction temperature. These results were compared with those in the literature in order to verify the operation of the new metal plate reformer. The main conclusions of this study are listed below.

6.2 Summary of Results

A single channel test reactor was successfully designed and built. The design provided a single narrow rectangular channel with laminar flow over a thin layer of catalyst.

The Biot number for the catalyst coated metal plate confirmed that the metal plate should provide isothermal conditions along the reaction channel. This was further determined experimentally by the six thermocouples closely measure the temperature along the reactor. The maximum variation in temperature along the length was 3 °C at 260°C.

The initial sealing procedure and reactor assembly was found to be insufficient in terms of achieving consistent leak free performance of the reactor. Modifications partially corrected the problem. Problems with gasket fabrication and consistent reactor assembly, however, still

persisted and would have required more time and effort than were available within the scope of this thesis.

Methanol conversion versus $W/F_{CH3OH,0}$ were found to be in acceptable agreement with those of Peppley *et al.* [59, 66]. Differences can be attributed to the improved heat transfer in the plate reactor.

The gas composition relative to the water-gas shift equilibrium was also in acceptable agreement with the results of Peppley *et al.* [66]. The marginal increase in CO concentration is most likely due to the average temperature in the catalyst layer being higher for the same set point temperature than observed in the packed bed by Peppley.

Based on the data acceptable determination of the first order rate constant for various temperatures were obtained. These results were in reasonably good agreement with previously published literature for the steam reforming of methanol over $Cu/ZnO/Al_2O_3$ catalyst. From an Arrhenius plot the activation energy was found to be 96±4 ($k.J.mol^{-1}$). This value compared well with values of found in the literature.

It was found that catalyst conditioning was critical and there was further significant deactivation after the first 24 hours of conditioning.

Reproducibility of the result has not been shown to this point because of the problems in sealing and catalyst deactivation. Improvements in the sealing procedure of the reactor as well as better catalyst preconditioning are required before reproducibility can be shown conclusively.

6.3 Recommendation for Design Improvements and Future Work

The following are a number of suggestions for design improvement and future work for the development of the plate reactor.

In terms of the thermocouple orientation in the reformer, it would be helpful to have thermocouples measuring the temperature on the surface of the catalyst as well as the catalyst

plate underneath the catalyst. As was discussed in Section 5.5.4 there was an indication that the catalyst in contact with the metal plate was slightly at a higher in temperature than the catalyst surface facing the flowing process stream. Temperature measurements of the catalyst surface would help in validating the modeling process.

It would be beneficial to reduce the total mass of the reformer and make the walls thinner. This would facilitate reaching steady state operational temperature more rapidly although this might require changing the method of sealing the reactor.

In terms of the operation of the catalyst, as was stated previously, catalyst conditioning was critical. A longer conditioning period than 24 hours is suggested for the catalyst.

References

[1]Asif, M.; Muneer, T. Energy supply, its demand and security issues for developed and emerging economies. *Renewable and Sustainable Energy Reviews* **2007**, *11*, 1388-1413.

[2]Song, C. Fuel processing for low-temperature and high-temperature fuel cells: Challenges, and opportunities for sustainable development in the 21st century. *Catalysis Today* **2002**, *77*, 17-49.

[3]U.S. Energy Information Administration International Energy Outlook 2011. , *DOE/EIA-0484 (2011)*.

[4]International Energy Agency Key World Energy Statistics from the IEA. **2011**.

[5]National Climate Data Centre NCDC: Climate of 2001 - Annual Review. http://lwf.ncdc.noaa.gov/oa/climate/research/2001/preann2001/preann2001.html (accessed 12/29/2011, 2011).

[6]Kolb, G. In *Fuel processing: for fuel cells;* Vch Verlagsgesellschaft Mbh: 2008; .

[7]Larminie, J.; Dicks, A. Fuel Cell Systems Explained (2nd Edition).

[8]Hirschenhofer, J.; Stauffer, D.; Engleman, R.; Klett, M. Fuel cell handbook. *US Department of Energy, Morgantown, WV* **1998**, *3*.

[9]Brant A. Peppley Personal communication **December 2011**, *At Hydrogen and Fuel Cell Conference, Mexico*.

[10]Christiansen, N.; Hansen, J. B.; Holm-Larsen, H.; Linderoth, S.; Larsen, P. H.; Hendriksen, P. V.; Mogensen, M. Solid oxide fuel cell development at Topsoe Fuel Cell and Risø. *Fuel Cells Bulletin* **2006**, *2006*, 12-15.

[11]Avila, P.; Montes, M.; Miro, E. E. Monolithic reactors for environmental applications:: A review on preparation technologies. *Chem. Eng. J.* **2005**, *109*, 11-36.

[12]Cybulski, A.; Moulijn, J. A. In *Structured catalysts and reactors;* CRC Press: 2006; Vol. 110.

[13]Giroux, T.; Hwang, S.; Liu, Y.; Ruettinger, W.; Shore, L. Monolithic structures as alternatives to particulate catalysts for the reforming of hydrocarbons for hydrogen generation. *Applied Catalysis B: Environmental* **2005**, *56*, 95-110.

[14]Redlingshöfer, H.; Kröcher, O.; Böck, W.; Huthmacher, K.; Emig, G. Catalytic wall reactor as a tool for isothermal investigations in the heterogeneously catalyzed oxidation of propene to acrolein. *Ind Eng Chem Res* **2002**, *41*, 1445-1453.

[15]Giornelli, T.; Löfberg, A.; Guillou, L.; Paul, S.; Le Courtois, V.; Bordes-Richard, E. Catalytic wall reactor:: Catalytic coatings of stainless steel by VOx/TiO2 and Co/SiO2 catalysts. *Catalysis Today* **2007**, *128*, 201-207.

[16]Meille, V. Review on methods to deposit catalysts on structured surfaces. *Applied Catalysis A: General* **2006**, *315*, 1-17.

[17]Heck, R. M.; Gulatiand Robert, J. The application of monoliths for gas phase catalytic reactions. *Chem. Eng. J.* **2001**, *82*, 149-156.

[18]Kolb, G.; Hessel, V. Micro-structured reactors for gas phase reactions. *Chem. Eng. J.* **2004**, *98*, 1-38.

[19]Thormann, J.; Pfeifer, P.; Kunz, U.; Schubert, K. Reforming of diesel fuel in a micro reactor. *International Journal of Chemical Reactor Engineering* **2008**, *6*, 1.

[20]Thormann, J.; Pfeifer, P.; Schubert, K.; Kunz, U. Reforming of diesel fuel in a micro reactor for APU systems. *Chem. Eng. J.* **2008**, *135*, S74-S81.

[21]Yu, X.; Tu, S.; Wang, Z.; Qi, Y. On-board production of hydrogen for fuel cells over Cu/ZnO/Al2O3 catalyst coating in a micro-channel reactor. *J. Power Sources* **2005**, *150*, 57-66.

[22]Pfeifer, P.; Schubert, K.; Emig, G. Preparation of copper catalyst washcoats for methanol steam reforming in microchannels based on nanoparticles. *Applied Catalysis A: General* **2005**, *286*, 175-185.

[23]Lim, M. S.; Kim, M. R.; Noh, J.; Woo, S. I. A plate-type reactor coated with zirconia-sol and catalyst mixture for methanol steam-reforming. *J. Power Sources* **2005**, *140*, 66-71.

[24]Karim, A.; Bravo, J.; Gorm, D.; Conant, T.; Datye, A. Comparison of wall-coated and packed-bed reactors for steam reforming of methanol. *Catalysis today* **2005**, *110*, 86-91.

[25]Bravo, J.; Karim, A.; Conant, T.; Lopez, G. P.; Datye, A. Wall coating of a CuO/ZnO/Al2O3 methanol steam reforming catalyst for micro-channel reformers. *Chem. Eng. J.* **2004**, *101*, 113-121.

[26]Kolb, G.; Zapf, R.; Hessel, V.; Lowe, H. Propane steam reforming in micro-channels--results from catalyst screening and optimisation. *Applied Catalysis A: General* **2004**, *277*, 155-166.

[27]Men, Y.; Gnaser, H.; Zapf, R.; Hessel, V.; Ziegler, C.; Kolb, G. Steam reforming of methanol over Cu/CeO2/[gamma]-Al2O3 catalysts in a microchannel reactor. *Applied Catalysis A: General* **2004**, *277*, 83-90.

[28]Zapf, R.; Becker-Willinger, C.; Berresheim, K.; Bolz, H.; Gnaser, H.; Hessel, V.; Kolb, G. Detailed characterization of various porous alumina-based catalyst coatings within microchannels and their testing for methanol steam reforming. *Chem. Eng. Res. Design* **2003**, *81*, 721-729.

[29]Cominos, V.; Hardt, S.; Hessel, V.; Kolb, G.; Lowe, H.; Wichert, M.; Zapf, R. A methanol steam micro-reformer for low power fuel cell applications. *Chem. Eng. Commun.* **2005**, *192*, 685-698.

[30]Hwang, S. M.; Kwon, O. J.; Kim, J. J. Method of catalyst coating in micro-reactors for methanol steam reforming. *Applied Catalysis A: General* **2007**, *316*, 83-89.

[31]Kim, T.; Kwon, S. Design, fabrication and testing of a catalytic microreactor for hydrogen production. *J Micromech Microengineering* **2006**, *16*, 1760.

[32]Kundu, A.; Ahn, J. E.; Park, S. S.; Shul, Y. G.; Han, H. S. Process intensification by micro-channel reactor for steam reforming of methanol. *Chem. Eng. J.* **2008**, *135*, 113-119.

[33]Kundu, A.; Park, J.; Ahn, J.; Park, S.; Shul, Y.; Han, H. Micro-channel reactor for steam reforming of methanol. *Fuel* **2007**, *86*, 1331-1336.

[34]Park, G. G.; Seo, D. J.; Park, S. H.; Yoon, Y. G.; Kim, C. S.; Yoon, W. L. Development of microchannel methanol steam reformer. *Chem. Eng. J.* **2004**, *101*, 87-92.

[35]Reuse, P.; Renken, A.; Haas-Santo, K.; Gorke, O.; Schubert, K. Hydrogen production for fuel cell application in an autothermal micro-channel reactor. *Chem. Eng. J.* **2004**, *101*, 133-141.

[36]Sekizawa, K.; Yano, S.; Eguchi, K.; Arai, H. Selective removal of CO in methanol reformed gas over Cu-supported mixed metal oxides. *Applied Catalysis A: General* **1998**, *169*, 291-297.

[37]Won, J. Y.; Jun, H. K.; Jeon, M. K.; Woo, S. I. Performance of microchannel reactor combined with combustor for methanol steam reforming. *Catalysis today* **2006**, *111*, 158-163.

[38]Haas-Santo, K.; Fichtner, M.; Schubert, K. Preparation of microstructure compatible porous supports by sol-gel synthesis for catalyst coatings. *Applied Catalysis A: General* **2001**, *220*, 79-92.

[39]Kiwi-Minsker, L.; Renken, A. Microstructured reactors for catalytic reactions. *Catalysis today* **2005**, *110*, 2-14.

[40]Alie, C.; Ferauche, F.; Léonard, A.; Lambert, S.; Tcherkassova, N.; Heinrichs, B.; Crine, M.; Marchot, P.; Loukine, E.; Pirard, J. P. Pd-Ag/SiO2 xerogel catalyst forming by impregnation on alumina foams. *Chem. Eng. J.* **2006**, *117*, 13-22.

[41]Giani, L.; Cristiani, C.; Groppi, G.; Tronconi, E. Washcoating method for Pd/[gamma]-Al2O3 deposition on metallic foams. *Applied Catalysis B: Environmental* **2006**, *62*, 121-131.

[42]Giani, L.; Groppi, G.; Tronconi, E. Mass-transfer characterization of metallic foams as supports for structured catalysts. *Ind Eng Chem Res* **2005**, *44*, 4993-5002.

[43]Giani, L.; Groppi, G.; Tronconi, E. Heat transfer characterization of metallic foams. *Ind Eng Chem Res* **2005**, *44*, 9078-9085.

[44]Chin, P.; Sun, X.; Roberts, G. W.; Spivey, J. J. Preferential oxidation of carbon monoxide with iron-promoted platinum catalysts supported on metal foams. *Applied Catalysis A: General* **2006**, *302*, 22-31.

[45]Yu, X.; Tu, S. T.; Wang, Z.; Qi, Y. Development of a microchannel reactor concerning steam reforming of methanol. *Chem. Eng. J.* **2006**, *116*, 123-132.

[46]Chen, G.; Li, S.; Yuan, Q. Pd-Zn/Cu-Zn-Al catalysts prepared for methanol oxidation reforming in microchannel reactors. *Catalysis today* **2007**, *120*, 63-70.

[47]Men, Y.; Gnaser, H.; Zapf, R.; Hessel, V.; Ziegler, C. Parallel screening of Cu/CeO2/γ-Al2O3 catalysts for steam reforming of methanol in a 10-channel micro-structured reactor. *Catalysis Communications* **2004**, *5*, 671-675.

[48]Eleta, A.; Navarro, P.; Costa, L.; Montes, M. Deposition of zeolitic coatings onto Fecralloy microchannels: Washcoating vs. in situ growing. *Microporous and Mesoporous Materials* **2009**, *123*, 113-122.

[49]Kolb, G.; Baier, T.; Schürer, J.; Tiemann, D.; Ziogas, A.; Specchia, S.; Galletti, C.; Germani, G.; Schuurman, Y. A micro-structured 5 kW complete fuel processor for iso-octane as hydrogen supply system for mobile auxiliary power units:: Part II--Development of water-gas shift and preferential oxidation catalysts reactors and assembly of the fuel processor. *Chem. Eng. J.* **2008**, *138*, 474-489.

[50]Stefanescu, A.; Van Veen, A.; Mirodatos, C.; Beziat, J.; Duval-Brunel, E. Wall coating optimization for microchannel reactors. *Catalysis today* **2007**, *125*, 16-23.

[51]Zapf, R.; Kolb, G.; Pennemann, H.; Hessel, V. Basic Study of Adhesion of Several Alumina-based Washcoats Deposited on Stainless Steel Microchannels. *Chem. Eng. Technol.* **2006**, *29*, 1509-1512.

[52]Sun, H.; Quan, X.; Chen, S.; Zhao, H.; Zhao, Y. Preparation of well-adhered [gamma]-Al2O3 washcoat on metallic wire mesh monoliths by electrophoretic deposition. *Appl. Surf. Sci.* **2007**, *253*, 3303-3310.

[53]Zhao, S.; Zhang, J.; Weng, D.; Wu, X. A method to form well-adhered [gamma]-Al2O3 layers on FeCrAl metallic supports. *Surface and Coatings Technology* **2003**, *167*, 97-105.

[54]Ming, Q.; Healey, T.; Allen, L.; Irving, P. Steam reforming of hydrocarbon fuels. *Catalysis today* **2002**, *77*, 51-64.

[55]Fauteux-Lefebvre, C.; Abatzoglou, N.; Blanchard, J.; Gitzhofer, F. Steam reforming of liquid hydrocarbons over a nickel–alumina spinel catalyst. *J. Power Sources* **2010**, *195*, 3275-3283.

[56]Goud, S. K.; Whittenberger, W. A.; Chattopadhyay, S.; Abraham, M. A. Steam reforming of n-hexadecane using a Pd/ZrO2 catalyst: Kinetics of catalyst deactivation. *Int J Hydrogen Energy* **2007**, *32*, 2868-2874.

[57]Rabe, S.; Truong, T. B.; Vogel, F. Catalytic autothermal reforming of methane: Performance of a kW scale reformer using pure oxygen as oxidant. *Applied Catalysis A: General* **2007**, *318*, 54-62.

[58]Krummenacher, J. J.; West, K. N.; Schmidt, L. D. Catalytic partial oxidation of higher hydrocarbons at millisecond contact times: decane, hexadecane, and diesel fuel. *Journal of Catalysis* **2003**, *215*, 332-343.

[59]Peppley, B. A.; Amphlett, J. C.; Kearns, L. M.; Mann, R. F. Methanol-steam reforming on Cu/ZnO/Al2O3. Part 1: the reaction network. *Applied Catalysis A: General* **1999**, *179*, 21-29.

[60]Pfeifer, P.; Schubert, K.; Liauw, M.; Emig, G. PdZn catalysts prepared by washcoating microstructured reactors. *Applied Catalysis A: General* **2004**, *270*, 165-175.

[61]Solbrig, C. W.; Gidaspow, D. Convective diffusion in a rectangular duct with one catalytic wall—laminar flow—arbitrary reaction order. *AICHE J.* **1967**, *13*, 346-351.

[62]Walpole, R. E.; Myers, R. H.; Myers, S. L.; Ye, K. In *Probability and statistics for engineers and scientists;* Prentice Hall Upper Saddle River, NJ: 1998; Vol. 6.

[63]McNair, H. M.; Miller, J. M.; Franke, S. In *Basic gas chromatography;* Wiley Online Library: 1969; .

[64]Brant A. Peppley A comprehensive kinetics model of methanol-steam reforming on $Cu/ZnO/Al_2O_3$ catalyst, Royal Military College of Canada, Ph.D. thesis, 1997.

[65]CRC Handbook of Chemistry and Physics; Page D-217; 1981-1982 .

[66]Peppley, B. A.; Amphlett, J. C.; Kearns, L. M.; Mann, R. F. Methanol-steam reforming on Cu/ZnO/Al2O3 catalysts. Part 2. A comprehensive kinetic model. *Applied Catalysis A: General* **1999**, *179*, 31-49.

[67]Amphlett, J.; Mann, R.; Weir, R. Hydrogen production by the catalytic steam reforming of methanol: Part 3: Kinetics of methanol decomposition using C18HC catalyst. *The Canadian Journal of Chemical Engineering* **1988**, *66*, 950-956.

[68]Jiang, C.; Trimm, D.; Wainwright, M.; Cant, N. Kinetic study of steam reforming of methanol over copper-based catalysts. *Applied Catalysis A: General* **1993**, *93*, 245-255.

[69]Agrell, J.; Birgersson, H.; Boutonnet, M. Steam reforming of methanol over a Cu/ZnO/Al2O3 catalyst: a kinetic analysis and strategies for suppression of CO formation. *J. Power Sources* **2002**, *106*, 249-257.

[70]Santacesaria, E.; Carra, S. Kinetics of catalytic steam reforming of methanol in a CSTR reactor. *Applied Catalysis* **1983**, *5*, 345-358.

[71]Levenspiel, O. Chemical Reaction Engineering (3rd Edition).

Appendix A: Gas Chromatograph, Pressure Transducers, Mass Flow Meter, and pump Calibrations

GC Calibrations

The gas chromatograph was calibrated by injecting the same volume of known gas composition and concentration. The response from the detector was integrated to obtain peak areas for H_2, N_2, CO, and CO_2. Following figures show the fit of the calibration curves for these components with 95% confidence intervals of the predicted values. These graphs have been expanded in the range of the range of concentrations which were measured during the experimental program. Equation for the best fit and coefficient of determination are also shown for each component.

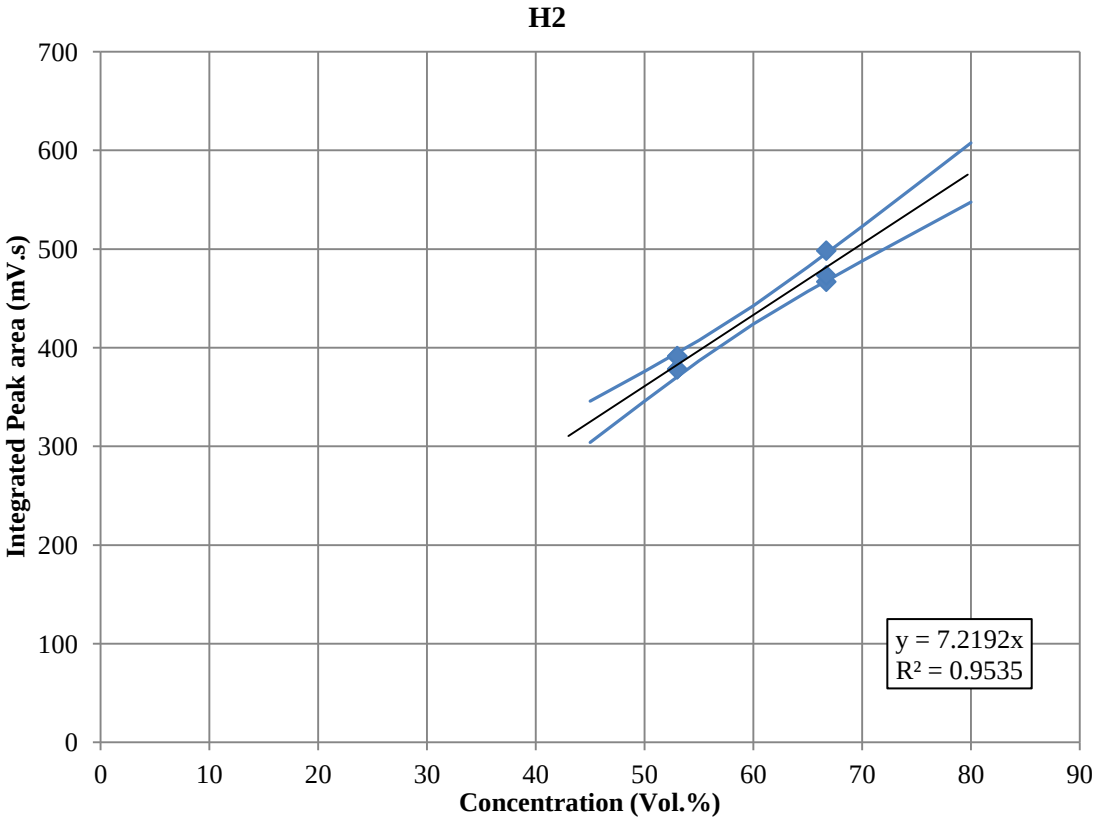

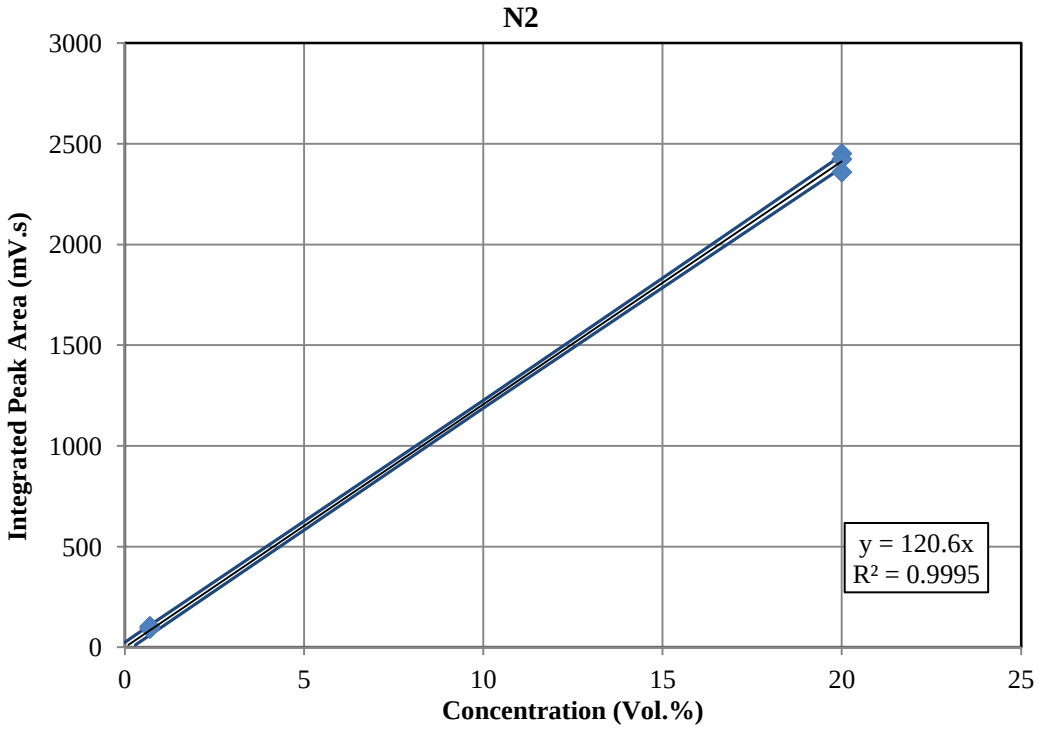
N2
Integrated Peak Area (mV.s)
3000
2500
2000
1500
1000
500
0
0
5
10
15
20
25
Concentration (Vol.%)
y = 120.6x
R² = 0.9995

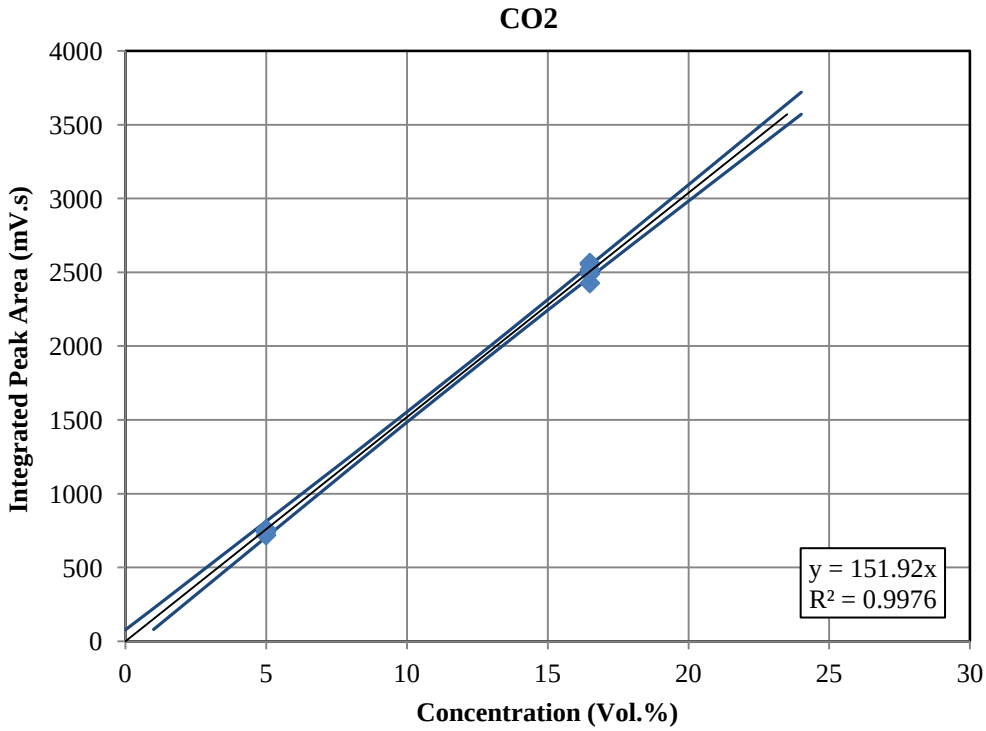
CO2
Integrated Peak Area (mV.s)
4000
3500
3000
2500
2000
1500
1000
500
0
0
5
10
15
20
25
30
Concentration (Vol.%)
y = 151.92x
R² = 0.9976

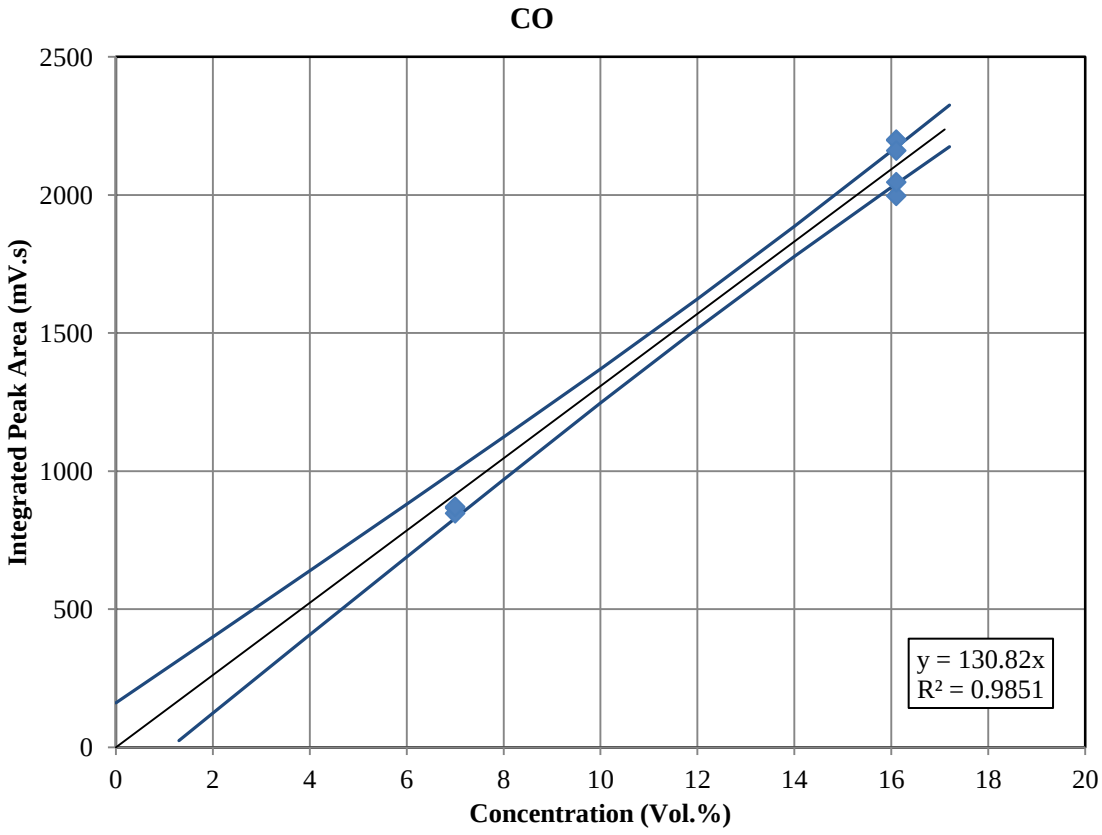

Nitrogen Mass Flow Controller (FE-101)

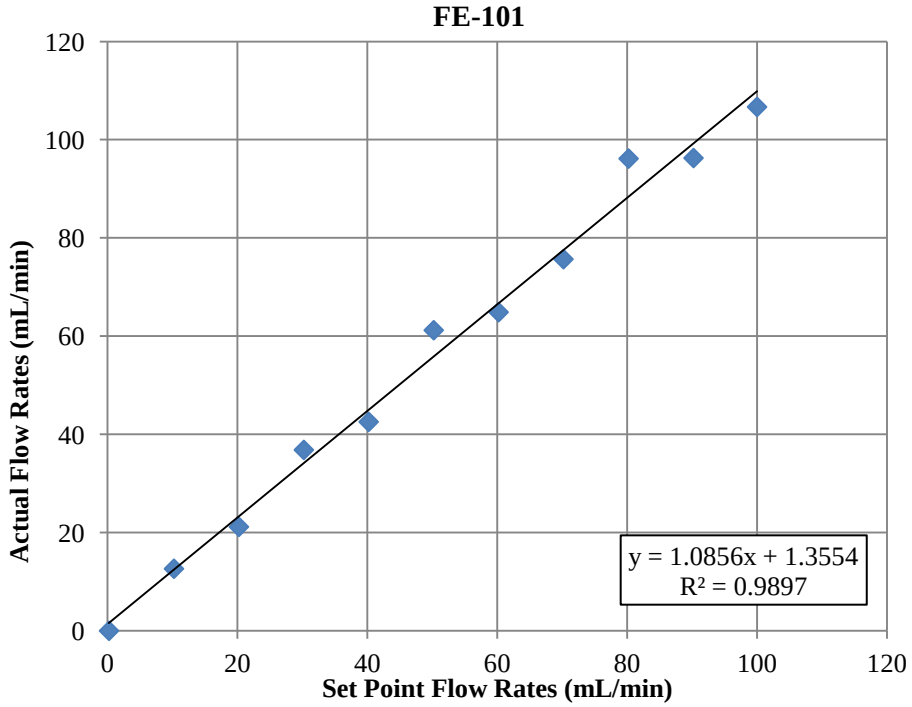

Reactor inlet (PE-301), outlet (PE-404), and soap bubble meter (PE-501) pressure sensors

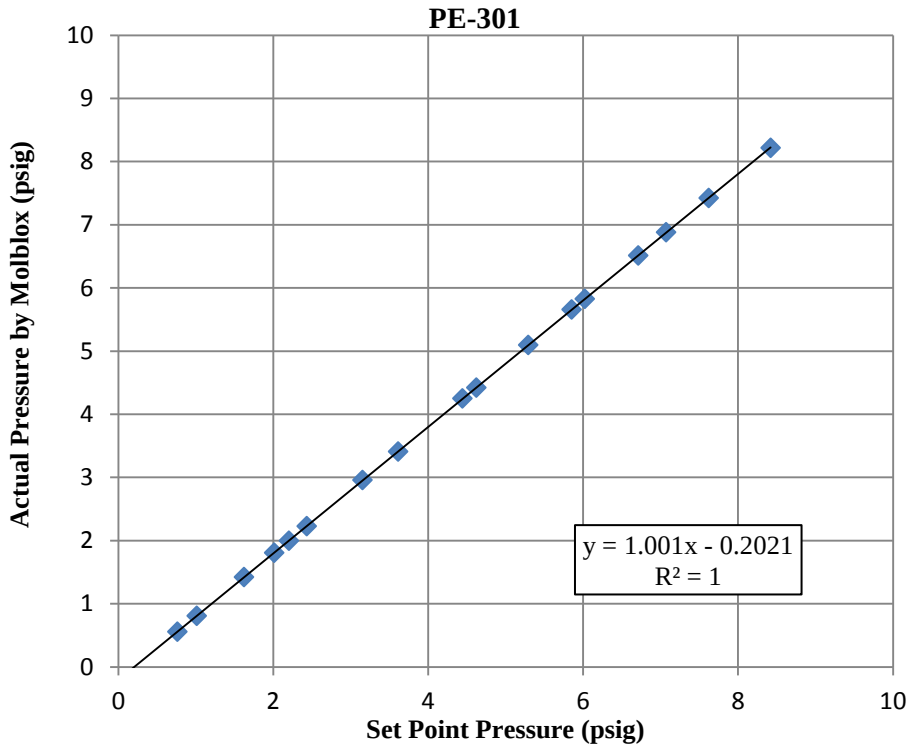

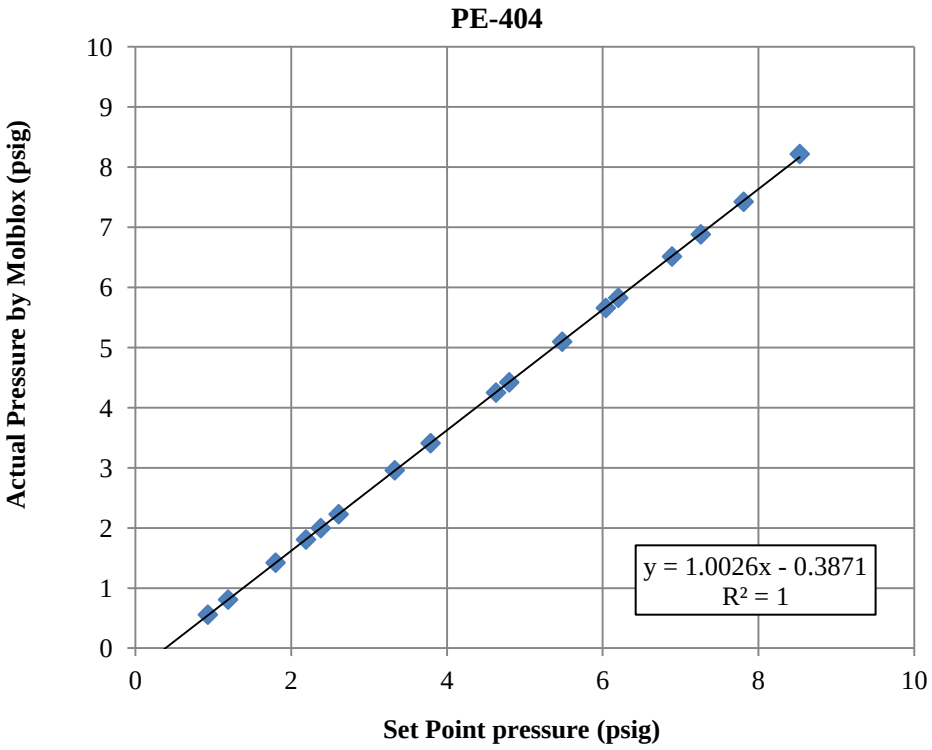

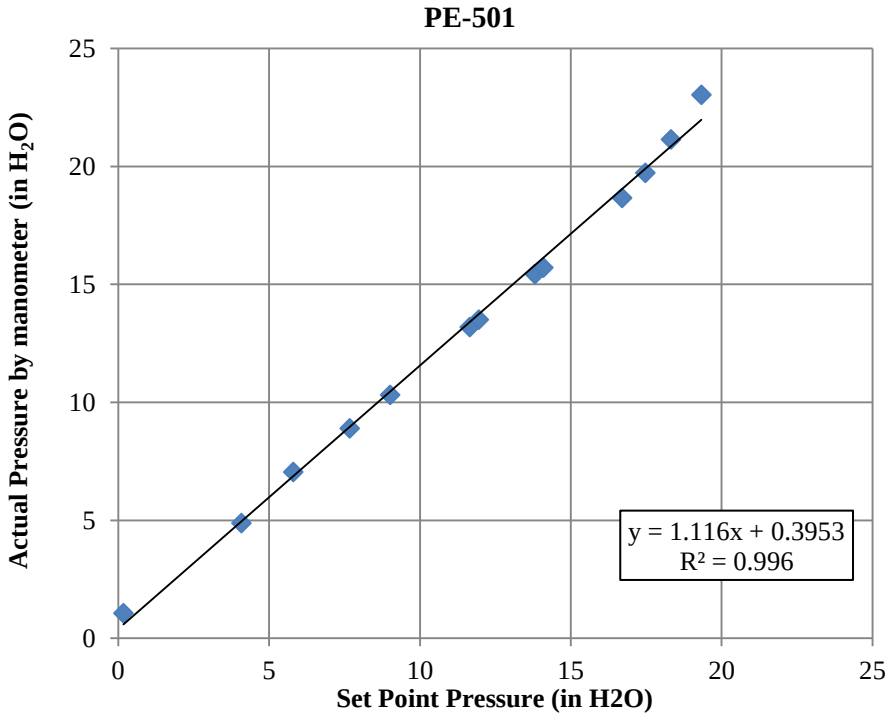

Pump Calibration

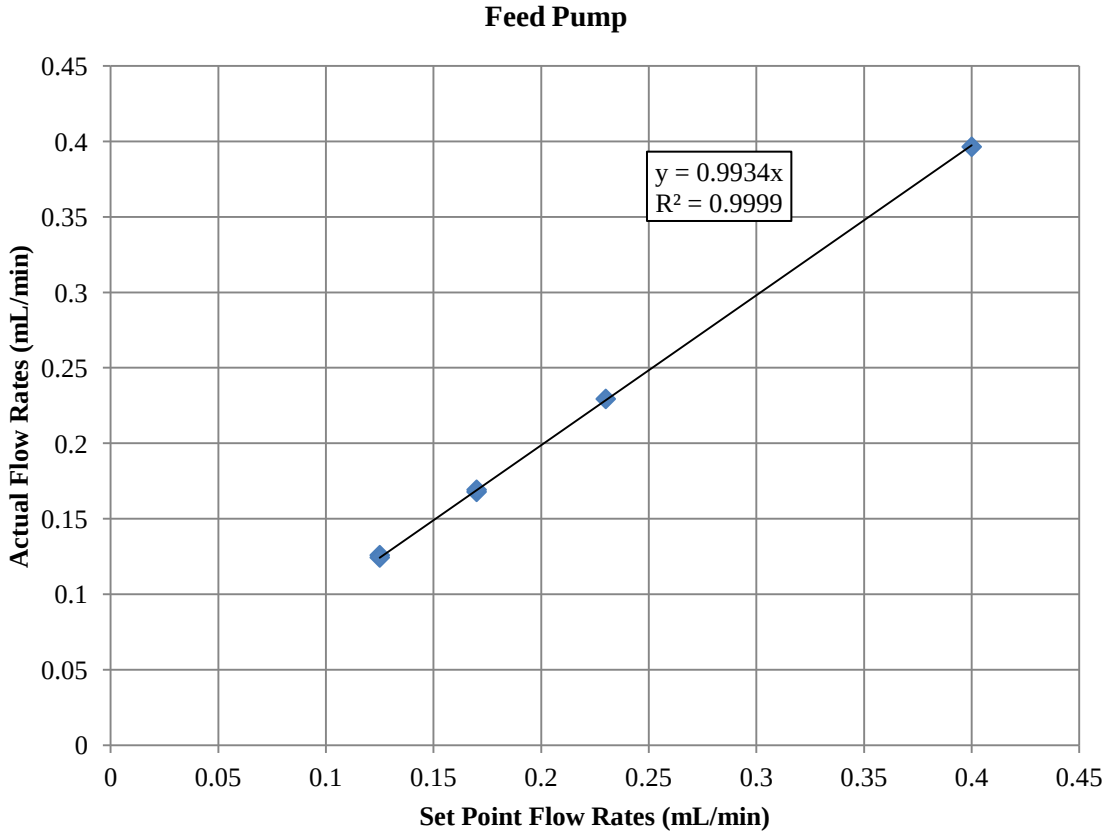

Appendix B: Experimental data for the reactor performance measurements

						Feed Composition						Molar Feed Rates	
Run	Wt. Cat. (g)	Reactor Temp. (°C)	Feed Total Volumetric flow rate (ml/s)	Density bottle empty (g)	Density bottle full (g)	Feed mass (g)	H_2O mass (g)	Sp. Gr. 20/20	Feed Density (g/cm^3)	wt.% Methanol	S/C	$F_{CH3OH,0}$ (mol/s)	$W/F_{CH3OH,0}$ (kg.s/mol)
April14a	0.7	220	0.0021	18.7906	27.5766	8.786	9.8615	0.8909	0.88934	62.46237	1.068	3.567E-05	19.62583
April14b	0.7	220	0.0021	18.7906	27.5766	8.786	9.8615	0.8909	0.88934	62.46237	1.068	3.567E-05	19.62583
April14c	0.7	220	0.0021	18.7906	27.5766	8.786	9.8615	0.8909	0.88934	62.46237	1.068	3.567E-05	19.62583
April14d	0.7	220	0.0021	18.7906	27.5766	8.786	9.8615	0.8909	0.88934	62.46237	1.068	4.851E-05	14.43076
April14e	0.7	220	0.0028	18.7906	27.5766	8.786	9.8615	0.8909	0.88934	62.46237	1.068	4.851E-05	14.43076
April14f	0.7	220	0.0028	18.7906	27.5766	8.786	9.8615	0.8909	0.88934	62.46237	1.068	4.851E-05	14.43076
April14g	0.7	220	0.0038	18.7906	27.5766	8.786	9.8615	0.8909	0.88934	62.46237	1.068	6.563E-05	10.66621
April14h	0.7	220	0.0038	18.7906	27.5766	8.786	9.8615	0.8909	0.88934	62.46237	1.068	6.563E-05	10.66621
April14i	0.7	220	0.0038	18.7906	27.5766	8.786	9.8615	0.8909	0.88934	62.46237	1.068	6.563E-05	10.66621
April14j	0.7	220	0.0066	18.7906	27.5766	8.786	9.8615	0.8909	0.88934	62.46237	1.068	0.0001141	6.13307
April14k	0.7	220	0.0066	18.7906	27.5766	8.786	9.8615	0.8909	0.88934	62.46237	1.068	0.0001141	6.13307
April14l	0.7	220	0.0066	18.7906	27.5766	8.786	9.8615	0.8909	0.88934	62.46237	1.068	0.0001141	6.13307
April15a	0.7	240	0.0021	18.7909	27.5671	8.7762	9.8608	0.8900	0.88841	62.89859	1.048	3.588E-05	19.51010
April15b	0.7	240	0.0021	18.7909	27.5671	8.7762	9.8608	0.8900	0.88841	62.89859	1.048	3.588E-05	19.51010
April15c	0.7	240	0.0021	18.7909	27.5671	8.7762	9.8608	0.8900	0.88841	62.89859	1.048	3.588E-05	19.51010
April15d	0.7	240	0.0028	18.7909	27.5671	8.7762	9.8608	0.8900	0.88841	62.89859	1.048	4.88E-05	14.34566
April15e	0.7	240	0.0028	18.7909	27.5671	8.7762	9.8608	0.8900	0.88841	62.89859	1.048	4.88E-05	14.34566
April15f	0.7	240	0.0028	18.7909	27.5671	8.7762	9.8608	0.8900	0.88841	62.89859	1.048	4.88E-05	14.34566
April15h	0.7	240	0.0038	18.7909	27.5671	8.7762	9.8608	0.8900	0.88841	62.89859	1.048	6.602E-05	10.60331

						Feed Composition						Molar Feed Rates	
Run	Wt. Cat. (g)	Reactor Temp. (°C)	Feed Total Volumetric flow rate (ml/s)	Density bottle empty (g)	Density bottle full (g)	Feed mass (g)	H_2O mass (g)	Sp. Gr. 20/20	Feed Density (g/cm^3)	wt.% Methanol	S/C	$F_{CH3OH,0}$ (mol/s)	$W/F_{CH3OH,0}$ (kg.s/mol)
April15i	0.7	240	0.0038	18.7909	27.5671	8.7762	9.8608	0.8900	0.88841	62.89859	1.048	6.602E-05	10.60331
April15j	0.7	240	0.0038	18.7909	27.5671	8.7762	9.8608	0.8900	0.88841	62.89859	1.048	6.602E-05	10.60331
April15k	0.7	240	0.0066	18.7909	27.5671	8.7762	9.8608	0.8900	0.88841	62.89859	1.048	0.0001148	6.09691
April15l	0.7	240	0.0066	18.7909	27.5671	8.7762	9.8608	0.8900	0.88841	62.89859	1.048	0.0001148	6.09691
April15m	0.7	240	0.0066	18.7909	27.5671	8.7762	9.8608	0.8900	0.88841	62.89859	1.048	0.0001148	6.09691
April16a	0.7	260	0.0021	18.7914	27.5735	8.7821	9.8635	0.8904	0.88876	62.73261	1.056	3.58E-05	19.55393
April16c	0.7	260	0.0021	18.7914	27.5735	8.7821	9.8635	0.8904	0.88876	62.73261	1.056	3.58E-05	19.55393
April16d	0.7	260	0.0021	18.7914	27.5735	8.7821	9.8635	0.8904	0.88876	62.73261	1.056	3.58E-05	19.55393
April16e	0.7	260	0.0028	18.7914	27.5735	8.7821	9.8635	0.8904	0.88876	62.73261	1.056	4.869E-05	14.37789
APril16f	0.7	260	0.0028	18.7914	27.5735	8.7821	9.8635	0.8904	0.88876	62.73261	1.056	4.869E-05	14.37789
April16g	0.7	260	0.0028	18.7914	27.5735	8.7821	9.8635	0.8904	0.88876	62.73261	1.056	4.869E-05	14.37789
April16h	0.7	260	0.0038	18.7914	27.5735	8.7821	9.8635	0.8904	0.88876	62.73261	1.056	6.587E-05	10.62714
April16i	0.7	260	0.0038	18.7914	27.5735	8.7821	9.8635	0.8904	0.88876	62.73261	1.056	6.587E-05	10.62714
April16j	0.7	260	0.0038	18.7914	27.5735	8.7821	9.8635	0.8904	0.88876	62.73261	1.056	6.587E-05	10.62714
April16k	0.7	260	0.0066	18.7914	27.5735	8.7821	9.8635	0.8904	0.88876	62.73261	1.056	0.0001146	6.11060
April16l	0.7	260	0.0066	18.7914	27.5735	8.7821	9.8635	0.8904	0.88876	62.73261	1.056	0.0001146	6.11060
April16m	0.7	260	0.0066	18.7914	27.5735	8.7821	9.8635	0.8904	0.88876	62.73261	1.056	0.0001146	6.11060
April17a	0.7	240	0.0021	18.7908	27.5764	8.7856	9.8628	0.8908	0.88918	62.53655	1.065	3.57E-05	19.60603
April17b	0.7	240	0.0021	18.7908	27.5764	8.7856	9.8628	0.8908	0.88918	62.53655	1.065	3.57E-05	19.60603
April17c	0.7	240	0.0021	18.7908	27.5764	8.7856	9.8628	0.8908	0.88918	62.53655	1.065	3.57E-05	19.60603
April17d	0.7	240	0.0028	18.7908	27.5764	8.7856	9.8628	0.8908	0.88918	62.53655	1.065	4.856E-05	14.41620
April17e	0.7	240	0.0028	18.7908	27.5764	8.7856	9.8628	0.8908	0.88918	62.53655	1.065	4.856E-05	14.41620
April17f	0.7	240	0.0028	18.7908	27.5764	8.7856	9.8628	0.8908	0.88918	62.53655	1.065	4.856E-05	14.41620
April17g	0.7	240	0.0038	18.7908	27.5764	8.7856	9.8628	0.8908	0.88918	62.53655	1.065	6.569E-05	10.65545

					Feed Composition							Molar Feed Rates	
Run	Wt. Cat. (g)	Reactor Temp. (°C)	Feed Total Volumetric flow rate (ml/s)	Density bottle empty (g)	Density bottle full (g)	Feed mass (g)	H_2O mass (g)	Sp. Gr. 20/20	Feed Density (g/cm^3)	wt.% Methanol	S/C	$F_{CH3OH,0}$ (mol/s)	$W/F_{CH3OH,0}$ (kg.s/mol)
April17h	0.7	240	0.0038	18.7908	27.5764	8.7856	9.8628	0.8908	0.88918	62.53655	1.065	6.569E-05	10.65545
April17i	0.7	240	0.0038	18.7908	27.5764	8.7856	9.8628	0.8908	0.88918	62.53655	1.065	6.569E-05	10.65545
April17j	0.7	240	0.0066	18.7908	27.5764	8.7856	9.8628	0.8908	0.88918	62.53655	1.065	0.0001143	6.12688
April17k	0.7	240	0.0066	18.7908	27.5764	8.7856	9.8628	0.8908	0.88918	62.53655	1.065	0.0001143	6.12688
April17l	0.7	240	0.0066	18.7908	27.5764	8.7856	9.8628	0.8908	0.88918	62.53655	1.065	0.0001143	6.12688
April19b	0.7	260	0.0021	18.7913	27.5826	8.7913	9.864	0.8913	0.88965	62.31596	1.075	3.56E-05	19.66507
April19c	0.7	260	0.0021	18.7913	27.5826	8.7913	9.864	0.8913	0.88965	62.31596	1.075	3.56E-05	19.66507
April19d	0.7	260	0.0021	18.7913	27.5826	8.7913	9.864	0.8913	0.88965	62.31596	1.075	3.56E-05	19.66507
April19e	0.7	260	0.0028	18.7913	27.5826	8.7913	9.864	0.8913	0.88965	62.31596	1.075	4.841E-05	14.45961
April19f	0.7	260	0.0028	18.7913	27.5826	8.7913	9.864	0.8913	0.88965	62.31596	1.075	4.841E-05	14.45961
April19h	0.7	260	0.0028	18.7913	27.5826	8.7913	9.864	0.8913	0.88965	62.31596	1.075	4.841E-05	14.45961
April19i	0.7	260	0.0038	18.7913	27.5826	8.7913	9.864	0.8913	0.88965	62.31596	1.075	6.55E-05	10.68754
April19j	0.7	260	0.0038	18.7913	27.5826	8.7913	9.864	0.8913	0.88965	62.31596	1.075	6.55E-05	10.68754
April19k	0.7	260	0.0038	18.7913	27.5826	8.7913	9.864	0.8913	0.88965	62.31596	1.075	6.55E-05	10.68754
April19l	0.7	260	0.0066	18.7913	27.5826	8.7913	9.864	0.8913	0.88965	62.31596	1.075	0.0001139	6.14533
April19m	0.7	260	0.0066	18.7913	27.5826	8.7913	9.864	0.8913	0.88965	62.31596	1.075	0.0001139	6.14533
April19n	0.7	260	0.0066	18.7913	27.5826	8.7913	9.864	0.8913	0.88965	62.31596	1.075	0.0001139	6.14533
April 24a	0.7	240	0.0074	18.7913	27.5950	8.8037	9.8666	0.8922	0.89067	61.83426	1.097	0.0001697	4.12408
April24b	0.7	240	0.0074	18.7913	27.5950	8.8037	9.8666	0.8922	0.89067	61.83426	1.097	0.0001273	5.49877
April 26a	0.7	220	0.0066	18.7906	27.5658	8.7752	9.861	0.8899	0.88829	62.95447	1.046	0.0001149	6.09231
April 26b	0.7	220	0.0066	18.7906	27.5658	8.7752	9.861	0.8899	0.88829	62.95447	1.046	0.0001149	6.09231
April26c	0.7	220	0.0066	18.7906	27.5658	8.7752	9.861	0.8899	0.88829	62.95447	1.046	0.0001149	6.09231

Dry Product Gas composition and Molar Flow Rate

Run	Dry product gas total volumetric flow rate V_F (cm^3/s)	Dry product gas P (PE-501) (H_2O" gauge)	Dry product gas flowrate STP (ml/s)	H_2 peak area	$y_{(H2)}$ Normalized	F_{H2} (mol/s)	CO peak area	$y_{(CO)}$ Normalized	F_{CO} (mol/s)	CO_2 peak area	$y_{(CO2)}$ Normalized	F_{CO2} (mol/s)
April14a	1.1086475	21.63	1.0741584	642.19	0.7702218	3.80969E-05	20.7546	0.00149965	7.4176E-08	3974.5673	0.22652585	1.12045E-05
April14b	1.3550136	22.2	1.3146168	577.2876	0.76948871	4.65186E-05	19.4586	0.00156259	9.44644E-08	3590.9373	0.22745395	1.37505E-05
April14c	1.2771392	21.61	1.2373505	567.7481	0.76864748	4.37972E-05	18.8713	0.0015392	8.7703E-08	3547.4517	0.22822523	1.30042E-05
April14d	1.3831259	22.43	1.3380786	634.2547	0.77172532	4.76217E-05	20.5845	0.0015089	9.31117E-08	3897.066	0.2253266	1.39045E-05
April14e	1.4992504	22.4	1.450319	587.3722	0.7702422	5.15208E-05	19.6337	0.00155109	1.03751E-07	3639.5531	0.22679717	1.51702E-05
April14f	1.5576324	22.5	1.5071487	569.7813	0.76949659	5.34752E-05	19.8917	0.00161843	1.1247E-07	3546.9704	0.22763117	1.58189E-05
April14g	1.5503876	22.19	1.4990494	607.4049	0.77203013	5.34017E-05	20.5922	0.00157682	1.09069E-07	3727.3015	0.22512625	1.55721E-05
April14h	1.55521	21.5	1.5012799	557.4212	0.76892865	5.33526E-05	18.2486	0.00151654	1.05226E-07	3478.9532	0.22804828	1.58233E-05
April14i	1.6129032	22.3	1.559897	568.9494	0.77038626	5.54367E-05	19.4985	0.00159059	1.14458E-07	3523.8715	0.22674128	1.63162E-05
April14j	1.7889088	21.7	1.7335422	613.0168	0.77214469	6.16265E-05	21.3065	0.00161682	1.29042E-07	3759.8993	0.22504956	1.79617E-05
April14k	1.6583748	21.85	1.6076139	563.7686	0.76991084	5.69645E-05	19.2072	0.00158025	1.1692E-07	3501.1412	0.22720863	1.68108E-05
April14l	1.754386	22.3	1.6967301	551.6153	0.76940121	6.02225E-05	19.481	0.001637	1.28132E-07	3435.3117	0.22769755	1.78223E-05
April15a	1.8975332	22.18	1.8290922	613.7461	0.76892171	6.50957E-05	34.7827	0.0026253	2.22254E-07	3819.659	0.22740165	1.92515E-05
April15b	2.0366599	22.1	1.9628303	571.7822	0.7686829	6.98468E-05	32.1289	0.00260216	2.36447E-07	3565.9898	0.22780976	2.07001E-05
April15c	2.0283976	22.35	1.9494125	567.6487	0.7679751	6.94994E-05	34.7877	0.00283541	2.56596E-07	3549.2399	0.22818048	2.06496E-05
April15d	2.1367521	22.39	2.0537415	600.7977	0.77137423	7.3536E-05	31.2156	0.00241452	2.30179E-07	3692.6986	0.2252975	2.14779E-05
April15e	2.3419204	22.1	2.2493999	573.7066	0.77031389	8.04861E-05	29.4832	0.00238492	2.49188E-07	3547.671	0.22635853	2.3651E-05
April15f	2.1008403	22.33	2.0189392	569.0062	0.76972538	7.21456E-05	32.6421	0.00266023	2.49341E-07	3525.1379	0.22660556	2.12395E-05
April15h	2.3809524	21.88	2.2934508	636.1988	0.77283346	8.20952E-05	33.8841	0.00247977	2.63416E-07	3878.225	0.223873	2.37812E-05
April15i	2.4509804	22.1	2.3541514	572.5312	0.76864469	8.40517E-05	31.5445	0.00255136	2.78993E-07	3571.0005	0.2278201	2.49122E-05

Dry Product Gas composition and Molar Flow Rate

Run	Dry product gas flow rate by soap meter V_F (cm^3/s)	Dry product gas P (PE-501) (H_2O" gauge)	Dry product gas flow rate STP (ml/s)	H_2 peak area	$y_{(H2)}$ Normalized	F_{H2} (mol/s)	CO peak area	$y_{(CO)}$ Normalized	F_{CO} (mol/s)	CO_2 peak area	$y_{(CO2)}$ Normalized	F_{CO2} (mol/s)
April15j	2.3980815	22.41	2.3050273	568.8235	0.76843922	8.22156E-05	29.1697	0.00237403	2.53998E-07	3557.336	0.22836657	2.4433E-05
April15k	2.7247956	22.07	2.6169639	574.1551	0.76890225	9.3473E-05	27.9882	0.00225808	2.74507E-07	3584.0618	0.22808307	2.77273E-05
April15l	2.9498525	21.6	2.829972	563.3693	0.76950082	0.000101272	28.7088	0.0023624	3.1091E-07	3504.6351	0.22747536	2.99375E-05
April15m	2.9673591	22.02	2.8495918	558.417	0.76865691	0.000101762	29.288	0.00242877	3.21541E-07	3489.6482	0.22826073	3.02191E-05
April16a	2.5575448	22.3	2.4502162	556.5544	0.75977789	8.66943E-05	53.3769	0.0043899	5.00909E-07	3624.6356	0.23513595	2.68302E-05
April16c	3.021148	22.18	2.8741227	566.7727	0.76602408	0.000103251	53.1023	0.00432383	5.82803E-07	3564.6302	0.22894103	3.08586E-05
April16d	2.5641026	22.06	2.4468377	550.5853	0.7605009	8.69994E-05	53.3754	0.00444159	5.08107E-07	3569.7502	0.2343088	2.68043E-05
April16e	3.164557	22.83	3.0050991	605.4158	0.76826157	0.000108468	51.9455	0.00397123	5.60685E-07	3766.3168	0.22711606	3.20658E-05
APril16f	2.9850746	22.57	2.8234762	594.9447	0.76779771	0.000102255	54.7197	0.00425438	5.66594E-07	3705.4918	0.22724363	3.02641E-05
April16g	2.8248588	22.83	2.6735762	581.9213	0.7692745	9.69525E-05	51.3814	0.00409209	5.15731E-07	3596.0648	0.22590208	2.84707E-05
April16h	3.4482759	22.58	3.2616789	580.8157	0.77011797	0.000118479	47.4112	0.00378723	5.82646E-07	3578.7977	0.22549229	3.46908E-05
April16i	3.2258065	22.83	3.0530515	583.0927	0.77563541	0.000111629	49.9725	0.00400473	5.76358E-07	3476.0404	0.21972551	3.16228E-05
April16j	3.0959752	22.7	2.9292732	562.3609	0.7672522	0.000105978	50.4193	0.00414421	5.72427E-07	3515.712	0.2279355	3.1484E-05
April16k	4.2553191	22.36	4.0229571	557.8165	0.75700891	0.000143719	42.306	0.00345887	6.56669E-07	3706.857	0.2390513	4.53841E-05
April16l	4.4642857	22.57	4.2226095	550.7828	0.7652303	0.000152414	42.0105	0.00351635	7.00365E-07	3495.9692	0.23081022	4.59714E-05
April16m	4.5248869	22.4	4.2782098	554.6697	0.76690499	0.000154821	42.0283	0.00350083	7.0674E-07	3482.7796	0.22882779	4.61953E-05
April17a	1.7152659	22.06	1.6629583	577.1596	0.7658745	5.86098E-05	36.9353	0.00295274	2.25963E-07	3648.1507	0.23004357	1.76044E-05
April17b	1.5649452	22.43	1.5185341	554.2087	0.76307606	5.3278E-05	37.1002	0.00307746	2.14869E-07	3554.7571	0.23258413	1.6239E-05
April17c	1.7301038	22.08	1.6774222	556.4156	0.76299143	5.88942E-05	36.5392	0.00301857	2.32999E-07	3571.5773	0.23273198	1.79643E-05
April17d	1.7889088	22.41	1.7357746	573.8211	0.76561677	6.11055E-05	34.2816	0.00275561	2.19931E-07	3635.0155	0.23047129	1.83944E-05
April17e	1.8450185	22.04	1.782648	572.4577	0.76545099	6.30085E-05	35.7759	0.00288195	2.37229E-07	3628.2639	0.23054117	1.89771E-05
April17f	1.9493177	22.4	1.8850066	587.9206	0.76651593	6.6663E-05	42.6825	0.00335254	2.91567E-07	3697.6921	0.22909146	1.99238E-05

Dry Product Gas composition and Molar Flow Rate

Run	Dry product gas flow rate by soap meter V_F (cm^3/s)	Dry product gas P (PE-501) (H_2O" gauge)	Dry product gas flow rate STP (ml/s)	H_2 peak area	$y_{(H2)}$ Normalized	F_{H2} (mol/s)	CO peak area	$y_{(CO)}$ Normalized	F_{CO} (mol/s)	CO_2 peak area	$y_{(CO2)}$ Normalized	F_{CO2} (mol/s)
April17g	1.8656716	22.16	1.8092003	552.0871	0.76402471	6.35951E-05	33.7531	0.00281407	2.34235E-07	3526.6379	0.231919	1.93042E-05
April17h	2.1141649	22.28	2.0438421	563.5565	0.76657251	7.23058E-05	37.0509	0.00303624	2.86389E-07	3543.3827	0.22903902	2.16038E-05
April17i	1.8761726	22.07	1.8128761	552.8521	0.7663264	6.41457E-05	35.635	0.0029758	2.49091E-07	3484.0767	0.22949233	1.92098E-05
April17j	1.9762846	22.38	1.9174506	553.8126	0.76442557	6.74009E-05	33.4727	0.00278346	2.45423E-07	3533.953	0.23179752	2.0438E-05
April17k	2.2026432	22.54	2.1451162	556.8411	0.76487262	7.51647E-05	33.9784	0.00281179	2.76317E-07	3545.3214	0.23141371	2.27412E-05
April17l	1.934236	22.07	1.8752947	555.8736	0.76418139	6.59457E-05	31.7276	0.00262772	2.26762E-07	3553.5704	0.23214588	2.00332E-05
April19b	2.1367521	22.38	2.051878	542.8183	0.76274047	7.2713E-05	75.7492	0.00641243	6.11305E-07	3443.1941	0.22991085	2.19177E-05
April19c	1.9646365	22.1	1.8853522	536.0652	0.76249234	6.68342E-05	62.0038	0.00531323	4.65716E-07	3419.9395	0.2311596	2.02617E-05
April19d	1.9379845	22.17	1.8600832	548.7329	0.76262649	6.59391E-05	58.3516	0.00488569	4.22432E-07	3503.7612	0.23139876	2.00075E-05
April19e	2.4213075	22.14	2.3238134	611.3734	0.76701382	8.28579E-05	68.9272	0.00520966	5.62782E-07	3807.2831	0.22697994	2.45199E-05
April19f	2.2675737	22.1	2.1760641	558.9375	0.76409393	7.73017E-05	56.6294	0.00466388	4.71835E-07	3546.0995	0.23036159	2.33052E-05
April19h	2.0703934	22.5	1.9887181	568.005	0.75415178	6.96615E-05	56.9422	0.00455473	4.20724E-07	3809.1931	0.24033401	2.21998E-05
April19i	2.3923445	22	2.2952575	537.3427	0.7623029	8.1364E-05	50.3387	0.0043023	4.59203E-07	3449.6727	0.23255718	2.48219E-05
April19j	2.2779043	22.52	2.1881462	559.3934	0.76363611	7.76073E-05	57.1319	0.00469862	4.77514E-07	3557.7406	0.2307911	2.3455E-05
April19k	2.5125628	22.48	2.4215113	566.3161	0.76456578	8.57063E-05	55.5735	0.00452008	5.06692E-07	3587.1826	0.23013628	2.57978E-05
April19l	2.2883295	21.93	2.2025416	602.5199	0.76671548	7.82769E-05	55.0256	0.00421842	4.30675E-07	3775.5934	0.22830935	2.3309E-05
April19m	2.8409091	22.29	2.7274855	565.397	0.76435889	9.68803E-05	49.2143	0.00400827	5.08037E-07	3594.8652	0.23094155	2.92712E-05
April19n	2.8089888	21.74	2.702468	555.8107	0.76520254	9.58975E-05	49.2474	0.00408465	5.11901E-07	3515.8175	0.23001252	2.88259E-05
April 24a	1.3812155	22.07	1.3056028	640.5036	0.77515068	4.77671E-05	48.8658	0.0035628	2.1955E-07	3822.8968	0.2198532	1.3548E-05
April24b	1.4144272	22.44	1.3381825	589.481	0.77553405	4.89398E-05	46.2265	0.00366391	2.3121E-07	3510.7948	0.21948869	1.38508E-05
April 26a	0.5980861	18.81	0.5638289	637.112	0.77462372	2.06698E-05	46.0653	0.0033742	9.00359E-08	3790.4288	0.21899742	5.84364E-06

Dry Product Gas composition and Molar Flow Rate

Run	Dry product gas flow rate by soap meter V_F (cm^3/s)	Dry product gas P (PE-501) (H_2O" gauge)	Dry product gas flow rate STP (ml/s)	H_2 peak area	$y_{(H2)}$ Normalized	F_{H2} (mol/s)	CO peak area	$y_{(CO)}$ Normalized	F_{CO} (mol/s)	CO_2 peak area	$y_{(CO2)}$ Normalized	F_{CO2} (mol/s)
April 26b	0.6119951	18.81	0.5769412	597.8319	0.77345836	2.11186E-05	43.7735	0.00341186	9.3158E-08	3583.629	0.22032133	6.01569E-06
April26c	0.6269592	18.8	0.591034	586.7124	0.77319676	2.16277E-05	42.9941	0.00341347	9.54808E-08	3523.2189	0.22063786	6.17164E-06

Run	Temperature (°C)	K_w	Mass Action Coefficient	Φ_w	Conversion	space Time ($kg.s/m^3$)	-2 ln (1-X)-X	Rate Constant ($m^3/kg.s$)
April14a	220	149.4821	66.1837047	0.442753	0.36	338232.33	0.525658	1.55E-06
April14b	220	149.4821	82.7417283	0.553523	0.44	338232.33	0.708457	2.09E-06
April14c	220	149.4821	77.9251554	0.521301	0.41	338232.33	0.645581	1.91E-06
April14d	220	149.4821	58.8077375	0.39341	0.33	248700.25	0.466769	1.88E-06
April14e	220	149.4821	63.6336998	0.425694	0.36	248700.25	0.521490	2.1E-06
April14f	220	149.4821	64.241439	0.42976	0.37	248700.25	0.550258	2.21E-06
April14g	220	149.4821	44.8216955	0.299847	0.27	183821.92	0.362540	1.97E-06
April14h	220	149.4821	47.3032235	0.316447	0.27	183821.92	0.362071	1.97E-06
April14i	220	149.4821	46.8692446	0.313544	0.28	183821.92	0.380844	2.07E-06
April14j	220	149.4821	27.3068881	0.182677	0.18	105697.60	0.217416	2.06E-06
April14k	220	149.4821	25.8822856	0.173146	0.17	105697.60	0.198032	1.87E-06
April14l	220	149.4821	26.6420538	0.178229	0.18	105697.60	0.211533	2E-06
April15a	240	102.5072	79.8109999	0.778589	0.61	338232.33	1.260229	3.73E-06
April15b	240	102.5072	90.272632	0.880647	0.65	338232.33	1.454887	4.3E-06
April15c	240	102.5072	82.4705455	0.804534	0.65	338232.33	1.440574	4.26E-06
April15d	240	102.5072	65.0003491	0.634105	0.50	248700.25	0.898105	3.61E-06
April15e	240	102.5072	75.4873058	0.73641	0.55	248700.25	1.052276	4.23E-06
April15f	240	102.5072	57.9659111	0.565481	0.49	248700.25	0.870059	3.5E-06
April15h	240	102.5072	48.3080638	0.471265	0.42	183821.92	0.659331	3.59E-06
April15i	240	102.5072	49.6562077	0.484417	0.43	183821.92	0.683760	3.72E-06
April15j	240	102.5072	51.9866305	0.507151	0.42	183821.92	0.660691	3.59E-06
April15k	240	102.5072	32.0846815	0.312999	0.27	105697.60	0.363215	3.44E-06
April15l	240	102.5072	33.6478361	0.328248	0.30	105697.60	0.403977	3.82E-06
April15m	240	102.5072	33.065527	0.322568	0.30	105697.60	0.406647	3.85E-06

Run	Temperature (°C)	K_w	Mass Action Coefficient	Φ_w	Conversion	space Time ($Kg.s/m^3$)	-2 ln (1-X)-X	Rate Constant k ($m^3/kg.s$)
April16a	260	72.3122	84.069665	1.162593	0.81	338232.33	2.529754	7.48E-06
April16c	260	72.3122	116.081363	1.60528	0.96	338232.33	5.845979	1.73E-05
April16d	260	72.3122	83.0234552	1.148125	0.81	338232.33	2.558000	7.56E-06
April16e	260	72.3122	73.7729142	1.0202	0.75	248700.25	1.998142	8.03E-06
APril16f	260	72.3122	62.2897418	0.8614	0.70	248700.25	1.730660	6.96E-06
April16g	260	72.3122	58.6082063	0.810489	0.67	248700.25	1.533865	6.17E-06
April16h	260	72.3122	53.7157966	0.742832	0.60	183821.92	1.242679	6.76E-06
April16i	260	72.3122	44.5537085	0.61613	0.57	183821.92	1.110004	6.04E-06
April16j	260	72.3122	42.3153813	0.585176	0.54	183821.92	1.010395	5.5E-06
April16k	260	72.3122	38.4033977	0.531078	0.42	105697.60	0.669713	6.34E-06
April16l	260	72.3122	38.8630572	0.537434	0.45	105697.60	0.733965	6.94E-06
April16m	260	72.3122	39.3806805	0.544592	0.45	105697.60	0.752436	7.12E-06
April17a	240	102.5072	61.715354	0.602059	0.55	338232.33	1.044614	3.09E-06
April17b	240	102.5072	52.47714	0.511936	0.50	338232.33	0.884556	2.62E-06
April17c	240	102.5072	61.9800871	0.604641	0.55	338232.33	1.054006	3.12E-06
April17d	240	102.5072	45.7101578	0.445921	0.42	248700.25	0.671882	2.7E-06
April17e	240	102.5072	45.5630486	0.444486	0.43	248700.2	0.704759	2.83E-06
April17f	240	102.5072	41.9165745	0.408913	0.45	248700.25	0.771381	3.1E-06
April17g	240	102.5072	32.2539666	0.314651	0.32	183821.92	0.458872	2.5E-06
April17h	240	102.5072	34.5554998	0.337103	0.37	183821.92	0.550455	2.99E-06
April17i	240	102.5072	30.4106578	0.296668	0.33	183821.92	0.464508	2.53E-06
April17j	240	102.5072	18.1629363	0.177187	0.20	105697.60	0.242341	2.29E-06
April17k	240	102.5072	20.3228057	0.198257	0.22	105697.60	0.277085	2.62E-06
April17l	240	102.5072	18.8019354	0.183421	0.20	105697.60	0.235955	2.23E-06
April19b	260	72.3122	40.1048043	0.554606	0.69	338232.33	1.634120	4.83E-06

Run	Temperature (°C)	K_w	Mass Action Coefficient	Φ_w	Conversion	space Time ($Kg.s/m^3$)	-2 ln (1-X)-X	Rate Constant k ($m^3/kg.s$)
April19c	260	72.3122	42.4710871	0.587329	0.63	338232.33	1.359463	4.02E-06
April19d	260	72.3122	45.2516118	0.625781	0.63	338232.33	1.321280	3.91E-06
April19e	260	72.3122	36.3721554	0.502988	0.58	248700.25	1.134094	4.56E-06
April19f	260	72.3122	37.5161297	0.518808	0.54	248700.25	0.998126	4.01E-06
April19h	260	72.3122	35.3317347	0.4886	0.48	248700.25	0.835142	3.36E-06
April19i	260	72.3122	29.0704866	0.402014	0.42	183821.92	0.660734	3.59E-06
April19j	260	72.3122	24.7523752	0.342299	0.40	183821.92	0.615597	3.35E-06
April19k	260	72.3122	29.2294323	0.404212	0.49	183821.92	0.716463	3.9E-06
April19l	260	72.3122	13.9726669	0.193227	0.23	105697.60	0.293250	2.77E-06
April19m	260	72.3122	19.1686957	0.265082	0.28	105697.60	0.385931	3.65E-06
April19n	260	72.3122	18.488237	0.255672	0.28	105697.60	0.380799	3.6E-06
April 24a	240	102.5072	5.91455937	0.057699	0.09	70465.07	0.103719	1.47E-06
April24b	240	102.5072	8.00315015	0.078074	0.13	93953.43	0.146905	1.56E-06
April 26a	220	149.4821	3.96676202	0.026537	0.06	105697.60	0.064006	6.06E-07
April 26b	220	149.4821	4.03654642	0.027004	0.06	105697.60	0.065487	6.2E-07
April26c	220	149.4821	4.14168915	0.027707	0.06	105697.60	0.067167	6.35E-07

Appendix C: Sample Calculations

Calculation of Molar Flow Rate of Methanol

The sample calculation and error analysis presented is related to Run 5 which was the first run for at 240°C for the total flow rate of 0.124 ml/min

i) Feed Solution Density

The density of the feed solution was determined using a calibrated density bottle. The balance used in the measurements was accurate to 0.1 mg. All liquids were at 20°C.

Wight of bottle empty = $18.7909 \pm 0.0001\ g$

Weight of bottle filled = $27.5671 \pm 0.0001 g$

Weight of feed solution = $8.7762 \pm (\sqrt{(0.0001)^2 + (0.0001)^2} = 8.7752 \pm 0.0001 g$

Weight of same volume of DI water = $9.8608 \pm 0.0001 g$

The specific gravity of the feed solution is determined as:

$$D_{20}^{20} = \frac{8.7762 \pm 0.0001\ g}{9.8608 \pm 0.0001\ g} = 0.8884 \pm \left[\sqrt{\left(\frac{0.0001}{8.7762}\right)^2 + \left(\frac{0.0001}{9.8608}\right)^2} \times \frac{8.7762}{9.8608} \right] =$$

0.89001 ± 0.00002

Density of feed solution is:

$$\rho_F = \rho_{H_2O} \times D_{20}^{20} = 0.9982 \times (0.89001 \pm 0.00002) = 0.88841 \pm 0.00002\ \left(g\ cm^{-3}\right)$$

ii) Volumetric Flow Rate of Feed

The total volume of the feed delivers to the reformer during the experiment was controlled directly from the pump control panel. The pump was calibrated before head to ensure the precision of the delivered amount of feed (see Appendix A). Based on 6 data points for 95% confidence interval it was determined.

$$Q_F = 0.002 \left(\text{ml s}^{-1}\right)$$
$$\Delta Q_F = 0.001 \left(\text{ml s}^{-1}\right)$$

iii) Calculation of Weight % of Methanol in Feed Solution

Data for concentrative properties of methanol and water solution from Handbook of Chemistry and Physics [65] was used to determine weight% of methanol according to the solution density. The relation was found to have a slight curve so a second order polynomial was used as a fit with the below equation:

$$w\%methanol = -1014.1(\rho_F)^2 + 1333.2(\rho_F) - 321.13$$

The R^2 for this fit was greater than 0.999 and standard error of the predicted values for this model was 3.2971.

$$w_{CH_3OH} = -1014.1(0.88841)^2 + 1333.2(0.88841) - 321.13 = 62.90\%$$

$$\Delta w_{CH_3OH} = \sqrt{\left(-1014.1 \times 2 \times \left(\frac{\Delta\rho_F}{\rho_F}\right) \times (\rho_F)^2\right)^2 + (1333.2 \times \Delta\rho_F)^2}$$

$$= \sqrt{\left(-1014.1 \times 2 \times \frac{0.00002}{0.88841} \times (0.88841)^2\right)^2 + (1333.2 \times 0.00002)^2} = 0.04\%$$

iv) Calculation of Molar Flow Rate of Methanol

The above calculations can now be substituted into the below equation to determine the molar flow rate of methanol.

$$F_{CH3OH,0} = \frac{\rho_F . Q_F . w_{CH3OH}}{60 \times M_{CH3OH}} \left(\text{mol s}^{-1}\right)$$

Where F_{CH_3OH} is the molar flow rate of methanol (mol s^{-1})

ρ_F is the density of the fees mixture (g cm^{-3})

Q_F is the volumetric flow rate of the feed mixture (cm^3 min^{-1})

w_{CH_3OH} is the weight fraction of methanol in the feed mixture based on the density of the feed mixture

M_{CH_3OH} is the molecular weight of methanol (=32.02 g gmol^{-1}).

$$F_{CH_3OH,0} = \frac{\rho_F . Q_F . w_{CH_3OH}}{M_{CH_3OH}} = \frac{(0.88841)\times(0.002056)\times(62.90/100)}{32.02}$$

$$= 3.612\times10^{-5}\ \left(\frac{\text{mol}}{\text{s}}\right) = 36\ \left(\frac{\mu\text{mol}}{\text{s}}\right)$$

$$\Delta F_{CH_3OH,0} = \frac{1}{32.02}\times\sqrt{\left(\frac{\Delta\rho_F}{\rho_F}\right)^2 + \left(\frac{\sqrt{\left(\frac{\Delta Q_F}{Q_F}\right)^2 + \left(\frac{\Delta w_{CH_3OH}}{w_{CH_3OH}}\right)^2}\times\left(Q_F\times w_{CH_3OH}\right)}{Q_F\times w_{CH_3OH}}\right)^2}\times\left(\rho_F\times Q_F\times w_{CH_3OH}\right)$$

$$= \frac{1}{32.02}\times\sqrt{\left(\frac{0.00002}{0.88841}\right)^2 + \left(\frac{\sqrt{\left(\frac{0.000049}{0.002056}\right)^2 + \left(\frac{0.04}{62.90}\right)^2}\times(0.002056\times0.6290)}{0.002056\times0.6290}\right)^2}$$

$$\times(0.88841\times0.002056\times0.6290) =$$

$$1\times10^{-6}\ \left(\frac{\text{mol}}{\text{s}}\right) = 1\ \left(\frac{\mu\text{mol}}{\text{s}}\right)$$

Calculation of Product Gas Component Molar Flow Rates

v) Gas Chromatograph Results

The percentage of H_2, CO and CO_2 in the sample loop was determined using the thermal conductivity detector response and the chromatograph calibration. The result from last two or more chromatograms, when the steady state was achieved, for each set of experimental conditions were pooled for each experiment. The average chromatography results for the specific discussed run including the standard deviations are shown in Table C. 1.

Table C. 1: Gas chromatograph results for Run16

Component	Integrated Peak Area (mV.s)	Std. Deviation (mV.s)	C.O.V (%)
H_2	592.2721	7.8626	1.32
CO	43.3838	0.5511	1.27
CO_2	3553.4239	42.7163	1.2021

vi) Calculation of Each Component Percentage in the Sample Loop

The calibration equations presented in Appendix A were used to convert the chromatograph response to percentage. The calculation for H_2 is shown as an example.

$$H_2\% = 0.1385 \times 613.7461 = 85.0$$

The error in this calculation will be the sum of the error associated with the variation in the chromatograph readings and the error in the calibration model.

$$\Delta H_2\% = t_{(df=5,0.05)} \times \hat{\sigma}\left(\text{chromatographs composition}\right) = 0.404 \times 2.015 = 0.8$$

Similar calculations for CO and CO_2 gives:

$$CO\% = 0.29$$
$$\Delta CO\% = 0.02$$
$$CO_2\% = 25.1$$
$$\Delta CO_2\% = 0.2$$

vii) Calculation of Normalized Fraction for Components

Usually the summation of above component percentages would not be equal to 100 due to GC readings and calibration errors. These amounts were then normalized with respect to other components available in the sample loop so that the total percentage was 100%. Traces of N_2

were sometimes identified as one of the components, so it was considered in normalization calculations.

$$\text{total}\% = H_2\% + CO\% + CO_2\% + N_2\% = 85.0 + 0.29 + 25.1 + 0.12 = 110.6$$

$$\Delta\text{total}\% = \sqrt{(\Delta H_2\%)^2 + (\Delta CO\%)^2 + (\Delta CO_2\%)^2 + (\Delta N_2\%)^2}$$
$$= \sqrt{(0.8158)^2 + (0.2902)^2 + (0.1514)^2 + (0.0223)^2} = 0.8$$

The normalized amount for H_2 is:

$$y_{H_2} = \frac{H_2\%}{\text{total}\%} = \frac{85.0}{110.6} = 0.7689$$

$$\Delta y_{H_2} = \sqrt{\left(\frac{\Delta H_2\%}{H_2\%}\right)^2 + \left(\frac{\Delta\text{total}\%}{\text{total}\%}\right)^2} \times \frac{H_2\%}{\text{total}\%} = \sqrt{\left(\frac{0.8}{85.0}\right)^2 + \left(\frac{0.8}{110.6}\right)^2} \times \frac{85.0}{110.6}$$
$$= 0.0009$$

Similarly:

$$y_{CO} = 0.0026,\ \Delta y_{CO} = 0.0002$$

$$y_{CO_2} = 0.227,\ \Delta y_{CO_2} = 0.002$$

i) Calculation Total Volumetric Flow Rate of Dry Product Gas

The total volumetric flow rate of dry product gas was determined by averaging the individual readings using the soap film meter and a stop watch for each run. At least 6 readings were taken for each run and below data is the average for last 2 runs at the specific condition.

$$V_F = \frac{10 \text{ ml}}{5.27 \text{ s}} = 1.898 \left(\frac{\text{ml}}{\text{s}}\right)$$

$$\Delta V_F = \frac{10}{t^2}\Delta t = \frac{10}{(5.27)^2} 0.01 = 0.003 \left(\frac{\text{ml}}{\text{s}}\right)$$

ii) Calculation of Molar Flow Rate of Gases

The average flow rate of dry product gas, in standard ml/min, was used to obtain the total molar flow rate using the ideal gas law. The total flow rate was then multiplied by the mole fraction of each component to obtain the individual molar flow rated of each component in the product gas.

$$F_i = y_i \frac{P^\circ \times V_F}{R \times T^\circ} \left(\frac{\text{mol}}{\text{s}}\right)$$

where P° is standard pressure = 1 atm (abs)

V is flow rate of dry product gas (mL s^{-1})

T° is standard temperature = 273.15 (K)

R is the gas constant = 82.05 (cm^3 atm $mole^{-1}$ K^{-1}).

Using the below equation, the molar flow rate of each component in the dry product gas stream can be calculated.

$$F_i = y_i \times V_F \times \frac{P^\circ}{RT^\circ} = y_i \times V_F \left(4.4615 \times 10^{-5}\right) \left(\frac{\text{mol}}{\text{s}}\right)$$

$$\Delta F_i = \sqrt{\left(\frac{\Delta y_i}{y_i}\right)^2 + \left(\frac{\Delta V_F}{V_F}\right)^2} \times y_i \times V_F \left(4.4615 \times 10^{-5}\right) \left(\frac{mol}{s}\right)$$

For H_2, CO and CO_2:

$$F_{H_2} = 65.1 \ \frac{\mu mol}{s} \quad , \quad \Delta F_{H_2} = 0.8 \ \frac{\mu mol}{s}$$

$$F_{CO} = 0.22 \ \frac{\mu mol}{s} \ , \ \Delta F_{CO} = 0.02 \ \frac{\mu mol}{s}$$

$$F_{CO_2} = 19.3 \ \frac{\mu mol}{s} \quad , \ \Delta F_{CO_2} = 0.1 \ \frac{\mu mol}{s}$$

iii) Calculation of Methanol Conversion

Combining above results and using Equation 5.8:

$$X_{CH_3OH} = \frac{F_{H_2} + F_{CO}}{3F_{CH_3OH,0}} = \frac{65.1 + 0.22}{3 \times 36} = 0.63$$

$$\Delta X_{CH_3OH} = \sqrt{\left(\frac{\sqrt{\left(\Delta F_{H_2}\right)^2 + \left(\Delta F_{CO}\right)^2}}{F_{H_2} + F_{CO}} \right)^2 + \left(\frac{3\Delta F_{CH_3OH}}{3F_{CH_3OH}} \right)^2} \times \left(\frac{F_{H_2} + F_{CO}}{3F_{CH_3OH}} \right)$$

$$= \sqrt{\left(\frac{\sqrt{(0.8)^2 + (0.02)^2}}{65.1 + 0.22} \right)^2 + \left(\frac{1}{36} \right)^2} \times \left(\frac{65.1 + 0.22}{3 \times 36} \right) = 0.02$$

The estimate relative error in the calculation of the methanol conversion is therefore approximately 2% for this particular run.

Appendix D: Overall mass balance of the system

Mass balances were calculated to validate the system performance. It was ensured that the condenser was completely empty before starting the run. A 10 ml density bottle was used to determine the specific gravity of the condensate solution. The actual composition of this solution was then determined using the specific gravity versus composition data from CRC Handbook of Chemistry and Physics [65]. Table D. 1 shows the mass balance for the selected runs.

Table D. 1: System overall mass balances for run 20, 21, and 22

Run	Duration (s)	Mass In (g) ($m_{CH3OH,0}+m_{H2O,0}$)	Mass Out (g) ($m_{H2}+m_{CO}+m_{CO2}+m_{CH3OH}+m_{H2O}$)	In-Out	Error (%)
20	5820	34.3873	36.1601	-1.7727	5
21	4680	31.1449	32.5873	-1.4424	4.6
22	8640	50.9687	53.3911	-2.4223	4.7

Appendix E: Preliminary analysis for the first order rate constant

Rate data are experimental measurements of the change in the number of moles of each component between the feed stream and the product stream for a known space time and a given set of operating conditions.

Space Time

Space time, τ_v, is the proper performance measure of flow reactor as time, t, is the natural measure for a batch reactor. Space time is defined as the time required to process one reactor volume of feed measured at specified conditions. For a given volumetric feed rate, Q_F, to a reactor with void volume, V, the space time, τ_v, is defined as:

$$\tau_v = \frac{V}{Q_F} = \frac{C_{A,0}V}{F_{A,0}} \qquad \text{[time]} \qquad \textbf{E. 1}$$

Where $F_{A,0}$ and $C_{A,0}$ are the molar flow rate and molar concentration of component 'A'. It is also common for some applications to base the space time on the weight of catalyst, W, instead of volume of the reactor resulting in a modified space time.

$$\tau_w = \frac{W}{Q_F} = \frac{C_{A,0}W}{F_{A,0}} \qquad \text{[mass of catalyst . time/ volume of feed]} \qquad \textbf{E. 2}$$

Throughout the remainder this work the symbol τ is referred to the space time based on the mass of catalyst and subscript is omitted.

The design equation for the flow reactors is well known [71] that the composition of the gas varies from point to point along the flow path. Therefore a material balance can be made for a differential element of volume or catalyst weight. For the catalyst coated plate used in this thesis calculations have been based on the weight of the catalyst.

$$F_{CH_3OH,0}dX = -r_{CH_3OH}dW \qquad \textbf{E. 3}$$

$$\int_0^W \frac{dW}{F_{CH_3OH,0}} = \int_{X=X_{CH_3OH,0}}^{X=X_{CH_3OH,f}} \frac{dX_{CH_3OH}}{-r_{CH_3OH}} \qquad \textbf{E. 4}$$

After integration and considering Equation E. 2, Equation E. 4 can be written as:

$$\frac{W}{F_{CH_3OH,0}} = \frac{\tau}{C_{CH_3OH,0}} = \int_{X=X_{CH_3OH,0}}^{X=X_{CH_3OH,f}} \frac{dX_{CH_3OH}}{-r_{CH_3OH}} \qquad \textbf{E. 5}$$

$$\tau = \frac{C_{CH_3OH,0}W}{F_{CH_3OH,0}} = C_{CH_3OH,0} \int_{X=X_{CH_3OH,0}}^{X=X_{CH_3OH,f}} \frac{dX_{CH_3OH}}{-r_{CH_3OH}} \qquad \textbf{E. 6}$$

The reaction has been assumed to be a first-order irreversible reaction, and for those types of reactions the kinetic equation can be written according to Equation E. 7 as Levenspiel [71].

$$k\tau = -\left(1+\varepsilon_{CH_3OH}\right)\ln\left(1-X_{CH_3OH}\right) - \varepsilon_{CH_3OH}X_{CH_3OH} \qquad \textbf{E. 7}$$

Where, k is the first-order forward rate constant [$m^3\ kg^{-1}\ s^{-1}$]

$F_{CH_3OH,0}$ is the molar flow rate of methanol entering the reactor [$mol\ s^{-1}$]

$C_{CH_3OH,0}$ is the concentration of methanol at the reactor entrance [$mol\ m^{-3}$]

W is the mass of catalyst [kg]

$\varepsilon_{CH_3OH} = \dfrac{V_{X_{CH_3OH}=1} - V_{X_{CH_3OH}=0}}{V_{X_{CH_3OH}=0}}$ is the fractional change in volume of the system between no conversion and complete conversion of methanol [71]

X_{CH_3OH} is the degree of conversion of methanol (see Equation 5.8).

Confirmation of First Order Mechanism

For the assumed irreversible methanol steam reforming reaction ε_{CH_3OH} equals to 1; therefore, Equation E. 7 will become:

$$k\tau = -2\ln\left(1-X_{CH_3OH}\right) - X_{CH_3OH} \qquad \textbf{E. 8}$$

Figure E.1 shows the value of the right hand side of Equation E. 8 plotted against τ at different temperatures. A first order reaction should yield a straight line with an intercept of zero and a slope equal to the rate constant, k, at different temperatures.

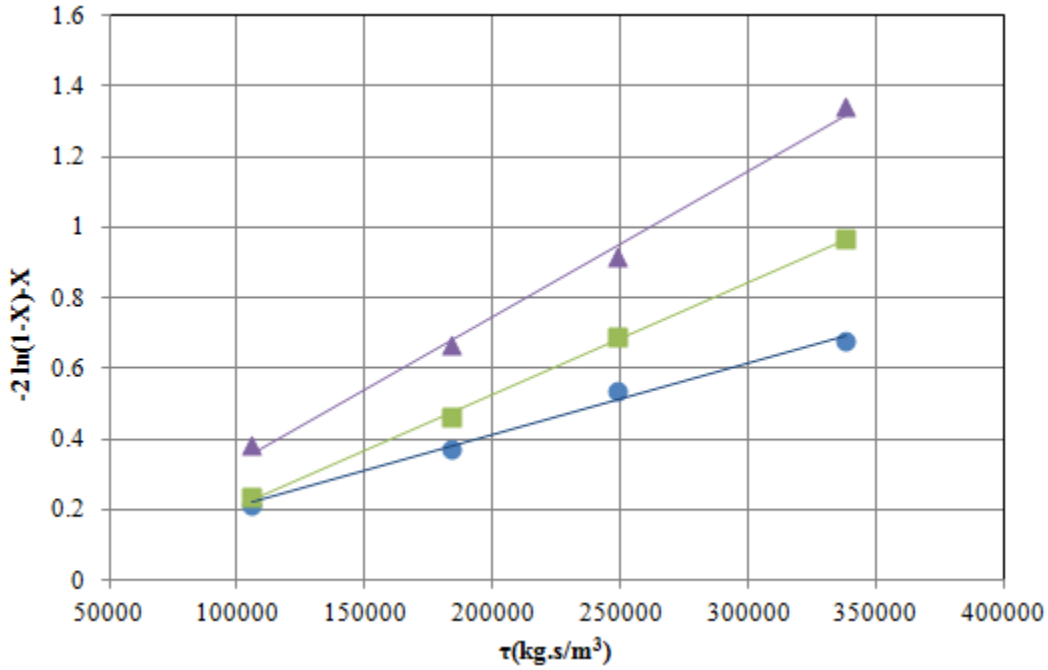

Figure E.1: Evaluation of first order reaction assumption, experimental results for (▲) 260, (■) 240, and (●) 220°C

The lines shown in Figure E.1 validate the irreversible first order assumption for the steam reforming reaction as a linear correlation exists between the right hand side of Equation E. 8 and τ. The trend in the slope of the lines is as expected with the increase in rate constant as the temperature increases.